1988ApJS...68..643B

THE ASTROPHYSICAL JOURNAL SUPPLEMENT SERIES, 68:643–714, 1988 December
© 1988. The American Astronomical Society. All rights reserved. Printed in U.S.A.

# EXTENDED OPTICAL-LINE–EMITTING GAS IN RADIO GALAXIES: BROAD-BAND OPTICAL, NARROW-BAND OPTICAL, AND RADIO IMAGING OF A REPRESENTATIVE SAMPLE

STEFI A. BAUM,[1,2,3,4] TIMOTHY HECKMAN,[3,4] ALAN BRIDLE,[2] WIL VAN BREUGEL,[5] AND GEORGE MILEY[6,7]
*Received 1987 December 8; accepted 1988 March 15*

## ABSTRACT

We have conducted a search for extended optical-line–emitting gas in a representative sample of powerful radio galaxies in order to determine the frequency with which such gas is found in these galaxies and to assess the relationship of the gas to the radio source structure and the structure of the host galaxy. We have obtained optical images through broad-band ($R$ or $V$) filters and through narrow-band filters, which isolated redshifted H$\alpha$ + [N II] or [O III] of 38 galaxies from a representative, radio-flux–limited ($S_{408\ \mathrm{MHz}} > 8.5$ Jy), optically unbiased sample and of five specially selected, previously studied galaxies. We have used the Very Large Array to obtain high-resolution ($\sim 1''$–$10''$) radio images of most of the sources in the sample. In this, the first of a series of papers reporting the results of this research, we describe the sample, the observations, and the data processing and present contour maps of the broad-band, narrow-band, and radio images. In subsequent papers, the numerical and statistical results of this survey will be presented and their implications will be discussed. From the images presented here, it is clear that extended optical-line–emitting gas is common in powerful radio galaxies. In some cases the emission-line filaments show organized structure on scales of 40–100 kpc, and in a few sources long emission-line filaments appear to connect the host radio galaxy to an apparent companion galaxy. S-shaped regions of line emission are observed in five of the sources. Morphological peculiarities in the distribution of the optical continuum light from the host radio galaxy are also apparent in many of these sources.

*Subject headings:* galaxies: interstellar matter — galaxies: structure — radio sources: galaxies

## I. INTRODUCTION

In active galaxies which have strong sources of nuclear ionizing radiation, cold extranuclear gas may be ionized. Thus, cold gas ($T \sim 10^4$ K) in powerful radio galaxies can potentially be traced through observations of optical emission lines emitted as the gas recombines. There are now over a dozen powerful radio sources known to have line-emitting gas that is extended on scales of tens of of kiloparsecs (see, e.g., Fosbury 1986; van Breugel 1986; and references therein). They span a wide range in radio luminosity and radio source size, as well as in habitat, from the centers of very rich clusters to very isolated environments. In some sources, the line-emitting gas may cool out of a hot, intracluster or interstellar medium (e.g., van Breugel, Heckman, and Miley 1984), while in others the emission lines probably originate in cold gas in the galaxy's interstellar medium, which has been heated and ionized (e.g., 3C 305, Heckman *et al.* 1982). Since elliptical galaxies are not expected to have much cold gas tens of kiloparsecs from their nuclei, the discovery of extended line-emitting gas in these galaxies may suggest that the gas has been acquired during a tidal interaction with a gas-rich companion. Indeed, some of the radio galaxies with such gas have distorted optical continuum morphologies (e.g., van Breugel *et al.* 1986). In many of these sources, there is also spectroscopic (e.g., kinematic or excitational) and imaging (i.e., morphological) evidence to suggest that the extended radio source and the line-emitting gas are interacting.

However, most of the powerful radio sources that have thus far been searched for extended emission lines were chosen for study specifically because previous observations had indicated that they were unusual. For instance, several of the sources were observed because they were known to have peculiar radio properties (e.g., low fractional polarization, indicative of the presence of depolarizing thermal material around the radio source), others because their host galaxies appeared to have peculiar morphologies in deep broad-band optical images, others because previous spectroscopic observations indicated that they had spatially extended emission lines, and still others were observed because of their special locations in the centers of rich "cooling flow" clusters. While the studies of these individual objects have advanced our understanding of these extended radio sources and the histories of their host galaxies, they do not tell us how general the phenomena observed in these objects are. Thus, we do not know (1) the frequency of occurrence of extended optical-line–emitting gas in powerful radio galaxies, (2) whether properties in the structure and environment of these galaxies correlate with the presence of such gas, (3) whether the gas we observe in

[1]Netherlands Foundation for Radio Astronomy.
[2]National Radio Astronomy Observatory. NRAO is operated by Associated Universities, Inc., under contract with the National Science Foundation.
[3]University of Maryland.
[4]Visiting Astronomer Kitt Peak National Observatory, operated by AURA, Inc., under contract to the NSF.
[5]University of California, Berkeley.
[6]Space Telescope Science Institute, Homewood Campus.
[7]Affiliated with the Astrophysics Division, Space Department of the European Space Agency. On leave from Leiden University.



© American Astronomical Society • Provided by the NASA Astrophysics Data System

1988ApJS...68..643B



emission lines is a source of fuel for the "central" engine and a direct or indirect determinant of the radio source ejection axis, (4) whether the distribution, ionization, and kinematics of the line-emitting gas are affected by the interaction of the radio source with the gas or whether they are determined only by the properties of the central engine, and (5) how important interactions between the radio source and cold gas are in determining the physical properties of the extended radio sources.

We initiated the research described in this paper in order to begin addressing these questions. We have obtained optical images through broad-band ($R$ or $V$) filters and through narrow-band filters, which isolate redshifted H$\alpha$ + [N II] or [O III], of 38 galaxies from a representative, radio-flux–limited ($S_{408\ \mathrm{MHz}} > 8.5$ Jy), optically unbiased, sample and of five specially selected, previously studied galaxies. In addition, we have also used NRAO's Very Large Array synthesis radio telescope to obtain $\sim 1''$–$4''$ resolution radio images of most of the sources in the sample.

In this paper we describe the details of the sample selection, the observations, and the data reduction. We present contour maps and detailed descriptions for each source of the broad-band optical, narrow-band optical, and radio images obtained. Subsequent papers will present additional quantities derived from these data and will present the statistical results of the survey and discuss their implications for (*a*) correlations between the luminosity and extent of the optical-line–emitting gas and the optical luminosity, morphology, and environment of the host galaxy, as well as the morphology and power of the associated radio source, (*b*) the importance of interactions between the extended line-emitting gas and the radio source, and (*c*) the origin and ionization of the line-emitting gas.

## II. SAMPLE SELECTION

The sources that we observed can be divided into two categories: (1) those which form a representative, optically unbiased, radio-flux-density–selected sample and (2) those which were observed specifically because we had prior knowledge that they were optically interesting. The statistical results from this work and the conclusions drawn from them will be based only on the observations of the galaxies from the "representative sample."

The representative sample is comprised of 38 galaxies, selected as follows. Twenty-two of the galaxies come from a complete sample of 34 radio galaxies which satisfy the following criteria:

1. Radio flux density $S_{408\ \mathrm{MHz}} > 11$ Jy (on the Baars *et al.* [1977] flux density scale).
2. Declination $-30° < \delta < +20°$.
3. Redshift $z < 0.6$.
4. Galactic latitude $|b| \geq 10°$.
5. Radio source extent $> 5''$.

To this list of 22 sources, we added 16 sources satisfying criteria (3) and (4), but with $S_{408\ \mathrm{MHz}} > 8.5$ Jy and not necessarily restricted to equatorial declinations. These sources were chosen without prior knowledge of their optical properties, with preference given to sources which fulfilled criterion (2), which could be imaged through already employed narrow-band filters, and which best filled the available hour angles. Note that the main criteria by which the sources were selected are their radio flux density at a relatively low radio frequency (408 MHz) and the requirement that the radio source size be greater than 5″ in total extent. These two criteria bias the sample toward steep-spectrum, extended radio sources.

We also observed five additional sources (B2 0149+358, 3C 171, 3C 285, 3C 305, 3C 321), which we term the "special sample." We observed these sources specifically because we had prior information that they were optically interesting. In Table 1, we list the sources in our final source list and distinguish those sources which are members of the representative sample.

## III. IDENTIFICATION OF SOURCES

All the radio sources in our final sample had previously been optically identified. However, we chose to redetermine the optical identifications for the sources in the representative sample using the core radio positions measured from our high-resolution radio maps, since previous identifications had typically been made from much lower resolution radio maps. Our sample is dominated by sources within $\sim 30°$ of the equator; previous interferometric maps of many of these sources were of low resolution in declination, since many of those maps were made with east-west arrays. We used a two-axis Mann measuring engine to place a right ascension and declination scale on the region of sky surrounding the galaxy on the Palomar Sky Survey prints by assigning positions from the SAO (Smithsonian Astrophysical Observatory 1966) and AGK3 (Dieckvoss 1975) catalogs to between 10 and 15 stars on the prints. The root mean square error on the accuracy of the position scale was typically between 0.″3 and 0.″6. Of the 38 sources in the final representative sample, only one source, 3C 89, was found to have been previously misidentified.

## IV. OPTICAL IMAGING

### *a*) *Observations and Data Reduction*

We used the prime focus (f/2.7) CCD system with a Texas Instrument chip (TI-2) on the National Optical Astronomical Observatory's (NOAO) Mayall 4 m telescope on Kitt Peak. We imaged each galaxy through a narrow-band filter centered on either H$\alpha$ $\lambda$6563 + [N II] $\lambda$6584 and $\lambda$6548, or [O III] $\lambda$5007, as emitted in the rest frame of the galaxy and through a broad-band (Mould $R$ or $V$) filter. To flux calibrate our observations, we imaged standard stars through both the narrow- and broad-band filters, when the conditions were photometric. The parameters of the observations are given in Table 2.

Typically, the narrow-band filters were 80 Å wide, corresponding to a velocity width at 6000 Å of 4000 km s$^{-1}$. In most cases, we centered the CCD frame on the radio galaxy. However, when the angular size of the radio source was greater than the field of view ($\sim 4' \times 4'$), we instead positioned the radio galaxy in the frame so that both the radio galaxy and, where present, one of the radio source hotspots (typically, the brighter one) were in our field of view. In a few

© American Astronomical Society • Provided by the NASA Astrophysics Data System

1988ApJS...68..643B

TABLE 1

SAMPLE MEMBERS

| Source | Redshift[a] | R.A.[b] | Decl.[b] | $E_{B-V}$[c] | Scale (kpc arcsec$^{-1}$) |
|---|---|---|---|---|---|
| 3C 29[d] | 0.0447 | $00^h55^m01^s.56$ | $-01°39'39''.9$ | 0.043 | 0.81 |
| 3C 33[d] | 0.0595 | 01 06 14.55 | +13 04 15.4 | 0.03 | 1.06 |
| 3C 40[d] | 0.0177 | 01 23 27.55 | −01 36 18.9[e] | 0.043 | 0.33 |
| B2 0149+358 | 0.0162 | 01 49 50.01 | +35 54 20.5[e] | 0.04 | 0.31 |
| 3C 63[d] | 0.175 | 02 18 21.94 | −02 10 32.5 | 0.0 | 2.68 |
| 3C 75N | 0.0241 | 02 55 02.99 | +05 49 37.0[e] | 0.09 | 0.45 |
| 3C 75S[d] | 0.0241 | 02 55 03.08 | +05 49 20.9[e] | 0.09 | 0.45 |
| 3C 78[d] | 0.0288 | 03 05 49.05 | +03 55 13.1[e] | 0.09 | 0.54 |
| 3C 88[d] | 0.0302 | 03 25 18.20 | +02 23 20.0 | 0.09 | 0.56 |
| 3C 89[d] | 0.1386 | 03 31 43.01 | −01 20 55.9 | 0.06 | 2.22 |
| PKS 0349−278[d] | 0.066 | 03 49 31.77 | −27 53 31.3 | ... | 1.16 |
| 3C 98[d] | 0.0306 | 03 56 10.17 | +10 17 32.5 | 0.15 | 0.57 |
| 3C 105[d] | 0.0886 | 04 04 38.99 | +03 34 27.5 | 0.15 | 1.52 |
| 3C 109[d] | 0.3056 | 04 10 54.86 | +11 04 40.9 | 0.21 | 4.02 |
| PKS 0634−206[d] | 0.056 | 06 34 23.27 | −20 32 18.5 | 0.50 | 1.00 |
| 3C 171 | 0.2384 | 06 51 10.92 | +54 12 48.1[e] | 0.09 | 3.38 |
| PKS 0745−191[d] | 0.1028 | 07 45 18.45 | −19 10 11.6[f] | 0.3 | 1.73 |
| 3C 192[d] | 0.0598 | 08 02 32.31 | +24 18 54.9[e] | 0.03 | 1.06 |
| 3C 196.1[d] | 0.198 | 08 12 56.99 | −02 59 13.7[f] | 0.06 | 2.94 |
| 3C 218[d] | 0.055 | 09 15 41.20 | −11 53 04.9 | 0.03 | 0.98 |
| 3C 219[d] | 0.1744 | 09 17 50.68 | +45 51 43.8 | 0.0 | 2.67 |
| 3C 223[d] | 0.1368 | 09 36 50.86 | +36 07 35.5[f] | 0.0 | 2.20 |
| 3C 227[d] | 0.0861 | 09 45 06.54 | +07 39 17.4 | ... | 1.48 |
| 3C 264[d] | 0.0208 | 11 42 29.56 | +19 53 02.3 | 0.0 | 0.39 |
| 3C 272.1[d] | 0.0031 | 12 22 31.58 | +13 09 50.7 | 0.02 | 0.06 |
| 3C 274[d] | 0.0043 | 12 28 17.56 | +12 40 02.0 | 0.02 | 0.07 |
| 3C 275[d] | 0.480 | 12 39 44.91 | −04 29 53.9[f] | 0.007 | 5.28 |
| 3C 278[d] | 0.0145 | 12 51 58.56 | −12 17 51.9 | ... | 0.28 |
| 3C 285 | 0.0794 | 13 19 05.22 | +42 50 55.7[e] | 0.0 | 1.38 |
| PKS 1345+125[d] | 0.1218 | 13 45 06.17 | +12 32 20.3[e] | 0.0 | 1.99 |
| 3C 295[d] | 0.4614 | 14 09 33.38 | +52 26 13.6 | 0.0 | 5.16 |
| 3C 305 | 0.041 | 14 48 17.34 | +63 28 36.3[e] | 0.03 | 0.75 |
| 3C 313[d] | 0.461 | 15 08 33.04 | +08 02 58.5[f] | ... | 5.16 |
| 3C 317[d] | 0.035 | 15 14 17.00 | +07 12 16.7 | ... | 0.64 |
| 3C 321 | 0.096 | 15 29 33.49 | +24 14 26.0[f] | 0.03 | 1.63 |
| 3C 327[d] | 0.1039 | 15 59 55.65 | +02 06 12.8 | 0.075 | 1.74 |
| 3C 327.1[d] | 0.4628 | 16 02 13.02 | +01 25 58.2 | 0.075 | 5.17 |
| 3C 346[d] | 0.161 | 16 41 34.47 | +17 21 21.0 | 0.06 | 2.51 |
| 3C 353[d] | 0.0304 | 17 17 53.28 | −00 55 49.0 | 0.15 | 0.56 |
| 3C 390.3[d] | 0.0561 | 18 45 37.57 | +79 43 06.5[e] | 0.05 | 1.00 |
| 3C 403[d] | 0.059 | 19 49 44.54 | +02 22 37.6 | 0.30 | 1.05 |
| 3C 405[d] | 0.0565 | 19 57 44.36 | +40 35 46.6[f] | 0.36 | 1.01 |
| 3C 433[d] | 0.1016 | 21 21 30.53 | +24 15 33.0[e] | 0.03 | 1.71 |
| 3C 442[d] | 0.0263 | 22 12 20.40 | +13 35 31.1 | 0.06 | 0.49 |

[a] Redshift taken from either Burbidge and Crown 1979 or Spinrad *et al.* 1985, except for B2 0149+358 taken from Hu, Cowie, and Wang (1985).

[b] Right ascension and declination assigned to the host galaxy nucleus on the CCD images, in epoch 1950 coordinates. Unless otherwise noted, positions are the core radio positions from our highest resolution VLA radio maps. Typically, these positions should be good to $\pm 0''.2$ in R. A. and decl.

[c] Galactic reddening, determined from the maps of Burstein and Heiles 1982. When no H I data was available we assume $E_{B-V} = 0.0$. For PKS 0745−191, the $E_{B-V}$ value was taken from Fabian *et al.* 1985.

[d] Member of the representative sample.

[e] The position of the galaxy nucleus was assigned the radio source position as given in the following references: for 3C 40, O'Dea and Owen 1985; for B0149+358, McCarthy *et al.* 1988; for 3C 75, Owen *et al.* 1985; for 3C 78 Unger, Booler, and Pedlar 1984; for 3C 171, Heckman, van Breugel, and Miley 1984; for 3C 192 and 3C 285, Spinrad *et al.* 1985; for PKS 1345+125, Gilmore and Shaw 1986; for 3C 305, Heckman *et al.* 1982; for 3C 390.3, Harris 1972; for 3C 433, van Breugel *et al.* 1983.

[f] The position of the optical nucleus (taken in this context to mean the location of peak galaxy surface brightness on the broad-band image) was assigned by determining the position of stars on the CCD image using a Mann measuring engine and the prints of the sky survey. These positions should be good to $\pm 0''.65$ (see text for details).



© American Astronomical Society • Provided by the NASA Astrophysics Data System

1988ApJS...68..643B



TABLE 2

LOG OF OPTICAL OBSERVATIONS

| Source (1) | Telescope[a] (2) | Date of Observation (3) | Narrow-Band Central λ[b] (Å) (4) | Narrow-Band Δλ[c] (Å) (5) | Narrow-Band Integration Time[d] (5) (6) | Broad-Band Filter[e] (7) | Broad-Band Integration Time[f] (5) (8) | FWHM of PSF[g] (9) |
|---|---|---|---|---|---|---|---|---|
| 3C 29[h] | KPNO 4 m | 1985 Dec 18 | 6871 | 78 | 1200 | R | 300 | 1".4 |
| 3C 33[h] | KPNO 4 m | 1985 Dec 16 | 6961 | 79 | 1200 | R | 300 | 1.5 |
| 3C 40[h] | KPNO 4 m | 1985 Dec 17 | 6693 | 76 | 1200 | V | 600 | 2.0 |
| NGC 708 | KPNO 4 m | 1985 Dec 17 | 6693 | 76 | 1200 | R | 300 | 1.4 |
| 3C 63[h] | KPNO 4 m | 1985 Dec 17 | 7730 | 85 | 1200 | R | 300 | 2.1 |
| 3C 75[h] | KPNO 4 m | 1985 Dec 18 | 6737 | 76 | 1200 | R | 900 | 1.7 |
| 3C 78[h] | KPNO 4 m | 1985 Dec 17 | 6781 | 78 | 1200 | V | 900 | 2.3 |
| 3C 88[h] | KPNO 4 m | 1985 Dec 16 | 6781 | 78 | 1200 | V | 1200 | 1.7 |
| 3C 89[h] | KPNO 4 m | 1985 Dec 17 | 7482 | 84 | 1200 | R | 360 | 1.5 |
| PKS 0349−278[h] | Lick 3 m | ... | ... | ... | ... | V | ... | 2.4 |
| 3C 98[h] | KPNO 4 m | 1985 Dec 17 | 6781 | 78 | 1200 | R | 270 | 1.6 |
| 3C 105[h] | KPNO 4 m | 1985 Dec 15 | 7146 | 80 | 1200 | V | 300 | 2.8 |
| 3C 109[h] | KPNO 2.1 m | 1985 Dec 16 | 6562 | 82 | 1800 | V | 1200 | 1.8 |
| PKS 0634−206[h] | KPNO 4 m | 1985 Dec 16 | 6961 | 79 | 1200 | V | 1200 | 3.2 |
| 3C 171 | KPNO 4 m | 1986 Apr 14 | 6187 | 71 | 600 | R | 300 | 1.5 |
| PKS 0745−191[h] | KPNO 2.1 m | 1986 Nov 27 | 7240 | 82 | 1800 | R | 300 | 1.7 |
| 3C 192[h] | KPNO 4 m | 1986 Apr 14 | 6961 | 79 | 1200 | R | 300 | 1.4 |
| 3C 196.1[h] | KPNO 4 m | 1985 Dec 17 | 7883 | 86 | 1200 | V | 1200 | 1.6 |
| 3C 218[h] | KPNO 4 m | 1986 Apr 15 | 6916 | 78 | 1200 | V | 360 | 1.4 |
| 3C 219[h] | KPNO 4 m | 1985 Dec 17 | 7730 | 85 | 1200 | V | 1200 | 1.5 |
| 3C 223[h] | KPNO 4 m | 1985 Dec 18 | 7482 | 84 | 1200 | V | 1200 | 1.5 |
| 3C 227[h] | KPNO 4 m | 1985 Dec 16 | 7146 | 78 | 1200 | R | 300 | 2.4 |
| 3C 264[h] | KPNO 4 m | 1985 Dec 16 | 6693 | 76 | 1200 | V | 1200 | 2.4 |
| 3C 272.1[h] | KPNO 4 m | 1986 Apr 12 | 6606 | 75 | 1200 | R | 120 | 1.8 |
| 3C 274[h] | KPNO 4 m | 1985 Dec 16 | 6606 | 75 | 1200 | R | 70 | 3.2 |
| 3C 275[h] | KPNO 4 m | 1986 Apr 13 | 7433 | 84 | 1200 | R | 300 | 2.3 |
| 3C 278[h] | KPNO 4 m | 1986 Apr 14 | 6693 | 76 | 1200 | R | 300 | 1.5 |
| 3C 285 | KPNO 4 m | 1986 Apr 14 | 7099 | 80 | 1200 | R | 450 | 1.2 |
| PKS 1345+125[h] | KPNO 4 m | 1985 Dec 17 | 7384 | 84 | 1200 | R | 300 | 1.5 |
| 3C 295[h] | KPNO 4 m | 1986 Apr 14 | 7336 | 82 | 1200 | R | 300 | 1.3 |
| 3C 305 | KPNO 4 m | 1986 Apr 13 | 6826 | 78 | 900 | R | 600 | 1.8 |
| 3C 313[h] | KPNO 4 m | 1986 Apr 14 | 7336 | 82 | 1200 | R | 450 | 1.6 |
| 3C 317[h] | KPNO 4 m | 1986 Apr 12 | 6826 | 78 | 1200 | R | 360 | 2.0 |
| 3C 321 | KPNO 4 m | 1986 Apr 12 | 7193 | 80 | 1200 | R | 300 | 1.4 |
| 3C 327[h] | KPNO 4 m | 1986 Apr 13 | 7240 | 82 | 1200 | R | 300 | 1.6 |
| 3C 327.1[h] | KPNO 4 m | 1986 Apr 13 | 7336 | 82 | 1200 | R | 300 | 1.7 |
| 3C 346[h] | KPNO 4 m | 1986 Apr 13 | 7630 | 85 | 1200 | R | 600 | 2.0 |
| 3C 353[h] | KPNO 4 m | 1986 Apr 15 | 6781 | 78 | 1200 | V | 300 | 1.3 |
| 3C 390.3[h] | KPNO 4 m | 1986 Apr 15 | 5277 | 47 | 600 | V | 300 | 1.5 |
| 3C 403[h] | KPNO 4 m | 1986 Apr 12 | 6961 | 79 | 1800 | R | 360 | 1.7 |
| 3C 405[h] | KPNO 4 m | 1986 Apr 12 | 5277 | 47 | 600 | V | 300 | 1.4 |
| 3C 433[h] | KPNO 2.1 m | 1986 Nov 27 | 7240 | 82 | 1800 | R | 1800 | 1.7 |
| 3C 442[h] | KPNO 4 m | 1985 Dec 18 | 6737 | 76 | 1200 | R | 300 | 1.3 |

[a] Telescope where data was taken.
[b] Nominal central wavelength of the narrow-band filter. Actual central wavelength of narrow-band observations taken with the KPNO 4 m telescope is the nominal central wavelength minus 15 Å. See text for details.
[c] Nominal full width at half-power of narrow band filter response.
[d] Total integration time of narrow-band observation.
[e] Filter used for broad-band observation, either Mould R or Mould V filters.
[f] Total integration time of broad-band observation.
[g] Full width at half-maximum of the point spread function in the final images. See text for details.
[h] Member of the representative sample.

cases, the proximity of a very bright star also required moving the galaxy from the center of the frame.

In columns (6) and (8) of Table 2, we give the *total* integration times for the narrow- and broad-band filters. Typically, for each galaxy, we obtained two or three narrow-band exposures and 10–20 broad-band exposures, maintaining the galaxy counts within the regime where the CCD response is linear. The number of photons collected in the nonsource regions of the chip (i.e., from the sky) was sufffi-cient to allow for efficient charge transfer. We subsequently averaged the individual integrations to produce the final image frames.

For each frame, the average DC electrical offset of the chip was removed using the average value from a 32 column

© American Astronomical Society • Provided by the NASA Astrophysics Data System

1988ApJS...68..643B



overscan region of the chip. The low spatial frequency variations in the zero-point level across the chip were then removed by subtraction of a bias frame. Finally, pixel-to-pixel variations in sensitivity were removed by dividing each frame by a normalized dome flat-field frame. To reduce the effects of readout noise, we added together adjacent columns and rows of the CCD during the readout of the chip. The resultant "big" pixels were measured to be $0''.595 \pm 0''.01$ on a side. For the images taken on the 4 m telescope at KPNO, the images are 396 pixels on a side, so the final field of view of each image is $\sim 4'$ by $4'$.

A few sources were imaged with the 2.1 m telescope on Kitt Peak or the 3 m Shane Telescope of the University of California's Lick Observatory. The data reduction performed on these images is equivalent to that described in detail for the images taken on the KPNO 4 m telescope.

### *b) Image Processing*

Our goal was to obtain an image of each galaxy in emission lines only. We used the AIPS (Astronomical Image Processing System) data reduction package for this purpose and employed the following reduction routine. The level of sky emission was determined for each frame by taking the average value in a region of the image that was devoid of stars or galaxies. This value was then subtracted from each pixel in the frame. We then removed the continuum light from each narrow-band image by subtracting a flux-scaled version of the broad-band image, thereby producing an image of each galaxy in emission lines alone.

The use of a broad-band image for the continuum subtraction, though economical in observing time, did pose several problems. The first of these was that the plate scale in the broad-band and the narrow-band images were often discrepant (at a level of $\lesssim 0.3\%$). To compensate for this we determined the relative plate scale and the offset of the two images for each galaxy by determining the positions (to $\lesssim 0.1$ pixel) of two, spatially well-separated stars in each frame by fitting two-dimensional Gaussians to the stellar isophotes. The broad-band image of each galaxy was then geometrically scaled to the plate scale of the corresponding narrow-band image and was shifted to align with that image, using bicubic Everett interpolation to determine the values at the shifted pixel locations.

The second problem was that the point spread functions (PSFs) of the broad-band and narrow-band images were often different.

The reason for the discrepancy between the plate scales and the point spread functions in the broad-band and narrow-band images is unclear. Possibilities include the difference in the pedestal focus of the CCD (i.e., the distance between the detector and the filter) for the broad- and narrow-band observations and chromatic aberration in the fast optics of the 4 m prime focus.

To compensate for this, we convolved each image with a Gaussian whose width was chosen so as to equalize the Gaussian FWHM of the PSFs of the broad-band and narrow-band images. This also increased the signal-to-noise ratio in the images, although of course the resolutions of the final images were degraded slightly. The resulting Gaussian FWHM of the PSFs for the observations of each galaxy is given in column (9) of Table 2.

Finally, a flux-scaled version of the broad-band image was subtracted from each narrow-band image. The flux scale factor was determined empirically in each case. We produced a series of subtracted images using different broad-band scaling factors until we obtained an image in which the emission from the other (presumably inactive) galaxies in the field of view was negligible and/or the symmetric emission from the galaxy under study had been removed.

The success with which we could effectively remove the continuum light from the narrow-band images in this way varied. Undersampling of the PSF (i.e., seeing better than or equal to $1''.2$), occasionally made it difficult for the interpolation program used to "match" the broad-band and narrow-band images adequately. Any slight misalignment of the broad- and narrow-band images results in asymmetric, negative and positive emission on either side of a point source in the subtracted image, whereas differences in the point spread function between the two images result in annuli of positive or negative emission around a point source. Thus, spurious features in the subtracted image can arise in regions of the image where there is a steep gradient in the continuum light (e.g., near the galaxy nucleus). The line-only images of some sources showed subtraction problems near the nuclei of the radio sources. Extended emission lines detected close to such nuclei require spectroscopic confirmation. Where the detection is tentative, we have so noted in the individual source descriptions.

### *c) Absolute Flux Calibration*

The observations of standard stars through the narrow- and broad-band filters were used to calibrate the response of the CCD-filter-telescope system. The filter transmission was assumed to be a rectangular function in each case. The broad-band $R$ and $V$ filters were assumed to have widths of 1283 Å and 871 Å and central wavelengths of 6500 Å and 5400 Å, respectively. The narrow-band filter widths assumed are given in column (5) of Table 2. The nominal central wavelength of each interference filter used is given in column (4) of Table 2. However, at the 4 m f/2.7 prime focus, the rays of light from a point source converge, so that the light rays pass through the filter at angles ranging from 0°–10°.5 (NOAO Newsletter, 1987 March). The net effect is that the central wavelength of the interference filter response shifts $\sim 15$ Å to the blue (Eather and Reasoner 1969). In addition, the peak transmission drops and the bandpass widens slightly. The latter two effects appear to be relatively less important and were not taken into account. Thus, to summarize, for the narrow-band observations taken with the KPNO 4 m telescope, the actual central wavelengths observed are the nominal central wavelength, given in column (5) of Table 2, minus 15 Å.

The calibrations obtained from the standard star observations were applied to the emission-line and broad-band images, respectively, thereby placing the images on an absolute flux scale. For some sources, the observations were taken during nonphotometric conditions. For some of these sources, as noted in the individual figure captions, we used published spectrophotometry to calibrate the emission-line images.

© American Astronomical Society • Provided by the NASA Astrophysics Data System

1988ApJS...68..643B



The use of broad-band ($R$ or $V$) images to subtract the continuum light from the narrow-band galaxy images introduced an additional uncertainty into the final flux calibration, since these filters sometimes allowed the light of emission lines from the galaxy under study to pass into the broad-band images. The counts in the "subtracted" (i.e., the emission-line only) image are therefore reduced by the factor

$$f = 1 - \frac{\Delta_{nb} S_{nb}}{\Delta_{bb} S_{bb}},$$

where $\Delta_{nb}$ and $\Delta_{bb}$ are the filter widths of the narrow- and broad-band filters, respectively, and $S_{nb}$ and $S_{bb}$ are the surface brightnesses in emission lines in the narrow- and broad-band images, respectively. We calculated the correction factor for each galaxy, assuming an *average* nuclear narrow–emission-line radio galaxy spectrum for the gas (Koski 1978; Cohen and Osterbrock 1981). The correction factors range from 1.002 to 1.36, with a median value of 1.09. Since we do not know the actual line ratios, these correction factors were not applied to the data, but serve instead as an indication of the uncertainty introduced into the calibration.

Despite this added uncertainty, our absolute fluxes agree well with those in the literature. We have compared our emission line fluxes with spectrophotometric fluxes from the literature for 12 sources in our sample. We find an average absolute level of disagreement of 20%. For three sources, 3C 390.3, 3C 171, and 3C 405, the redshifted [O III] line fell on the blue edge of the transmission response curve of the narrow-band filter. For these sources, we used published spectrophotometry to calibrate the narrow-band images, but we caution that [O III] emission from blueshifted gas from the galaxy may be underrepresented in our emission-line images of these galaxies.

### *d*) *Calibration of the Optical Positions*

A right ascension and declination grid was assigned to each image in the following way. The location of the nucleus of the galaxy in each image was determined by fitting a two-dimensional Gaussian to the inner region of the galaxy image, within the region where the surface brightness is greater than 0.5 times the peak. Typically, the position of the galaxy nucleus was determined with an error of $\lesssim 0.1$ pixels, or $\lesssim 0''.06$. The nucleus was then assigned the epoch 1950.0 right ascension and declination coordinates of the radio core of the galaxy as determined from our VLA maps or from published radio positions, as given in Table 1. Then, using the derived plate scale of $0''.595$ per pixel, and employing a tangent-arc geometry, a right ascension and declination gird was assigned to the images. In general, since the plate scale is known to $\pm 0''.01$, under the assumption that the maximum brightness on the broad-band image corresponds to the radio core, the right ascension and declination scale so affixed should be good to better than $1''$ within $1'$ from the galaxy nucleus.

For seven sources in which the radio or optical position of the galaxy nucleus was ambiguous (3C 196.1, PKS 0745−191, 3C 223, 3C 275, 3C 313, 3C 321, and 3C 405), we chose to determine the right ascension and declination for the optical image in an alternate way. We used the NRAO Mann measuring engine, in conjunction with prints of the Palomar or Southern Sky Survey, to determine the right ascension and declination of between 4 and 10 stars on the broad-band image. We then used the known plate scale, in conjunction with the pixel locations of these stars on the broad-band image, to determine the position of the nucleus of the radio galaxy on the broad-band image to an accuracy of $\sim 0''.6$.

## V. RADIO OBSERVATIONS

The National Radio Astronomy Observatory's Very Large Array (Thompson *et al.* 1980) was used to obtain high-resolution radio snapshot images of many of the sources in the sample during the period 1982–1986. Typically, a source was observed at 6 cm in the B array with $\sim 1''.2$ resolution. For the larger sources, we also obtained lower resolution images at $\sim 3''$ or $10''$ resolution, using the VLA in its more compact configurations. The "snapshot" observations were typically 12 minutes in length, with the observing time separated into two 6 minute observations taken roughly 1 hr before and 1 hr after the source's zenith crossing. For the most extended sources, three separate observations were obtained at intervals of 1 hr. For a few of the more interesting sources we subsequently obtained more extensive, multihour VLA observations. A log of the VLA observations is given in Table 3.

We used 3C 48 and 3C 286 as primary flux density calibrators and adopted the flux density scale of Baars *et al.* (1977). We observed antenna complex gain calibrators at roughly 30 minute intervals. We separated the antenna instrumental polarizations from the source polarization and removed them from the cross-hand data through observations of an unresolved polarization calibrator through a large range of parallactic angle (Bignell and Perley 1985). The absolute polarization position angle was determined by observing a source (e.g., 3C 286, or 3C 138) whose position angle is assumed known.

The "calibrated" data were passed through several iterations of self-calibration (Schwab 1980) to remove any residual antenna-based phase and amplitude errors. We added a zero-spacing flux density (i.e., the total flux density in the source, taken in most cases from single-dish measurements in the literature) to the data prior to mapping. We used a weight for the zero-spacing flux density which was empirically chosen so that the mean value of the nonsource regions of the image would be close to zero in the final image. We employed the Hogbom (1974) clean algorithm (as implemented in the Cotton-Schwab "MX" algorithm [Schwab 1984]) to interpolate the missing spacings in the $(u, v)$-plane (i.e., the Fourier transform of the sky brightness plane). We produced clean images in the Stokes parameters $I$, $Q$, and $U$ from which we produced polarized intensity, fractional polarization, and polarization position angle images. The total intensity images were corrected for the primary beam pattern of the VLA antennas.

We corrected the polarized intensity maps for the Ricean bias (Vinokur 1965; Wardle and Kronberg 1974; Simmons and Stewart 1985; Killeen, Bicknell, and Ekers 1986).[8]

[8]The bias in the measurement of polarized intensity arises because the polarized intensity ($P$) is determined from measurements of the Stokes

© American Astronomical Society • Provided by the NASA Astrophysics Data System

1988ApJS...68..643B



TABLE 3

LOG OF RADIO OBSERVATIONS

| Source | Wavelength[a] (cm) | Bandwidth (MHz) | Array[b] | Flux on Shortest Spacing[c] (Jy) |
|---|---|---|---|---|
| 3C 29 | 6 | 2×50 | C | 1.2 (60%) |
| | 20 | 50 | A | 1.4 (25%) |
| 3C 33 | 6 | 12.5 | B | 2.5 (45%) |
| | 6 | 2×50 | C | 3.7 (70%) |
| 3C 63 | 6 | 12.5 | B | 0.85 (65%) |
| 3C 78 | 6 | 12.5 | B | 1.25 (30%) |
| | 6 | 2×50 | C | 2.9 (75%) |
| | 20 | 2×50 | C | 7.0 (90%) |
| 3C 88 | 6 | 2×50 | C | 0.6 (30%) |
| | 20 | 2×50 | C | 4.4 (85%) |
| 3C 89 | 6 | 12.5 | B | 0.34 (30%) |
| | 20 | 2×50 | C | 2.65 (100%) |
| PKS 0349−278 | 6 | 12.5 | B | 0.4 (20%) |
| | 20 | 12.5 | B/C* | 5.3 (95%) |
| 3C 98 | 6 | 12.5 | B | 0.94 (25%) |
| | 6 | 2×50 | C* | 2.5 (70%) |
| 3C 105 | 6 | 12.5 | B | 1.2 (45%) |
| | 6 | 2×50 | C | 1.6 (60%) |
| | 6 | 2×50 | D | 1.8 (70%) |
| 3C 109 | 6 | 12.5 | B | 0.60 (30%) |
| | 6 | 2×50 | C | 1.47 (75%) |
| PKS 0634−206 | 6 | 12.5 | A/B/C/D* | ... |
| PKS 0745−191 | 6 | 2×50 | B | 0.45 (95%) |
| | 20 | 2×25 | A | 2.2 (95%) |
| 3C 196.1 | 6 | 2×50 | B | 0.430 (95%) |
| 3C 218 | 2 | 2×50 | C | 3.6 (60%) |
| | 6 | 12.5 | B | 9.2 (65%) |
| | 6 | 2×50 | C | 13.2 (90%) |
| | 20 | 50 | A | 32.0 (70%) |
| | 20 | 2.×25 | B | 38.0 (85%) |
| | 20 | 2×25 | C | 40.0 (90%) |
| 3C 223 | 20 | 2×25 | B | 2.5 (70%) |
| 3C 227 | 6 | 12.5 | B | 0.78 (30%) |
| | 6 | 2×50 | C | 1.4 (50%) |
| | 6 | 2×50 | D | 2.6 (95%) |
| 3C 264 | 6 | 12.5 | B | 0.45 (20%) |
| | 6 | 2×50 | C | 0.95 (40%) |
| 3C 275 | 6 | 12.5 | B | 1.0 (90%) |
| 3C 278 | 6 | 2×50 | C | 0.9 (90%) |
| 3C 295 | 2 | 12.5? | A | 1.82 (>100%) |
| 3C 313 | 6 | 12.5 | B | 0.9 (75%) |
| 3C 317 | 6 | 12.5 | B | 0.73 (70%) |
| | 6 | 2×50 | C | 0.90 (90%) |
| | 6 | 2×50 | D | 0.91 (90%) |
| 3C 327 | 6 | 12.5 | B | 0.84 (30%) |
| | 6 | 2×50 | C | 1.7 (50%) |
| | 6 | 2×50 | D | 2.51 (80%) |
| 3C 327.1 | 6 | 12.5 | B | 1.4 (>100%) |
| 3C 346 | 6 | 12.5 | B | 1.44 (100%) |
| 3C 353 | 6 | 12.5 | B | 1.22 (5%) |
| | 6 | 2×50 | C | 6.5 (30%) |
| | 6 | 2×50 | D | 19.0 (90%) |
| 3C 403 | 6 | 12.5 | B | 0.5 (20%) |
| | 6 | 2×50 | C | 1.3 (50%) |
| 3C 442 | 6 | 12.5 | B | 0.04 (5%) |

[a]Approximate observing wavelength in cm.

[b]Array observed in. Unless otherwise noted, observations were ~12 minutes in total extent. An asterisk indicates that the source was observed for a duration of ~4 hr or more.

[c]Approximate source flux density seen at the shortest baseline, in janskys. In parentheses is given the corresponding fraction of the total source flux density, as given by single-dish measurements from the literature.

The fractional polarization data were discarded (i.e., the images blanked) whenever the polarized intensity was less than 4 times the noise in the $Q$ and $U$ maps and whenever the absolute error in the fractional polarization was greater than 15%.

Residual errors in the calibration of the antenna polarizations should result in errors in fractional polarization of only several tenths of a percent. In our radio snapshot images, therefore, errors in fractional polarization should be dominated by the signal-to-noise ratio in the $I$, $Q$, and $U$ images. Errors in the absolute calibration of the polarization position angle are $\sim \pm 1°$ at 6 cm, and may be as high as $\pm 5°$ at 20 cm (due mainly to increased Faraday rotation in the ionosphere at 20 cm). At 6 cm, errors in $\chi$ will be dominated by the noise in the $Q$ and $U$ images for regions of the image where the signal-to-noise ratio in the polarized intensity is less than ~30.

## VI. INDIVIDUAL SOURCE DESCRIPTIONS

We describe the radio, broad-band optical, and optical emission-line morphologies of each source in our sample. We use a Hubble constant $H_0 = 75$ km s$^{-1}$ Mpc$^{-1}$ and a deceleration parameter $q_0 = 0.0$ when converting from angular to linear size scales. We refer to the radio luminosities of the individual sources as either low, $L_{\rm radio} < 5\times10^{41}$ ergs s$^{-1}$, intermediate, $5\times10^{41}$ ergs s$^{-1} < L_{\rm radio} < 5\times10^{43}$ ergs s$^{-1}$, or high, $L_{\rm radio} > 5\times10^{43}$ ergs s$^{-1}$. A detailed parameterization of the radio and optical properties of the individual sources can be found in Baum and Heckman (1987).

Contours of the optical broad-band, emission-line, and radio images are shown in Figures 1–55 (at the end of this paper), and should be referred to along with the text. The optical images whose surface brightness contours we show have not been corrected for Galactic extinction; thus these contours represent the actual surface brightness observed. Superposed on the contours of the radio emission we often show emissivity-weighted, vector-averaged, electric field vectors, whose lengths indicate the fractional polarization and whose orientations indicate the position angle of the projected electric field vector. Negative contour levels are drawn as light lines. The linear scale in kpc arcsec$^{-1}$ is given in Table 1 for each source.

*3C 29 (0055+39).*—The host galaxy of 3C 29 is an apparently normal elliptical galaxy with no significant companions within 100 kpc. Sandage (1972, hereafter S72) suggested that it may be an outlying member of the cluster Abell 119. We detect nuclear H$\alpha$+[N II] emission and a possible trail of faint line-emitting gas extending 9″ (7 kpc) to the north. Our 6 cm, 6″ and 20 cm, 1.″5 resolution VLA radio snapshot images of 3C 29 show a possible jet to the south, ending in a feature that may be a dim southern hotspot. A possible counterjet knot is visible to the north and only diffuse emission is seen in the northern lobe.

*3C 33 (0106+13).*—The host galaxy of 3C 33 appears to be isolated (e.g., S72). As is readily apparent on our broad-

parameters $Q$ and $U$ as $P = (Q^2 + U^2)^{1/2}$. Even if the noise on the $Q$ and $U$ images is Gaussian with a mean of zero, the noise on the resulting $P$ image will no longer be Gaussian, but instead will be skewed toward positive values.

© American Astronomical Society • Provided by the NASA Astrophysics Data System

1988ApJS...68..643B



band ($R$) image and as discussed by Heckman *et al.* (1986; hereafter H86) and Simkin and Michel (1986), the host galaxy of 3C 33 has several morphological peculiarities. We note the curved, broad fan of emission to the southeast of the nucleus and a faint extension of diffuse emission to the north. The change in ellipticity and major axis position angle between 3″ and 14″ from the nucleus seen in our $R$-band image is partly due to contamination of the $R$-band image by emission lines from the oval region of emission lines present in the center of this galaxy. However, if we assume that the line emission has a spectrum characteristic of a Seyfert 2 or narrow-line radio galaxy (Koski 1978; Cohen and Osterbrock 1981), and use the emission-line–only image to subtract the contribution from line emission out of the $R$-band image, we still do not eliminate the twisting of isophotes. Thus, there appears to be a real change in the continuum light distribution in going from the inner to the outer part of the galaxy.

Our emission-line image of 3C 33 shows a flattened region of emission-line gas with a total extent of ~12″ (13 kpc), centered on the galaxy nucleus (and see also Hansen, Norgaard-Nielsen, and Jorgensen 1987). The minor axis of the emission-line ellipse is oriented at a position angle of 155°, virtually perpendicular to the short axis of the distribution of stellar light and askew by 44° to the axis of the large-scale radio source. Simkin (1979) and Heckman, Carty, and Bothun (1985) obtained long-slit spectroscopy of the extended line emission at many position angles and concluded that the line-emitting gas is rotating, with a rotation axis in a position angle of ~19°, along the radio source ejection axis, but askew to the minor axis of the gas distribution.

Our 3.″8 resolution, 6 cm VLA snapshot radio image of 3C 33 contains only roughly 70% of the total source flux density (as given by single-dish measurements), and thus only the bright, fine-scale, structure is well represented in the image. 3C 33 shows bright hotspots in both the northern and southern lobes, surrounded by filamentary emission. The southern radio lobe and hotspot is coincident with an extended region of optical emission (Simkin 1986 and references therein). Radio maps with better sensitivity which adequately represent the large-scale source structure are needed to determine whether there is radio source structure directly along the minor or rotation axes of the line-emitting gas.

*3C 40 (0123 − 01).*—3C 40 is associated with NGC 545 at the center of the richness class 0 cluster, Abell 194 (S72). A second galaxy of comparable size is projected on the envelope of NGC 545. The nuclei of the two galaxies are separated by ~30″ (9.6 kpc). Lauer (1987) finds no evidence for tidal distortion in the stellar isophotes of NGC 545, suggesting that the two are not interacting, though the radial velocities of the two galaxies differ by only 136 km s$^{-1}$ (Chincarini and Rood 1977). The minor axes of the two galaxies are oriented roughly 90° to one another, and the southern galaxy is identified with the radio source. O'Dea and Owen (1985) presented a high-resolution VLA radio map of 3C 40, showing that two oppositely directed jets emanate from the nucleus and display a wandering, helical morphology as they fade out of view. Schilizzi, Lockhart, and Wall (1972) have mapped the large-scale radio structure of 3C 40. Our emission-line image of this galaxy shows the presence of very diffuse gas with a diameter of ~10.″5 (3.5 kpc) associated with the radio galaxy. However, this result needs to be confirmed spectroscopically.

*B2 0149 + 358.*—B2 0149+358, the radio source associated with NGC 708, the elliptical galaxy at the center of the "cooling flow" cluster Abell 262, is a low-luminosity, Z-shaped radio source that is embedded within its parent galaxy (Parma *et al.* 1986). A detailed description of the optical and radio morphologies of NGC 708 can be found in McCarthy *et al.* (1988, in preparation). To summarize, NGC 708 has a dust lane at right angles to the radio source axis and possesses two distinct optical emission-line filaments, neither of which shows an obvious morphological connection to the radio source. One of these emission-line filaments extends along the dust lane and appears to be in rotation about the galaxy nucleus, although the line-emitting gas is asymmetrically distributed about the nucleus. The second filament is extended roughly perpendicular to the dust lane and exhibits a large velocity gradient. This filament extends over ~17″ (5 kpc) and shows kinematic evidence for both an interaction with the radio jet close to the galaxy nucleus and a tidal interaction with a nearby (in projection) SO galaxy (NGC 705).

*3C 63 (0218 − 02).*—Our H$\alpha$+[N II] image of the host galaxy of 3C 63 shows an S-shaped filament extending through the galaxy nucleus. The easternmost end of this filament appears to emanate from a continuum feature, perhaps a small companion galaxy. Our broad-band image shows four somewhat smaller galaxies within 125 projected kpc of the host galaxy of 3C 63. The radio source shows two bright hotspots separated by ~ 604 kpc, which are roughly collinear with the nucleus, and a wide bridge of lower surface brightness emission extending from the hotspots toward the galaxy nucleus. At the lowest levels, the bridge extends away from the galaxy toward the southwest, perpendicular to the radio source axis. The average level of fractional polarization at 6 cm in the radio source is high (~18%), though there appears to be a region of low fractional polarization just northwest of the southern hotspot, coincident with the location of the line-emitting gas.

*3C 75 (0255 + 05).*—3C 75 is associated with the central dumbell galaxy in Abell 400 (Mathews, Morgan, and Schmidt 1964, hereafter MMS). The two nuclei are separated by ~16.″5 (7.5 kpc). Owen *et al.* (1985) present VLA observations of 3C 75, which show it to be a pair of wide-angle-tail radio sources, with one jet system emerging from each of the two nuclei of the host galaxy. Our H$\alpha$+[N II] image shows only weak nuclear emission from each of the nuclei. Spectroscopic observations by O'Dea, Owen, and Keel (1986) confirm this result.

*3C 78 (0305 + 03).*—The radio source 3C 78 is identified with NGC 1218, which has been classified as an SOa galaxy (Schmidt 1965; Maltby, Mathews, and Moffet 1963). S72 describes the galaxy environment as isolated. There are two other galaxies visible on our broad-band image of 3C 78. One of the galaxies is a small elliptical, the other is an edge-on spiral galaxy, situated roughly 60 projected kpc from the nucleus of 3C 78. The spiral galaxy shows H$\alpha$+[N II] emission from the length of its disk in our emission-line images. NGC 1218, itself, contains a small region of line-emitting gas ~ 9″ (5 kpc) in extent, centered on its nucleus. The innermost

© American Astronomical Society • Provided by the NASA Astrophysics Data System

1988ApJS...68..643B



line-emitting gas is elongated roughly along the direction of the radio jet, but the gas also shows a broad, curved tail extending to the southeast, roughly perpendicular to the radio source axis.

The radio source 3C 78 has a very unusual morphology which has been described in detail by Unger, Booler, and Pedlar (1984) and Saikia *et al.* (1986). High-resolution images show a jet to the northeast and evidence of a weak counterjet to the southwest. At lower resolution the source can be seen to contain two broad jets which curve into an S shape before blending into an extended radio halo.

*3C 88 (0325 + 02).*—Our *V*-band image of the host galaxy of 3C 88 shows it to be a flattened elliptical with only two much smaller "nearby" galaxies within a projected distance of 65 kpc. MMS suggest that 3C 88 is a member of a poor cluster, though S72 describes its environment as isolated. Our emission-line image shows H$\alpha$ + [N II] emission from a elliptical region roughly centered on the galaxy nucleus, with an extent of 5″ (3 kpc) and with its minor axis askew by 49° from the major axis of the stellar isophotes and by 44° from the radio source ejection axis. We do not detect either of the two nearby (in projection) galaxies in H$\alpha$ + [N II]. The radio source 3C 88 has two roughly collinear hotspots, symmetrically located on either side of the core, extending along the minor axis of the galaxy's stellar isophotes. The lobes of 3C 88 are very broad and reach all the way back to the galaxy nucleus, giving the source a rectangular appearance. Our radio snapshot images show only core emission in the region of the source which overlaps the line emission. The large-scale radio structure of 3C 88 shows high levels of fractional polarization: greater than 10% over most of the source, even at 20 cm and 18″ resolution.

*3C 89 (0331 − 01).*—3C 89 is a wide-angle-tail radio galaxy.[9] It is associated with the northern galaxy in a pair of dominant galaxies (projected separation ~ 75 kpc) in what MMS described as a poor cluster. The radio source had been previously misidentified with the southern of the two galaxies (Wyndham 1966). The parent galaxy of 3C 89 appears highly flattened. The radio source extends roughly along the minor axis of the galaxy before bending back. The two bent jets show an oscillating shape superposed on their overall *V* morphology. Our emission-line observations of this galaxy are inconclusive; there does not appear to be any resolved emission associated with either the host galaxy of 3C 89 or the "nearby" galaxy, though both show signs of nuclear line emission, a result which needs to be confirmed spectroscopically.

*PKS 0349 − 278.*—Our *V*-band image of PKS 0349 − 278 shows that this elliptical galaxy is the largest galaxy in a region of relatively high local galaxy density, there being four elliptical galaxies within a projected distance of 80 kpc present on the image. None of the other galaxies in the image was detected as an [O III] emitter. The unusual appearance of this galaxy as seen through a *V*-band filter is due largely to contamination of the broad-band image by emission lines from extended gas.

The line-emitting gas in PKS 0349 − 278 has been studied in detail by Danziger *et al.* (1984) using long-slit spectroscopy. Combining their results with the results of our own [O III] imaging (and see also Hansen, Norgaard-Nielsen, and Jorgensen 1987), we note the following:

1. The strongest [O III] emission comes from an emission-line knot northeast of the nucleus, along the position angle of the extended radio source. Danziger *et al.* (1984) reported that the gas in this knot has a higher state of ionization then does the nebula as a whole. We note that the [O III] emission is brightest to the northeast, along the radio source position angle in the direction of the brighter hotspot (see below); the [O III] emission southwest of the nucleus is less extended and of lower surface brightness.

2. The emission lines come from a region which has roughly an S shape. The easternmost portion of this emission-line filament points directly at one of the galaxy's companion galaxies. The companion has a radial velocity only 280 (± 200) km s$^{-1}$ different from the host galaxy of PKS 0349 − 278. We detect no [O III] emission coincident with the companion.

In the radio, PKS 0349 − 278 has a very bright hotspot at the edge of the northeastern lobe (unresolved at 2″ resolution) and a dimmer hotspot in the southwestern lobe, which resolves into four individual components when viewed at 2″ resolution. The large-scale structure shows an X shape, with diffuse radio emission extending perpendicular to the radio source axis. The line-emitting gas is found in the region of the radio source where the cocoons (or bridges) from the two hotspots meet near the galaxy core. Our VLA images do not have sufficient sensitivity to show any fine-scale radio structure at the location of the emission-line nebula, and the association (if there is one) between the line-emitting gas and the radio source structure is unclear.

*3C 98 (0356 + 10).*—3C 98 is associated with an elliptical galaxy which appears to be located in a fairly sparse environment. Our H$\alpha$ + [N II] image of 3C 98 shows a wealth of extended line-emitting gas (and see also Simkin 1979; Hansen, Norgaard-Nielsen, and Jorgensen 1987). We note the following:

1. The "comma"-shaped elongation of the nuclear emission to the north;

2. The tangential filament of line-emitting gas to the south, which is curved convex to the nucleus, and the symmetrically placed but blobby filament of emission-line gas north of the nucleus, both of which define an axis which is askew by 44° to the radio source axis;

3. The presence of much fainter line-emitting gas ~ 45″ (25 kpc) northeast of the nucleus, along the radio source axis and of a very faint, curving, tangential filament of line-emitting gas ~ 30″ (17 kpc) due south of the nucleus, both of which are confirmed spectroscopically.

In the radio, at 3.″8 resolution, 3C 98 shows single hotspots in both the northern and the southern radio lobes, separated by ~ 310″ (175 kpc). A jet is present in the northern lobe, though it is strongly blended with diffuse lobe emission in the image shown in Fig. 14*b*. The jet is straight along most of its

[9] Wide-angle-tail radio sources (WATs) were defined as a class by Owen and Rudnick (1976) as C-shaped radio sources with edge-darkened (i.e., Fanaroff and Riley 1974, class I) radio morphologies, radio luminosities between $10^{42}$ and $10^{43}$ ergs s$^{-1}$, and associated with optically dominant galaxies in rich clusters of galaxies (see also O'Donoghue 1987).

© American Astronomical Society • Provided by the NASA Astrophysics Data System

1988ApJS...68..643B



length, but curves abruptly to the east at a bright knot ~120″ from the core, before merging into the northern hotspot. There is a ridge of bright emission curving to the south of the northern hotspot. The large-scale radio structure of 3C 98 is under represented in our maps, but 3C 98 does show a cocoon or bridge of lower surface brightness radio emission extending from the hotspots back toward the core, which, at least to the north, appears to show a tail of emission extending to the west of the radio source axis, near the radio core. The fractional polarization of the radio emission from 3C 98 at 3.″8 resolution and 6 cm is high throughout most of the source structure. The average fractional polarization over the source is 28%.

An understanding of the nature of the relationship between the extended line-emitting gas and the radio source structure awaits more detailed studies. As described above, the brightest extranuclear line-emitting gas is skewed with respect to the radio source axis, but the most distant line-emitting gas is located along the radio source axis.

*3C 105 (0404 + 03).*—The host galaxy of 3C 105 is a surprisingly small and underluminous galaxy to be associated with a high-luminosity radio source. We detect only nuclear Hα + [N II] emission from the host galaxy of 3C 105. In the radio, 3C 105 shows a bright southern hotspot and only a weak, resolved hotspot in the northern lobe (at 6″ resolution), separated by ~335″ (510 kpc). Narrow bridges of emission extend from the hotspots back toward the core.

*3C 109 (0410 + 11).*—The host galaxy of 3C 109 is an isolated, broad-line (Grandi and Osterbrock 1978), N galaxy (MMS). Our [O III] image shows resolved emission, 9″ (35 kpc) in extent, elongated along a position angle which is 44° from the radio source ejection axis. The radio source is 96″ (380 kpc) in total extent and shows a bright southern hotspot, a weaker northern hotspot, and bridges of emission extending back toward the galaxy nucleus.

*PKS 0634 − 206.*—The host galaxy of PKS 0634 − 206 appears to be very isolated, there being no other galaxies within 175″ (175 projected kpc) visible on our *V*-band image to the north, south, or west or within 75″ (75 projected kpc) to the east of the galaxy. Spectroscopic observations of extended emission-line gas have been reported by Fosbury *et al.* (1984), and imaging by Hansen, Norgaard-Nielsen, and Jorgensen (1987).

Our Hα + [N II] emission-line image shows a wealth of extended emission-line gas within 20″ (20 kpc) of the galaxy nucleus. We note in particular (1) the westward "curving" of the line-emitting gas just north of the nucleus and (2) the "tangential" filament or arc of line-emitting gas about 20″ due north of the nucleus, which is slightly curved, concave to the galaxy nucleus. The radio source shows two bright, roughly collinear hotspots, separated by ~870″ (870 kpc), and bridges of radio emission extending back toward the core from the hotspots. The "bridges" can be seen to widen and narrow several times between the core and the nucleus. The relationship between the line-emitting gas and the radio source structure is unclear. The line-emitting gas is elongated predominantly north-south along the radio source axis, but bears no obvious relation to the radio source structure.

*3C 171 (0651 + 54).*—Heckman, van Breugel, and Miley (1984) have discussed in detail the association of extended optical-line–emitting gas with the radio lobes in this small (34 kpc), high-luminosity, radio source. The radio source has two bright hotspots, extending east to west, roughly collinear with the nucleus. Fans of lower surface brightness radio emission extend perpendicular to the radio axis, north and south of each of the hotspots. The [O III] emission is coincident with the bright inner radio structure. Heckman, van Breugel, and Miley (1984) report very low fractional (<1%) polarization in the vicinity of the hotspots at 6 cm, a dramatic change in the velocity of the line-emitting gas east and west of the nucleus, and broad-line widths (~500–650 km $s^{-1}$) throughout the emission-line region. They interpret these results as evidence that the radio jets of 3C 171 have encountered a gas-rich environment within the host galaxy.

The optical spectra of Heckman, van Breugel, and Miley (1984) showed that there might be an optical continuum source roughly coincident with the eastern radio hotspot. Heckman, van Breugel, and Miley (1984) suggested that this continuum excess might provide a local source of photoionization for the emission-line gas. We have subtracted a flux-scaled version of our [O III] emission-line image from our broad-band (*R*) image of the host galaxy of 3C 171, in order to produce a "line-free" continuum image of 3C 171 by removing the contamination from emission lines from the broad-band image. We find that the galaxy itself appears to be elongated roughly north-south and appears to have a tail extending to the southwest. In addition, we find an unresolved optical continuum component just north of the location of the eastern hotspot, roughly where the spectra of Heckman, van Breugel, and Miley (1984) show the excess. This finding is supported by our *V*-band image of 3C 171 which is less contaminated by emission lines than the *R*-band image. We note that the host galaxy of 3C 171 appears to be very isolated; the closest galaxy visible on our *R*-band image is ~200 kpc away in projection.

*PKS 0745 − 191.*—PKS 0745 − 191 is associated with a giant galaxy at the center of a particularly X-ray–luminous cluster at a redshift of 0.1028 (Fabian *et al.* 1985; Bolton and Ekers 1966). The intracluster gas is purported to be cooling and accreting onto the host galaxy of PKS 0745 − 191 at the unprecedented rate of 1000 solar masses per year (Fabian *et al.* 1985; but see also Arnaud *et al.* 1987). We note the following:

1. The Hα + [N II] emission is spatially resolved, extending 13.″5 north (23 kpc) and 10″ (17 kpc) west of the galaxy nucleus.

2. The radio source has a peculiar morphology, with an amorphous halo of diffuse emission surrounding a bright core. At 6 cm we detect only low levels (≤1%) of polarized emission from the inner parts of the source and a patch of polarized emission in the northern extension of the source at the ~10% level.

3. The radio continuum and optical line emission are roughly cospatial, but the overall size of the line-emitting region appears to be roughly twice that of the radio source (our VLA images contain ~95% of the single-dish flux). The

© American Astronomical Society • Provided by the NASA Astrophysics Data System

1988ApJS...68..643B



radio source extends southwest of the line emission, and the line emission shows a broad trail of emission to the west, where we have not detected any radio emission.

4. Our *R*-band image of the host galaxy of PKS 0745−191 shows a peculiar "arc" of emission ~8″ (13 kpc) in extent, located ~20″ (35 kpc) to the west of the galaxy nucleus, well outside the visible edge of the galaxy. Our "emission-line–only image" shows no feature coincident with the arc, so it appears to be a continuum-dominated feature. Our data are of low signal-to-noise ratio. It would clearly be of interest to obtain deeper images of this field to confirm and clarify this result. It may be that this small arc of emission is related to the much larger and more complete arcs of optical continuum emission found about the central dominant galaxies in three clusters by Lynds and Petrosian (1986) and Soucail *et al.* (1987). Begelman and Blandford (1987) suggest that these arcs result from massive star formation induced in the intracluster medium by a bow shock, which precedes a dominant galaxy as it moves through the intracluster medium in a cooling accretion flow, and predict that clusters with such arcs should contain cooling flows, a condition met by the PKS 0745−191 cluster.

*3C 192 (0802 + 24).*—Our *R*-band image of the host galaxy of 3C 192 shows it to be a very round appearing elliptical galaxy with one similar sized neighbor 70″ (70 projected kpc) away. According to S72, 3C 192 is a member of a small group of galaxies. Our Hα+[N II] image shows extensive line-emitting filaments. Just west of the nucleus is a tangential filament, whose long axis is oriented perpendicular to the radial from the nucleus. A long filament extends ~30″ (30 kpc) from the southeast of the nucleus, and there is fainter line-emitting gas to the northeast of the nucleus which extends northward for ~25″ (25 kpc). 3C 192 has been mapped extensively in the radio by Hogbom (1979). We present a 20 cm VLA map at 3.″9 resolution (courtesy of Steve Spangler), showing bright hotspots at the ends of the northwestern and southeastern lobes, separated by ~190″ (200 kpc) and the very symmetric X-shaped morphology of the source on large scales.

The nature of the relationship between the extended radio source and the extensive filaments of line-emitting gas is unclear; however, we note that the line-emitting gas appears to be associated with the regions where the bridges or cocoons of emission which extend from the hotspots to the core meet either each other or the galaxy interstellar medium (ISM).

*3C 196.1 (0812 − 02).*—The host galaxy of 3C 196.1 appears to be the dominant galaxy in its environment. There are 14 smaller galaxies on our broad-band image within 350 kpc of the nucleus of the host galaxy of 3C 196.1. The galaxy appears to be a highly flattened elliptical with an extensive outer envelope extending ~30″ (80 kpc) from the galaxy nucleus to the northeast and southwest. A potential secondary nucleus can be seen ~4″ (11 kpc) north of the site of the primary nucleus.

Our Hα+[N II] image shows line-emitting gas which extends from the nucleus toward the northeast and which appears to be brightest off the nucleus. The radio structure of 3C 196.1 is unusual. We have identified the location of the core from the optically determined position of the nucleus of the host galaxy. The core appears to be weak and situated in the southwestern part of the radio source. A bright unresolved component is observed to the northwest, coincident with the bright extension of the optical line emission. Surrounding the weak core and bright knot is an amorphous radio halo. At 6 cm, ~1.″3 resolution, we detect only very low levels of radio polarization (<1%) from the inner parts of the radio source.

*3C 218 (0915 − 11).*—The host galaxy of 3C 218 (Hydra A) is the dominant galaxy in a poor (Bautz-Morgan type I, Abell richness class 0) cluster (Sandage and Hardy 1973). Our *V*-band image shows at least five galaxies within a projected distance of 40 kpc of the galaxy nucleus and a potential secondary nucleus ~10″ (10 kpc) from the primary nucleus of 3C 218. We detect emission lines from a flattened elliptical region (unresolved laterally), with a total extent of ~6″ (6 kpc) roughly centered on the primary nucleus, and from two, narrow, curved arms which extend from the northwestern and southeastern edges of this elliptical region. Thus, overall, the line-emitting gas has an S shape. Simkin (1979) and Heckman, Carty, and Bothun (1985) report that the emission-line region within 3″ of the nucleus is rotating about an axis at a position angle of ~29°, roughly along the minor axis of the flattened ellipse of gas and roughly perpendicular to the radio source axis.

3C 218 has an unusual radio morphology for its high radio luminosity. It has a bright core and two knots (or hotspots) of emission on either side of the core at ~10″ (10 kpc) from the core. Extending down from the northern knot is a narrow region of radio emission, which points slightly to the west of the core. Trailing away from the knots are tails of emission which bend to the northeast from the northern hotspot and to the southwest from the southern knot, giving the source an overall S or helical shape. The radio spectral index between 20 and 6 cm appears to steepen down these trails, reaching a value of $\alpha \sim -1.8$ ($F_\nu \propto \nu^\alpha$) at the ends of the tail. Excluding the absence of an overall C shape, the radio source morphology closely resembles the morphology of many wide-angle-tail radio sources (e.g., O'Donoghue and Owen 1987). Ekers and Simkin (1983) observed 3C 218 with the Fleurs synthesis telescope and reported that the source extends for 240″ (~240 kpc) to the south of the radio core. The relationship between this large-scale radio structure (which contains only ~10% of the total source flux) and the finer scale radio structure in our VLA radio maps is unclear.

The radio source shows very low fractional polarization at 6 cm and 1.″85 resolution in the regions of the source within ~15 kpc of the nucleus. The lowest levels of polarization appear to the south of the core, where the average detected level of polarization is 2%. The percent polarization rises rapidly at 2 cm, and there is evidence for a large amount of Faraday rotation. Specifically, we measure polarization position angle differences of at least 90° between 2 and 6 cm, corresponding to a (minimum absolute) *observed* Faraday rotation measure of 430 rad $m^{-2}$. This is consistent with the results of Kato *et al.* (1987), who report an integrated rotation measure of −1850 rad $m^{-2}$.

The relationship between the radio and extended line-emitting gas is unclear. The line-emitting gas spans the region

© American Astronomical Society • Provided by the NASA Astrophysics Data System

1988ApJS...68..643B



between the radio core and the radio "knots," shares the S symmetry of the radio emission and overlaps with the radio emission only at the edges of the radio knots, if at all.

*3C 219 (0917 + 45).*—3C 219 is a high-luminosity radio galaxy associated with the dominant member of a cluster of galaxies of richness class 2 ($z = 0.1745$) (Schmidt 1965; MMS 1964). The radio source was mapped in detail with the VLA by Bridle, Perley, and Henriksen (1986). A jet emanates to the southwest, pointing toward a hotspot in the southern lobe. To the northeast a knot in a possible counterjet is visible, pointing toward a more diffuse lobe. Our H$\alpha$ + [N II] image shows only unresolved nuclear emission.

*3C 223 (0936 + 36).*—According to S72, the host galaxy of 3C 223 is in a group of galaxies. There are ~12 much smaller galaxies apparent on our *V*-band image within 110″ (250 kpc) of the galaxy nucleus. Our *V*-band image of the galaxy shows it to be a flattened elliptical with an extensive envelope reaching ~ 25″ (55 kpc) northeast of the galaxy nucleus and ~ 20″ (45 kpc) southwest of the nucleus. Trails of light roughly 30″ (70 kpc) in length can be seen extending to the southeast and southwest from the edges of the galaxy's envelope. No emission lines were detected from these trails, thus they must be continuum features. We did detect line-emitting gas in the nucleus of the galaxy and extended gas along a position angle of 58° with an extent of ~ 4.″5 (10 kpc). Due to the presence of interference fringes from night-sky lines in the narrow-band image, this result is tentative and should be confirmed spectroscopically.

At 3.″8 resolution and 20 cm, the radio source has weak hotspots in each lobe separated by roughly 300″ (660 kpc). The northern, brighter hotspot shows a "hammerhead" morphology. No core was detected.

*3C 227 (0945 + 07).*—3C 227 is associated with an isolated N galaxy (S72) with broad nuclear emission lines (Osterbrock, Koski, and Phillips 1975, 1976). Our *R*-band image shows that the nearest galaxy to 3C 227 is ~ 75″ (110 kpc) away in projection. Our H$\alpha$ + [N II] image reveals an extensive network of emission-line filaments. One chain of emission-line knots runs northeast to southwest, extending ~ 35″ (50 kpc) on either side of the nucleus. A second smaller, but higher surface brightness, filament extends southeast to northwest, for ~ 9″ (13 kpc) on either side of the nucleus and has a faintly S-shaped morphology. The northwestern end of this smaller filament is coincident with a bright, unresolved continuum feature seen in the *R*-band image, a possible secondary nucleus or companion galaxy. Excluding this possible secondary nucleus, the broad-band contours of the host galaxy of 3C 227 show no obvious evidence of distortion.

The radio source 3C 227 has hotspots in its western and eastern lobes, separated by ~ 230″ (335 kpc) and displaced to the south relative to the core. Lower surface brightness emission (a cocoon or bridge) extends back from each hotspot to the core. The centroid of this low-level emission is displaced slightly to the south of the core. The radio source has fairly high levels of fractional polarization throughout (mean fractional polarization is 22% at 6.″5 resolution and 6 cm). The relationship between the very extended line-emitting gas and the radio source structure is unclear, but we note the tendency of the line-emitting gas to be found along the edges of the low-surface-brightness radio cocoon.

*3C 264 (1142 + 19).*—3C 264 is associated with NGC 3862 in a dense subcluster on the edge of the irregular, richness class 2 cluster, Abell 1367 (S72; Dickens and Moss 1976). A second galaxy can be seen projected on the envelope of NGC 3862, its nucleus being ~ 52″ (20 projected kpc) north of the nucleus of NGC 3862. Elvis *et al.* (1981) reported the detection of a point, possibly variable, *X*-ray source associated with NGC 3862. Our H$\alpha$ + [N II] image shows an oval region of line-emitting gas ~ 6.″3 (2.4 kpc) in extent, centered on the galaxy nucleus, oriented with its major axis almost due east–west, roughly perpendicular to the radio source ejection axis.

The radio source 3C 264 has been mapped on many scales. At 6 cm and 1.″15 resolution, the source has a jet extending to the northeast, which turns gently to the northwest roughly 4″ (1.5 kpc) from the nucleus. At 6 cm, the magnetic field appears to be parallel to the jet axis in close to the core and to flip to become perpendicular at roughly the point where the jet turns, thereafter becoming parallel again. At 6 cm and 3.″8 resolution, the source shows a very unusual, amorphous structure, with a secondary peak of emission roughly 30″ (12 kpc) northeast of the core, surrounded by very diffuse emission. The secondary peak is aligned with the initial direction of the jet. Bridle and Vallee (1981) and Gavazzi, Perola, and Jaffe (1981) have mapped the large-scale radio structure of 3C 264. On the largest scales, 3C 264 shows a two-tailed structure with forked emission extending ~ 360″ (140 kpc) to the north-northeast.

*3C 272.1 (1222 + 13).*—The radio source 3C 272.1 is associated with M84, one of the four prominent elliptical galaxies near the center of the Virgo cluster. M84 has been shown to be a source of resolved X-ray emission, and Forman and Jones (1982) suggest a cooling time for the X-ray–emitting gas of only $2 \times 10^7$ yr, corresponding to an estimate for the mass inflow rate onto M84 of 20 $M_\odot$ yr$^{-1}$. M84 has a dust lane running virtually perpendicular to the minor axis of the galaxy (Wade 1960).

Hansen, Norgaard-Nielsen, and Jorgensen (1985) presented optical narrow-band imaging and spectroscopy of the dust lane which revealed the presence of an elongated region of line-emitting gas coincident with the dust lane. Our own H$\alpha$ + [N II] image shows somewhat more clearly the apparent S shape of the emission-line region, which extends ~ 12″ (0.75 kpc) on either side of the nucleus. The radio source 3C 272.1 has been mapped in detail by Laing and Bridle (1987). It has twin jets which extend to the north and south. The jets lose collimation and bend ~ 50″ (3 kpc) from the galaxy nucleus, the northern jet to the east, the southern jet to the west, and fade into diffuse lobes. Thus, like the emission-line nebula, the radio source has an overall S-shaped symmetry. Interestingly, the sense of the curvature is the same (counterclockwise) for the radio source and the emission-line nebula. Laing and Bridle use polarization observations at 1.4 and 4.9 GHz to show that a Faraday rotating medium with an extent of ~ 10 kpc lies between the radio-emitting plasma and us, most likely within the interstellar medium of the galaxy itself.

© American Astronomical Society • Provided by the NASA Astrophysics Data System

1988ApJS...68..643B



*3C 274 (1228 + 12).*—The radio source 3C 274 (Virgo A) is associated with M87, the dominant galaxy in the Virgo cluster. The X-ray emission from this irregular, "cooling flow" cluster is peaked on M87 (Canizares, Stewart, and Fabian 1983), and the intracluster gas is purported to be cooling and accreting onto M87 at the rate of $\sim 10\ M_{\odot}$.

When imaged in the light of H$\alpha$ + [N II], the inner regions of M87 (i.e., within $\sim 75''$, or 5.4 kpc of the nucleus) show a system of emission-line filaments stretching predominantly east–west, along the radio axis. These filaments are largely displaced to the north of the jet axis, but share the overall distribution of the radio emission (Ford and Butcher 1979). Several of the optical emission-line filaments appear adjacent to radio features (e.g., next to the western jet, near an enhancement on the eastern edge of the eastern lobe and just below the northern edge of the source).

The large-scale radio emission of M87 has a total extent of $\sim 14'$ (60 kpc) and displays a rough Z shape (Kotanyi 1980; Feigelson *et al.* 1986; Rao 1987). Recently, Feigelson *et al.* (1986) have shown that the asymmetric X-ray emission from M87 is elongated $\sim 4'$ (18 kpc) due east of the nucleus of M87 and $\sim 4'$ to the southwest at a position angle of 220°. There is a strong spatial correspondence between this asymmetric X-ray emission and the large-scale radio structure of M87 (Feigelson *et al.* 1986).

We also detect an optical H$\alpha$ + [N II]–emitting filament $\sim 3\farcs3$ (14) kpc from the nucleus of M87, at a rough position angle of 78°. This filament is on the edge of the detected asymmetric X-ray emission, and well within the region of bright radio emission. The filament is extended $\sim 1$ kpc in the direction roughly perpendicular to the jet axis, is unresolved in the lateral direction, and shares the curvature of the eastern lobe of M87 (i.e., it is concave toward the radio axis).

*3C 275 (1239 − 04).*—The high-luminosity radio source 3C 275 is identified with a galaxy at a redshift of 0.480. Our broad-band image shows that it is the largest galaxy in a chain of five galaxies which is $\sim 34''$ (180 kpc) in length. Our [O III] image shows line-emitting gas with a total extent of $\sim 4\farcs4$ (23 kpc), which is elongated northeast to southwest along the position angle of the extended radio source. Using the positions of four stars measured off the Palomar sky survey, we determine that the location of the nucleus on the broad-band optical image is at $12^{h}39^{m}44\overset{s}{.}91 \pm 0\overset{s}{.}05$, $-04°29'53\farcs9 \pm 0\farcs75$. The radio source appears to be a small double. At 6 cm, $1\farcs4$ resolution, we detect two point sources separated by roughly $5''$ (26 kpc), the southwestern of which shows significantly lower fractional polarization. The nominal position of the galaxy nucleus as determined from the optical image is between the two radio point sources, closer to the southwestern point source.

*3C 278 (1252 − 12).*—3C 278 is associated with the southern nucleus in the dumbbell galaxy NGC 4782 (S72). The two nuclei are separated by $\sim 41''$ (11.5 kpc) in projection. Our optical *R*-band contours of the galaxy show that the southern nucleus appears to be displaced to the west of the centroid of the larger scale brightness contours, while the northern nucleus appears to be displaced eastward (also Alok Patnaik 1986, private communication). We detect nuclear H$\alpha$ + [N II] emission from the southern nucleus as well as an apparent extension of line emission to the east of the nucleus, surrounded by a low–surface-brightness region of line-emitting gas extending $\sim 3\farcs5$ (1 kpc) from the nucleus. These emission-line results need to be confirmed spectroscopically.

The radio source 3C 278 shows a wide-angle-tail radio morphology. The eastern jet bends sharply to the north shortly after extending from the galaxy nucleus, before merging with diffuse emission in the northeastern lobe. The western jet also bends to the north, but only at roughly 4 times the distance at which the eastern jet bends, and only once the jet has widened considerably.

*3C 285.*—According to S72, the host galaxy of 3C 285 is the brightest member of a group of galaxies. The peculiar optical morphology of the galaxy has been described by H86. The galaxy has a continuum-emitting S-shaped envelope which is aligned with an apparent companion galaxy to the north-northwest. Our emission-line image of 3C 285 shows two systems of gas. Running due east–west, along the direction of the radio source axis, is a compact, high–surface-brightness region of H$\alpha$ + [N II] emission which extends for $\sim 5\farcs5$ (8 kpc) on either side of the nucleus. Running north-northwest to south-southeast along the elongated optical continuum envelope of the galaxy is a much lower surface brightness filament of line-emitting gas. This filament extends $\sim 26''$ (35 kpc) to the north toward an apparent companion galaxy. The "companion galaxy" also appears to contain line-emitting gas at the approximate redshift of the host galaxy of 3C 285 (a result which needs to be confirmed spectroscopically).

A 20 cm VLA radio map of 3C 285 at $\sim 5''$ resolution has been presented by Leahy and Williams (1984). In the radio 3C 285 is as a slightly C-shaped classical double, with two hotspots and an eastern ridge showing curvature to the south-southeast, or roughly along the line from 3C 285 to the companion galaxy. The diffuse envelope or "bridge" emission in 3C 285 also extends to the south-southeast on both sides of the galaxy nucleus.

*PKS 1345 + 125.*—The continuum optical morphology of the host galaxy of PKS 1345+125 has been discussed by Gilmore and Shaw (1986) and H86, and the emission-line properties of the nuclei by Grandi (1977), and Gilmore and Shaw (1986). As is apparent in our *R*-band image, the continuum optical light is very distorted. The source shows a double nucleus, with a separation of $1\farcs8$ (11 kpc), inside of an asymmetrically shaped body. There are continuum extensions to the northeast and southwest and a looping filament to the northwest. The galaxy appears as if it may be the dominant member of a group of galaxies (H86). Our H$\alpha$ + [N II] image shows nuclear line-emitting gas associated with the northwestern nucleus, line-emitting gas extending to the northeast, and a tail of line-emitting gas emanating from the south of the nucleus which curves to the west. End to end, the emission-line region appears to be $\sim 8\farcs8$ (17 kpc). The radio source is unresolved at $0\farcs1$ resolution (see the VLA Calibrator Manual) and has been identified with the southeastern nucleus (Gilmore and Shaw 1986).

*3C 295 (1409 + 52).*—The very powerful radio source 3C 295 is associated with a large elliptical galaxy in a cluster at a

© American Astronomical Society • Provided by the NASA Astrophysics Data System

1988ApJS...68..643B



redshift of 0.461 (MMS). Henry and Henriksen (1986) describe the X-ray morphology of this cluster and suggest that there is evidence of a cooling flow of $\sim 145\ M_\odot\ \mathrm{yr}^{-1}$ onto the parent galaxy of 3C 295.

3C 295 is a very luminous classical double radio source with bright hotspots roughly collinear with the nucleus and a total linear extent of only $\sim 30$ kpc. The measured fractional polarization of the radio emission from 3C 295 is fairly high at 2 cm and 0".1 resolution (on average $\sim 18\%$), with the southern lobe showing polarization at the $\sim 22\%$ level, on average, and the northern lobe at the $\sim 11\%$ level. Kato *et al.* (1987) report an integrated *observed* Faraday rotation measure of $+2250$ rad $\mathrm{m}^{-2}$, so these percentages may be effected by beam depolarization resulting from the rotation measure substructure.

Our [O III] image of the host galaxy of 3C 295 shows that extranuclear line-emitting gas is present. This gas appears to be elongated to the northwest, directly along the radio axis of the source and is unresolved in the lateral direction.

*3C 305 (1448 + 63).*—Detailed radio and optical observations of 3C 305 have been presented by Heckman *et al.* (1982) and H86. We summarize the major results. The radio source 3C 305 is unusually small ($\sim 10$ kpc). The source has a core and two roughly collinear hotspots to the northeast and southwest, both of which exhibit trails of more diffuse emission extending roughly north to south. The central regions of the source have very low fractional linear polarization at 6 cm ($< 1\%$), with the fractional polarization rising to 10%–30% along the edges and more diffuse regions of the source.

Our new H$\alpha$ + [N II] image shows a roughly S-shaped region of line-emitting gas, which extends for $\sim 18''.4$ (14 kpc) to the east and west of the nucleus. The overlay of radio and emission-line contours shows that the optical line and bright inner radio emission are roughly cospatial. As described by Heckman *et al.* (1982) there is a detailed anticorrelation between the presence of line emission and the fractional polarization of the radio emission. The kinematic emission-line data and the radio data are consistent with a scenario in which the radio source plowed into a preexisting, rotating disk of gas.

Finally, we note the unusual optical continuum morphology of the host galaxy of 3C 305. It has two tails of emission each of which extends $\sim 75''$ (55 kpc) from the visible edge of the galaxy envelope, one to the southeast, the other to the northwest. There are no nearby companion galaxies present on our broad-band image within 80 projected kpc of the galaxy nucleus.

*3C 313 (1508 + 08).*—3C 313 is associated with a galaxy at a redshift of 0.461. Our image of the galaxy in [O III] shows that, while there is line emission associated with the galaxy nucleus, the peak [O III] emission comes from a region $\sim 2''$ (10 kpc) east of the nucleus. Our 2" resolution VLA radio snapshot image of 3C 313 contains only a small fraction of the total single dish flux from the source and shows only the fine-scale source structure. 3C 313 has two roughly collinear hotspots separated by $\sim 130''$ (670 kpc) and trails of emission extending from the hotspots back to the core. There is no evidence on these images that the radio emission is related to the line-emitting gas, though more sensitive maps are needed to address this question properly.

*3C 317 (1504 + 07).*—3C 317 is identified with the multiple nucleus cD galaxy at the center of the richness class 0, possible "cooling flow" cluster Abell 2052 (MMS; Abramopoulos and Ku 1983). The second, smaller nucleus lies 7" (4.5 kpc) northwest of the primary nucleus and has a radial velocity only $\sim 50$ km $\mathrm{s}^{-1}$ different from that of the primary nucleus (Hoessel, Borne, and Schneider 1985). Our emission-line image shows a thin arc of line-emitting gas $\sim 6''$ (4 kpc) north of the primary nucleus. This arc appears to loop around and pass just south of the primary nucleus before joining with the secondary nucleus. Thus it is tempting to associate the emission lines with gas that has been tidally stripped out of the second nucleus (or its galaxy) during the course of its merger with the host galaxy of 3C 317.

3C 317 is a source of intermediate radio luminosity. It has a strong core and a curved ridge of enhanced brightness (a jet?) to the south, surrounded by amorphous emission that stretches at least 35" (22 kpc) from the core. The source has an overall corkscrew shape. One possible explanation for the unusual radio morphology of 3C 317 is that its radio emission has been smeared out over a large area by the precession and possibly swinging (e.g., Wirth, Smarr, and Gallagher 1982) of the jet axis. At 6 cm, 4" resolution we detect polarized emission from patches within the main body of the source, with the average level of fractional polarization measured being only 5%. It is not yet clear whether there is a physical connection between the line-emitting gas and the radio-emitting plasma. However, they are cospatial (in projection) and have similar size scales.

*3C 321 (1529 + 24).*—The peculiar optical structure of the host galaxy of 3C 321 has been discussed by H86. The host galaxy of 3C 321 has two nuclei, separated by $\sim 3''$ (4.8 kpc). The southwestern nucleus is the brighter of the two and is most closely coincident with the location of the radio core. Specifically, we determine a position of $15^h29^m33^s.49$ ($\pm 0^s.044$) 24°14′26".0 ($\pm 0''.6$) for the position of the southern nucleus on our *R*-band images and a position of $15^h29^m33^s.32$ ($\pm 0^s.044$) 24°14′27".9 ($\pm 0''.6$) for the northern nucleus. The radio core is at $15^h29^m33^s.513$ ($\pm 0^s.015$) 24°14′26".76 ($\pm 0''.2$), as measured from our 20 cm, 1".37 resolution VLA image. Thus, to within the errors, the radio core is coincident with the southern nucleus (but is displaced at least 1".9 from the position of the northern nucleus).

The two nuclei are contained in an amorphous shaped halo of continuum light, which has a broad fan or tail emanating from the south and curving eastward. Our emission-line image shows an S-shaped region of line-emitting gas roughly 22" (35 kpc) across, which passes through both of the nuclei. There is also line-emitting gas 22" (35 kpc) to the northwest of the nuclei. The only other galaxy within 235" (380 kpc) of 3C 321 is a small galaxy 40" (65 kpc) to the northeast.

The 20 cm, 1".37 resolution VLA map of 3C 321 shows a jet emanating from the core to the northwest, which points toward the arc of line-emitting gas. The jet has a knot roughly 35" (6 kpc) from the core, after which it exhibits an S-shaped bend. A possible counterjet is barely visible (at the 3 $\sigma$ level) to the southeast. The putative counterjet aligns with the northern jet and the nucleus and is directed toward a break in the arc of line-emitting gas to the southeast. Finally, we note

© American Astronomical Society • Provided by the NASA Astrophysics Data System

1988ApJS...68..643B



that while the putative counterjet, core, and northern jet do align with one another, they do not point at the hotspots. They define, instead, an axis which deviates by 11° from the axis defined by the northern hotspot, core, and southern hotspot. The radio source is ~ 300″ (490 kpc) in total extent.

*3C 327 (1559 + 02).*—3C 327 is associated with a flattened elliptical galaxy, which appears to be near the edge of a richness class 0 cluster (MMS). From the center of the galaxy we detected emission lines from a small, roughly elliptical region, which is elongated roughly along the minor axis of the galaxy's stellar isophotes and perpendicular to the extended radio source, with a total extent of ~ 4″ (7 kpc). The radio source 3C 327 has two hotspots, of which the southeastern hotspot is the closer to the core and the brighter of the two. Lobes (or bridges) of emission extend back toward the core from the hotspots. The two lobes are strikingly different in overall shape. The east lobe has a wide bridge whereas the west lobe has a highly elongated conical structure that extends back to the core in a manner resembling a poorly collimated jet (though it does not have the brightness contrast usually associated with a "jet").

*3C 327.1 (1602 + 01).*—The very high radio luminosity source 3C 327.1 is associated with a galaxy at a redshift of 0.4268. We detect only unresolved nuclear line emission from the galaxy. The radio source shows hotspots in each lobe, which are displaced to the southeast of the core, and wide bridges joining the hotspots to the core. The total radio source extent is ~19″, or 100 kpc.

*3C 346 (1641 + 17).*—The host galaxy of 3C 346 ($z = 0.161$) has a diffuse outer envelope that extends roughly 16″ (40 kpc) from the galaxy nucleus in our broad-band image. A potential secondary nucleus is located 3.″2 (8 kpc) to the south-southeast of the primary nucleus, roughly aligned with the extension of the broad-band envelope. Our *R*-band image shows ~15 galaxies within ~120″ (300 kpc) of the core of 3C 346, of which the host galaxy of 3C 346 is by far the largest. Our Hα + [N II] images show strong nuclear emission from the primary nucleus plus possible line emission extending toward, and coincident with, the potential secondary nucleus. In the radio, 3C 346 has a complex edge-brightened morphology, with a hotspot south-southwest of the nucleus on the western edge of the source and a knot roughly 4.″5 east of the nucleus. Surrounding this finer scale structure is a broad region of lower surface brightness emission.

*3C 353 (1717 − 00).*—3C 353 is identified with a D2 galaxy which, according to MMS, is in a Zwicky cluster of which it is not the brightest member, and which, according to S72, is isolated. Four much smaller galaxies are visible on our broad-band image within 64 projected kpc of the galaxy's nucleus. Our Hα + [N II] image shows a small region of line-emitting gas ~ 7.″4 (4 kpc) in length, centered on the galaxy nucleus. The emission-line region extends north to south, roughly perpendicular to the radio source axis and along the minor axis of the host galaxy. In the radio, at 6 cm and 1.″2 resolution, 3C 353 shows a weak, resolved hotspot in each lobe. At lower resolution 3C 353 shows broad cocoons or bridges of emission extending from the hotspots back toward the core and a possible ring of emission to the west of the nucleus in the broad western lobe.

*3C 390.3 (1845 + 79).*—3C 390.3 is associated with a broad-line N galaxy (Wyndham 1966; Sandage 1966). Our *V*-band image shows six galaxies within 120″ (120 kpc) of the host galaxy of 3C 390.3, of which 3C 390.3 is the brightest. Maps of 3C 390.3 at 2.7 and 5 GHz at 12″ and 6″ resolution, respectively, have been presented by Harris (1972). The source has a bright southern hotspot, a much weaker northern hotspot and is ~ 200″ (200 kpc) in total extent. Burbidge and Burbidge (1971) have shown that the line emission from the galaxy comes from two separate velocity systems corresponding to $z \sim 0.043$ and $z \sim 0.057$. We detected only nuclear [O III] emission from the galaxy. Our filter only passed light from the low-velocity system. Recently, Clavel and Wamsteker (1987) have shown that the flux in the narrow core of the Lyα λ1216 and C IV λ1550 emission lines declined by a factor of 1.7 and 3.2, respectively, from 1978 to 1987, coincident with a decrease in the optical continuum flux over that time span. From the variability they set an upper limit to the size of the narrow-line region in 3C 390.3 of only 10 lt-yr.

*3C 403 (1949 + 02).*—3C 403 is associated with a galaxy at a Galactic latitude of 12°. Because of the crowded field, structure in the broad-band image of the galaxy is difficult to discern. However, there is a suggestion of a broad extension, or fan, in the continuum light to the south of the galaxy nucleus. Our Hα + [N II] image shows an elliptical region of line-emitting gas, ~13″ (14 kpc) in extent, centered on the galaxy nucleus, with its long axis roughly aligned with the southern continuum extension but askew by 54° to the radio source axis. We note the presence of a narrow, curved feature (tail) extending from the northern end of the emission-line region.

At 6 cm and 1.″4 resolution, 3C 403 shows a core, a single bright unresolved hotspot to the west, and a double hotspot to the east. A bright knot of emission is located roughly halfway between the core and the eastern hotspots, but is displaced to the north from the line joining the core and the northern of the two hotspots. At lower resolution, the source shows diffuse structure perpendicular to the radio source axis, giving the source an X shape. At 6 cm, 3.″2 resolution, we detect polarized emission from most parts of the source at levels between 10% and 40% in the main body of the source and approaching 60% in the low level X-shaped emission.

*3C 405 (1957 + 40).*—The very powerful radio galaxy 3C 405 (Cygnus A) has been studied in detail due to its proximity and radio brightness. The host galaxy appears to be a cD galaxy, the dominant member in a poor cluster of galaxies (MMS; Spinrad and Stauffer 1982). Fabbiano *et al.* (1979) and Arnaud *et al.* (1984) have shown that 3C 405 is a strong, extended X-ray source, and estimate that $\sim 90\ M_\odot\ \mathrm{yr}^{-1}$ of hot intracluster gas is accreting onto the galaxy. 3C 405 is a classical, double-lobed radio source with multiple hotspots in each lobe, a jet to the west, a very faint counterjet to the east, and detailed filamentary structure in the lobes (Hargrave and Ryle 1974; Perley, Dreher, and Cowan 1984). Recently, Dreher, Carilli, and Perley (1987) reported measurements of rotation measures toward Cygnus A as high as 4000 rad $\mathrm{m}^{-2}$ and rotation measure gradients exceeding 300 rad $\mathrm{m}^{-2}$ $\mathrm{arcsec}^{-1}$, which they argue are occurring in either (1) a sheath of magnetoionic material surrounding the radio source, (2) the

© American Astronomical Society • Provided by the NASA Astrophysics Data System

1988ApJS...68..643B

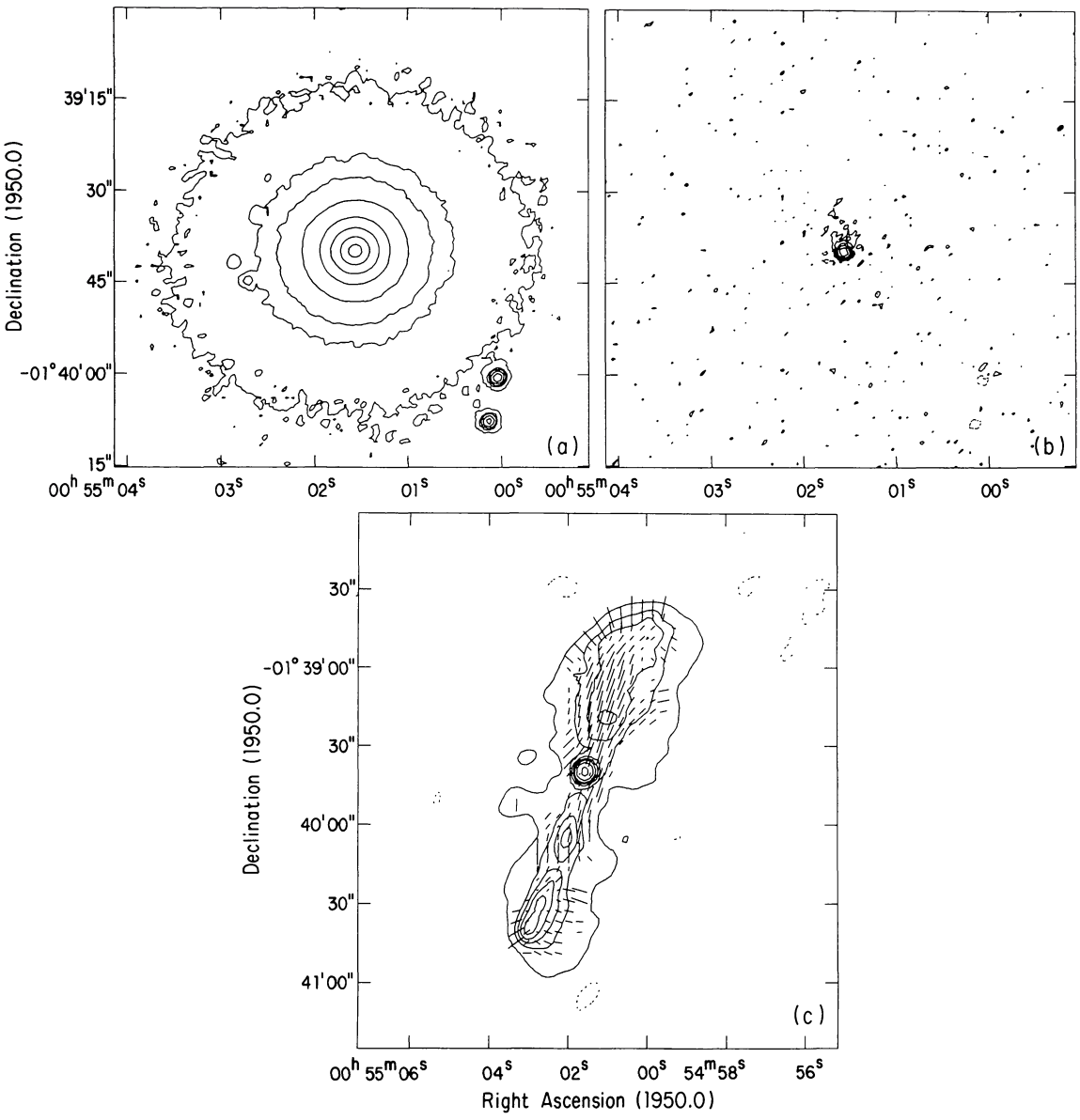


FIG. 1.—3C 29. (*a*) Contours of the *R*-band optical image of the host galaxy of 3C 29. Levels are $1\times10^{-16}\times(-10, 10, 30, 50, 100, 200, 350, 600, 1000)$ ergs $s^{-1}$ $cm^{-2}$ $arcsec^{-2}$. (*b*) Contours of the H$\alpha$+[N II] image. Levels are $1\times10^{-17}\times(-8, 8, 15, 30, 50, 100, 200)$ ergs $s^{-1}$ $cm^{-2}$ $arcsec^{-2}$. (*c*) Contours of the 6 cm VLA C array image. Levels are $1.3\times(-3, 3, 10, 15, 20, 25, 35, 55)$ mJy per restoring beam (6″ FWHM circular Gaussian). The lengths of the superposed vectors indicate the fractional polarization, and their orientations give the direction of the projected electric field. A vector of length 1″ represents a fractional polarization of 6.25%.

© American Astronomical Society • Provided by the NASA Astrophysics Data System

1988ApJS...68..643B

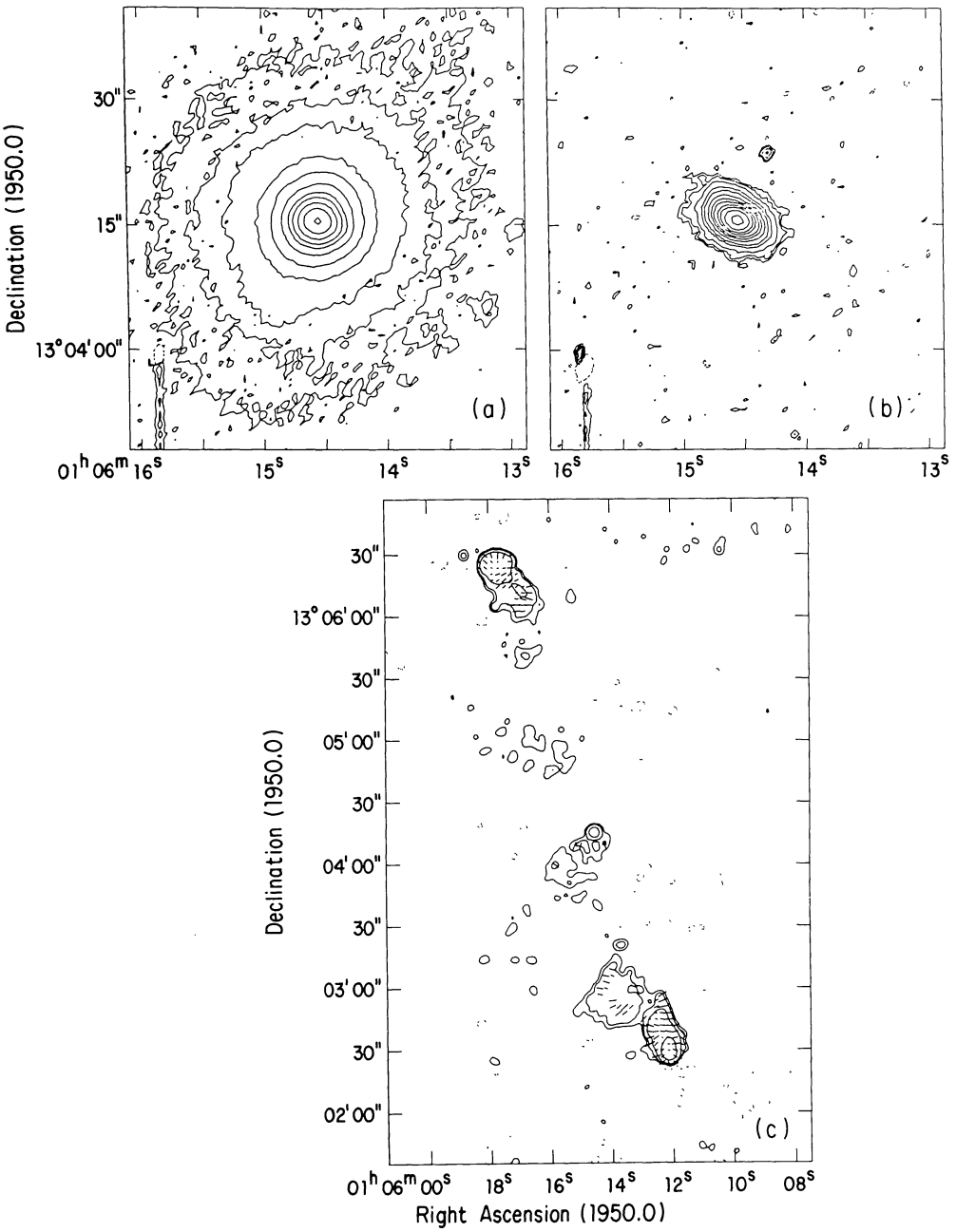


FIG. 2.—3C 33. (*a*) Contours of the *R*-band optical image of the host galaxy of 3C 33. Levels are $1\times10^{-16}\times(-4, 4, 8, 15, 35, 60, 100, 150, 200, 300, 500, 1000, 2000)$ ergs $s^{-1}$ $cm^{-2}$ $arcsec^{-2}$. (*b*) Contours of the H$\alpha$+[N II] emission. Levels are $1\times10^{-17}\times(-3, 3, 5, 10, 20, 30, 50, 75, 100, 150, 200, 300, 500, 1000)$ ergs $s^{-1}$ $cm^{-2}$ $arcsec^{-2}$. (*c*) Contours of the 6 cm C array VLA image of 3C 33. Levels are $7.0\times10^{-1}\times(-3, 3, 6, 25, 300)$ mJy per restoring beam (3".85 FWHM circular Gaussian). The lengths of the superposed vectors indicate the fractional polarization, and their orientations give the direction of the projected electric field. A vector of length 1" represents a fractional polarization of 8.3%.

© American Astronomical Society • Provided by the NASA Astrophysics Data System

1988ApJS...68..643B

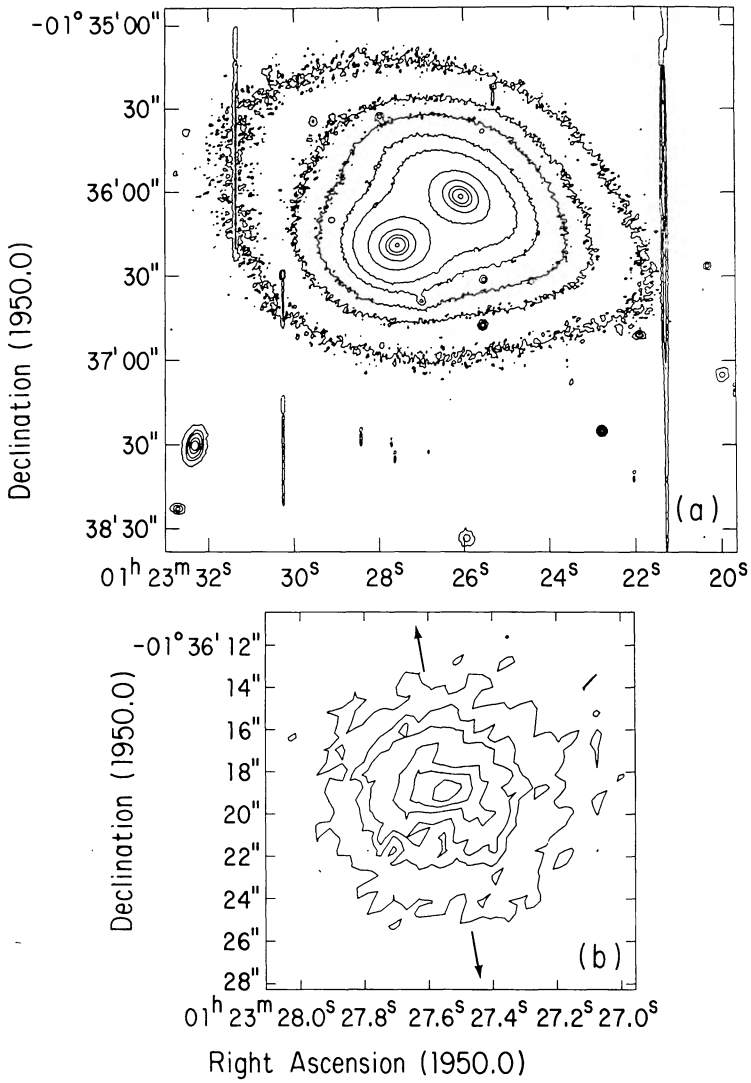


FIG. 3.—3C 40. (*a*) Contours of the *V*-band optical image of the host galaxy of 3C 40. Levels are $1\times10^{-15}\times(-1, 1, 2, 3, 5, 7.5, 15, 30, 60, 100, 300)$ ergs $s^{-1}$ $cm^{-2}$ $arcsec^{-2}$. (*b*) Contours of the H$\alpha$ + [N II] image. Levels are $1\times10^{-17}\times(-28, 8, 20, 30, 50, 75, 100, 200, 300, 500)$ ergs $s^{-1}$ $cm^{-2}$ $arcsec^{-2}$. Arrows indicate the radio source axis.

© American Astronomical Society • Provided by the NASA Astrophysics Data System

1988ApJS...68..643B

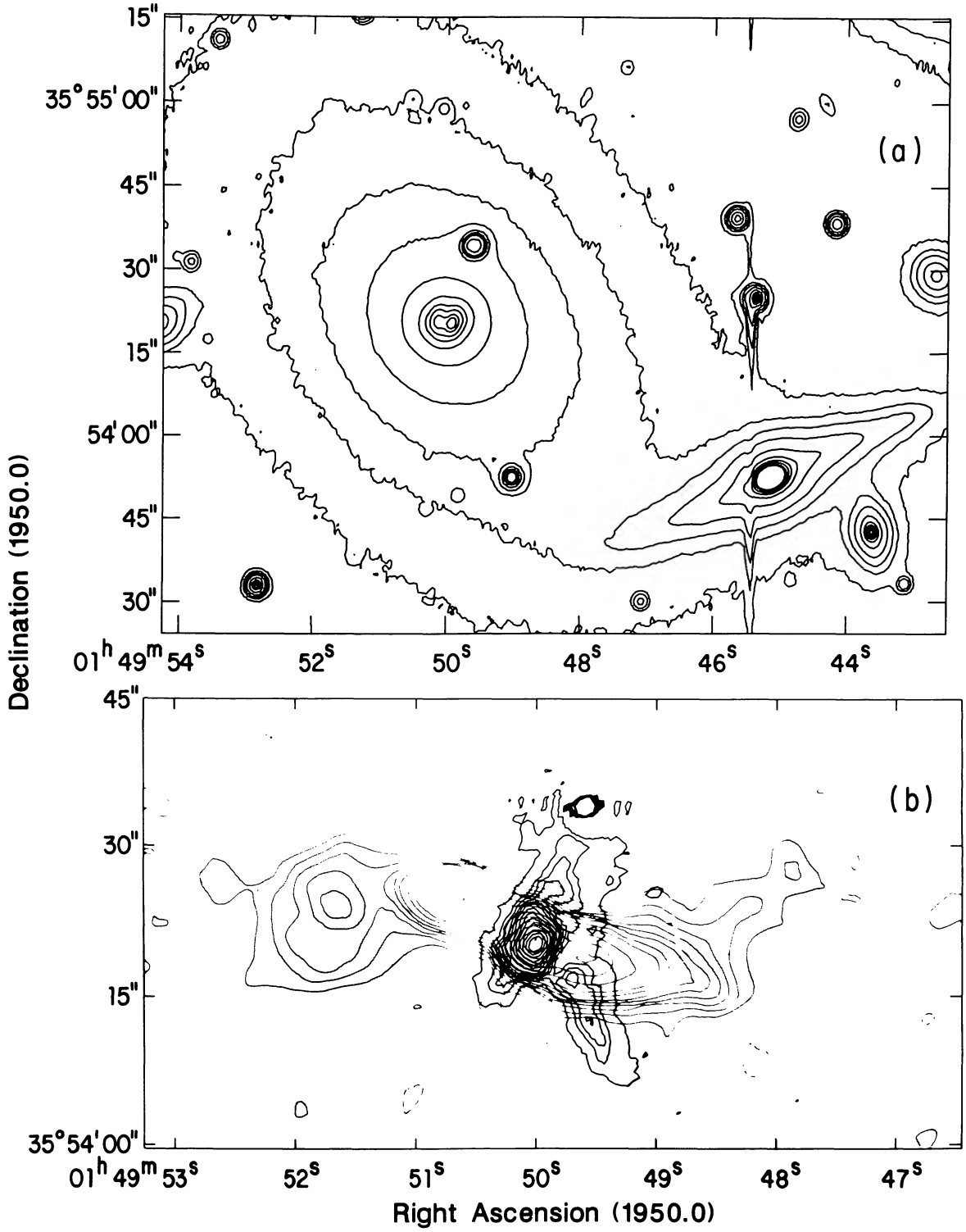


FIG. 4.—B2 0149+358. (*a*) Contours of the *R*-band optical image of NGC 708, the host galaxy of B2 0149+358. Levels are $1\times10^{-16}\times(-15, 15, 30, 50, 100, 250, 500, 700, 850, 1000, 1100, 3000)$ ergs $s^{-1}$ $cm^{-2}$ $arcsec^{-2}$. (*b*) Overlay of the contours of the H$\alpha$+[N II] emission (*dark lines*) on the contours of the 20 cm B array VLA image (*light lines*) (reproduced from Baum and Heckman 1987). H$\alpha$+[N II] contours are at levels of $1.5\times10^{-17}\times(3, 10, 15, 20, 25, 30, 40, 50, 60, 75, 100, 125, 150, 200, 300)$ ergs $s^{-1}$ $cm^{-2}$ $arcsec^{-2}$. Radio contour levels are $1.5\times10^{-1}\times(-2, 2, 4, 6, 8, 10, 12, 16, 20, 30, 40, 50, 60, 70, 80, 90, 100)$ mJy per restoring beam (4″ FWHM circular Gaussian).



© American Astronomical Society • Provided by the NASA Astrophysics Data System

1988ApJS...68..643B

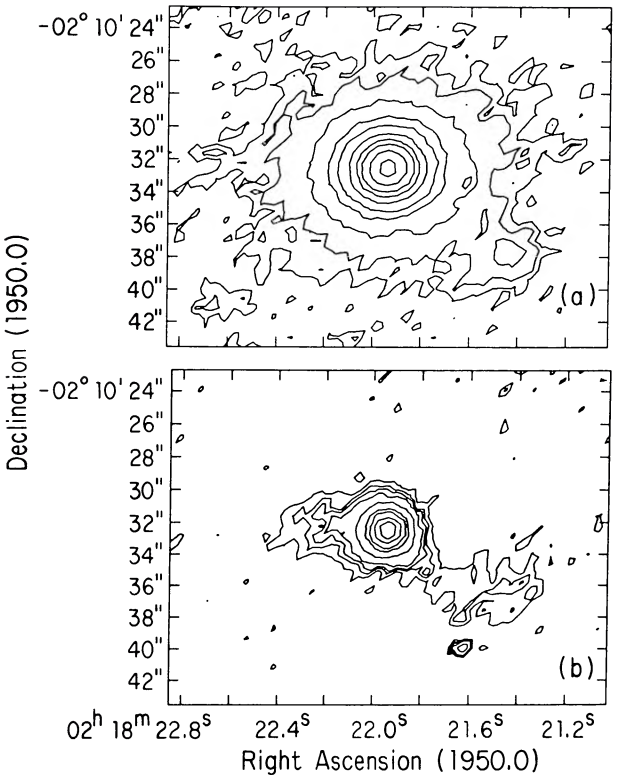


FIG. 5.—3C 63. (*a*) Contours of the *R*-band optical image of the host galaxy of 3C 63. Levels are $1\times10^{-16}\times(-3, 3, 5, 10, 20, 30, 50, 75, 100, 150, 225)$ ergs $s^{-1}$ $cm^{-2}$ $arcsec^{-2}$. (*b*) Contours of the H$\alpha$+[N II] image. Levels are $1\times10^{-17}\times(-8, 8, 12, 15, 20, 40, 75, 100, 150, 200)$ ergs $s^{-1}$ $cm^{-2}$ $arcsec^{-2}$.

© American Astronomical Society • Provided by the NASA Astrophysics Data System

1988ApJS...68..643B

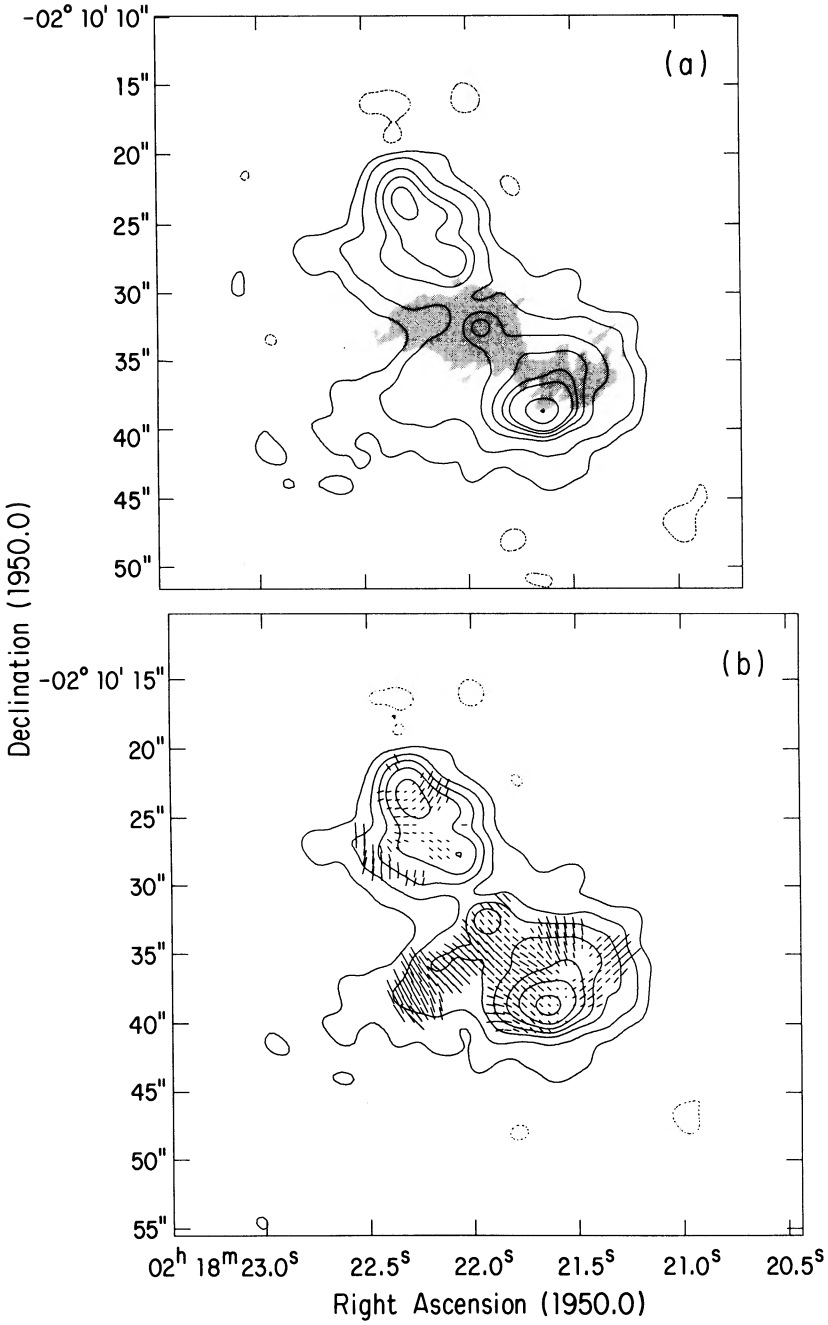


FIG. 6.—3C 63. (*a*) Silhouette of the H$\alpha$+[N II] image superposed on the contours of the 6 cm B array radio image. The radio contours are $3\times10^{-1}\times(-3, 3, 10, 30, 50, 75, 100, 200, 300, 400, 500, 750, 1000)$ mJy per restoring beam (1″.85 FWHM circular Gaussian). (*b*) Contours of the 6 cm VLA B array image. Levels are $3.5\times10^{-1}\times(-3, 3, 10, 20, 35, 60, 100, 200)$ mJy per restoring beam (1″.85 FWHM circular Gaussian). The lengths of the superposed vectors indicate the fractional polarization, and their orientations give the direction of the projected electric field. A vector of length 1″ represents a fractional polarization of 33%.



© American Astronomical Society • Provided by the NASA Astrophysics Data System

1988ApJS...68..643B

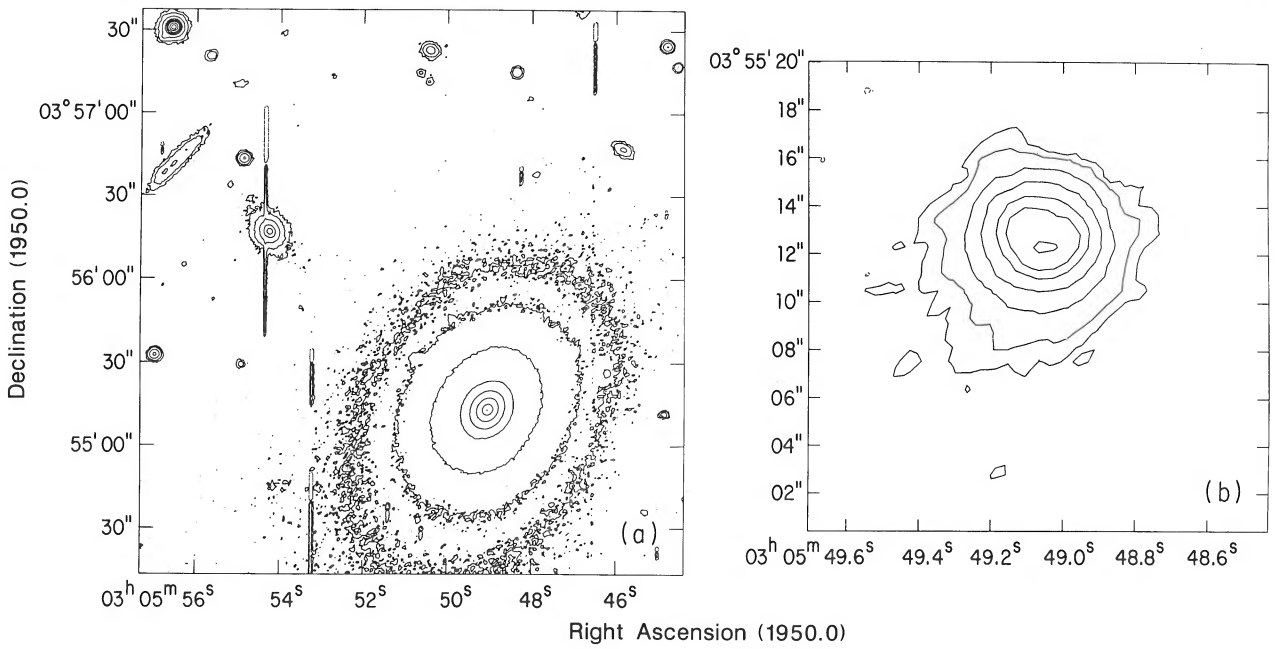


FIG. 7.—3C 78. (*a*) Contours of the *V*-band optical image of the host galaxy of 3C 78. Levels are $1\times10^{-16}\times(-5, 5, 10, 30, 100, 200, 400, 1000, 2000)$ ergs $s^{-1}$ $cm^{-2}$ arcsec$^{-2}$. (*b*) Contours of the H$\alpha$+[N II] emission. Levels are $1\times10^{-17}\times(-5, 5, 10, 25, 50, 90, 125, 185)$ ergs $s^{-1}$ $cm^{-2}$ arcsec$^{-2}$.



© American Astronomical Society • Provided by the NASA Astrophysics Data System

1988ApJS...68..643B

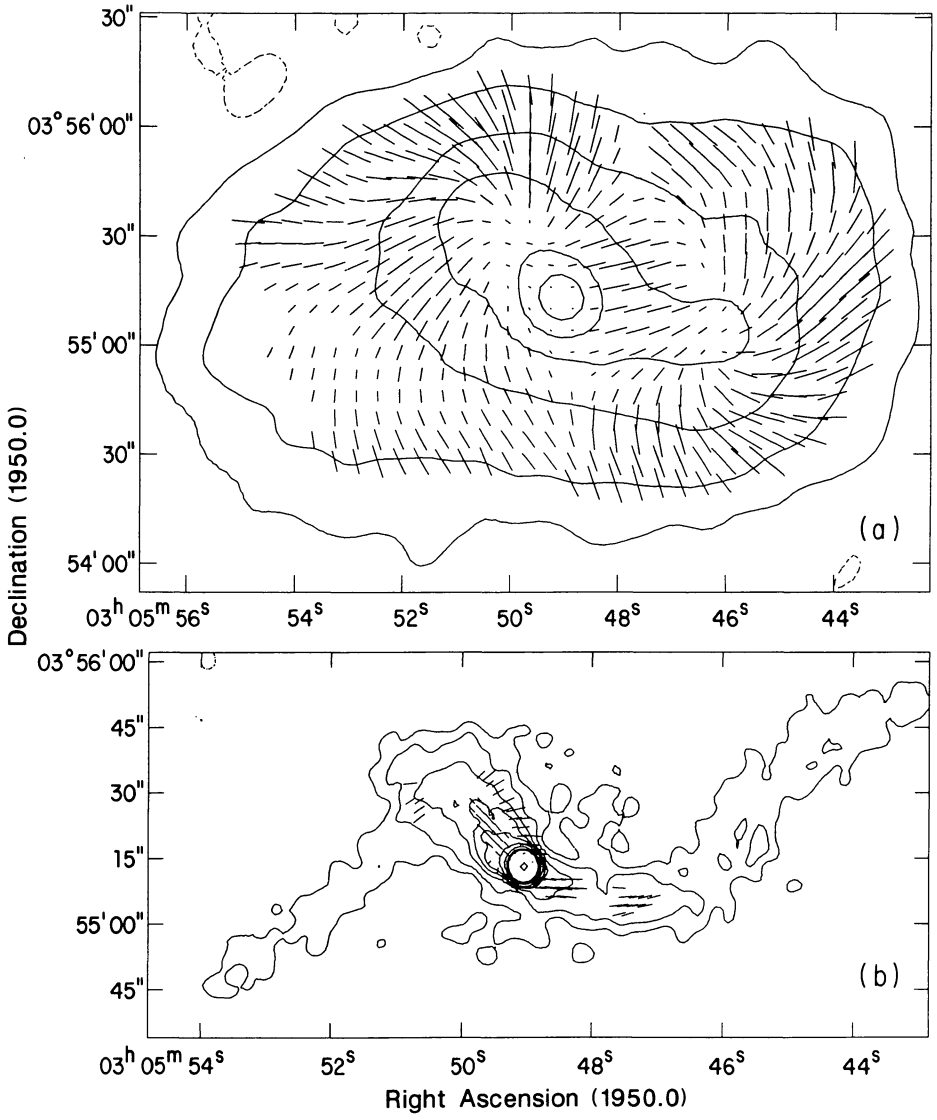


FIG. 8.—3C 78. (*a*) Contours of the 20 cm C array VLA image of 3C 78. Levels are $5.7\times10^{-1}\times(-3, 3, 25, 100, 200, 600, 1500)$ mJy per restoring beam (13".1×12".7 FWHM elliptical Gaussian). The lengths of the superposed vectors indicate the fractional polarization and their orientations give the direction of the projected electric field. A vector of length 1" represents a fractional polarization of 4.2%. (*b*) Contours of the 6 cm C array VLA image. Levels are (−3, 3, 5, 10, 15, 20, 30, 50, 75, 100, 750) mJy per restoring beam (3".5 FWHM circular Gaussian). The lengths of the superposed vectors indicate the fractional polarization, and their orientations give the direction of the projected electric field. A vector of length 1" represents a fractional polarization of 8.3%.

© American Astronomical Society • Provided by the NASA Astrophysics Data System

1988ApJS...68..643B

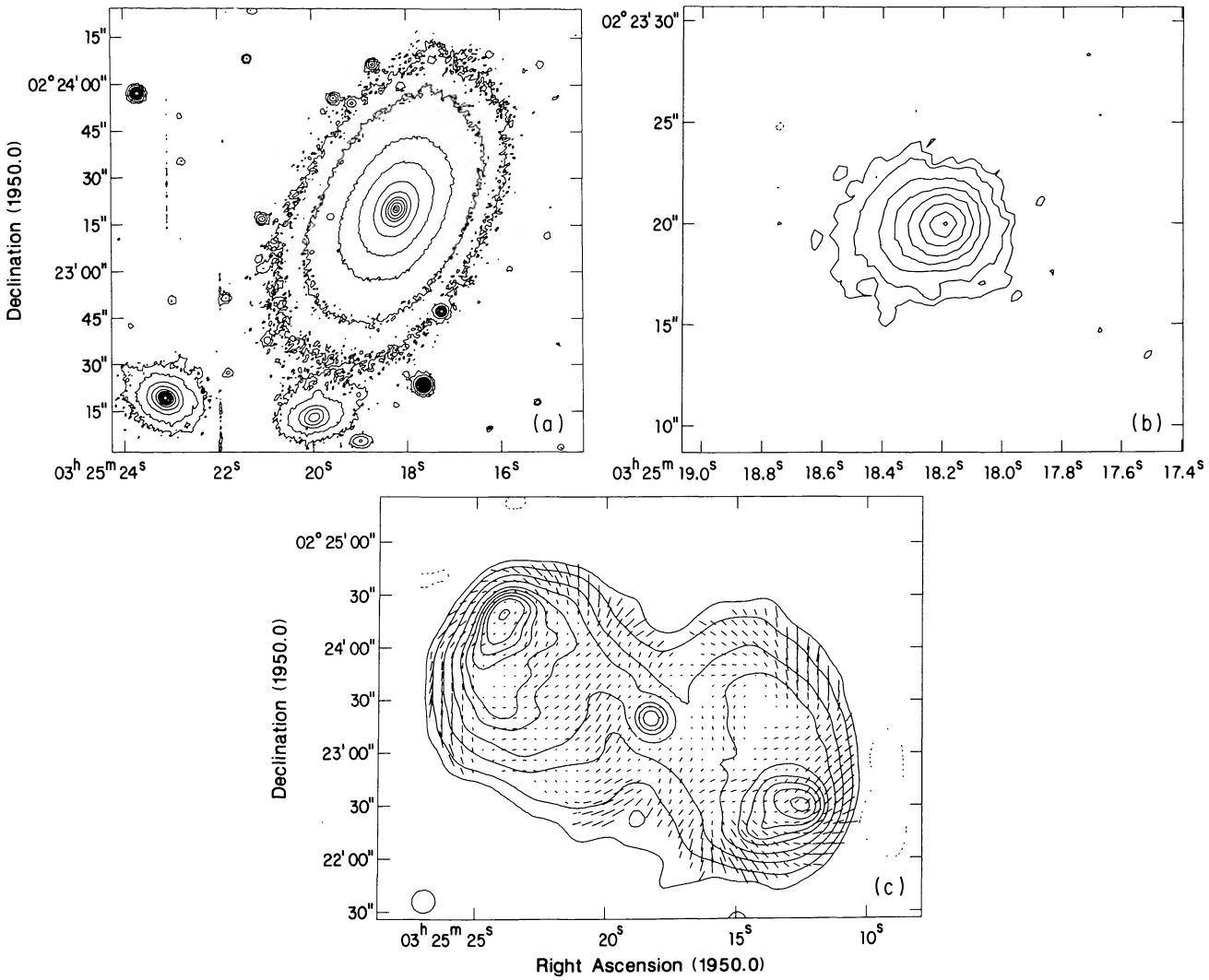


FIG. 9.—3C 88. (*a*) Contours of the *V*-band optical image of the host galaxy of 3C 88. Levels of $1\times10^{-16}\times(-3, 3, 6, 15, 30, 60, 100, 150, 200, 300, 450, 550)$ ergs $s^{-1}$ $cm^{-2}$ $arcsec^{-2}$. (*b*) Contours of the H$\alpha$+[N II] emission at levels of $1\times10^{-17}\times(-5, 5, 10, 25, 50, 100, 200, 350, 500)$ ergs $s^{-1}$ $cm^{-2}$ $arcsec^{-2}$. (*c*) Contours of the 20 cm C array VLA image of 3C 88. Levels are $8.5\times10^{-1}\times(-3, 3, 10, 30, 60, 100, 125, 150, 175, 200, 250)$ mJy per restoring beam (18″ FWHM circular Gaussian). The lengths of the superposed vectors indicate the fractional polarization, and their orientations give the direction of the projected electric field. A vector of length 1″ represents a fractional polarization of 4.2%.

© American Astronomical Society • Provided by the NASA Astrophysics Data System

1988ApJS...68..643B

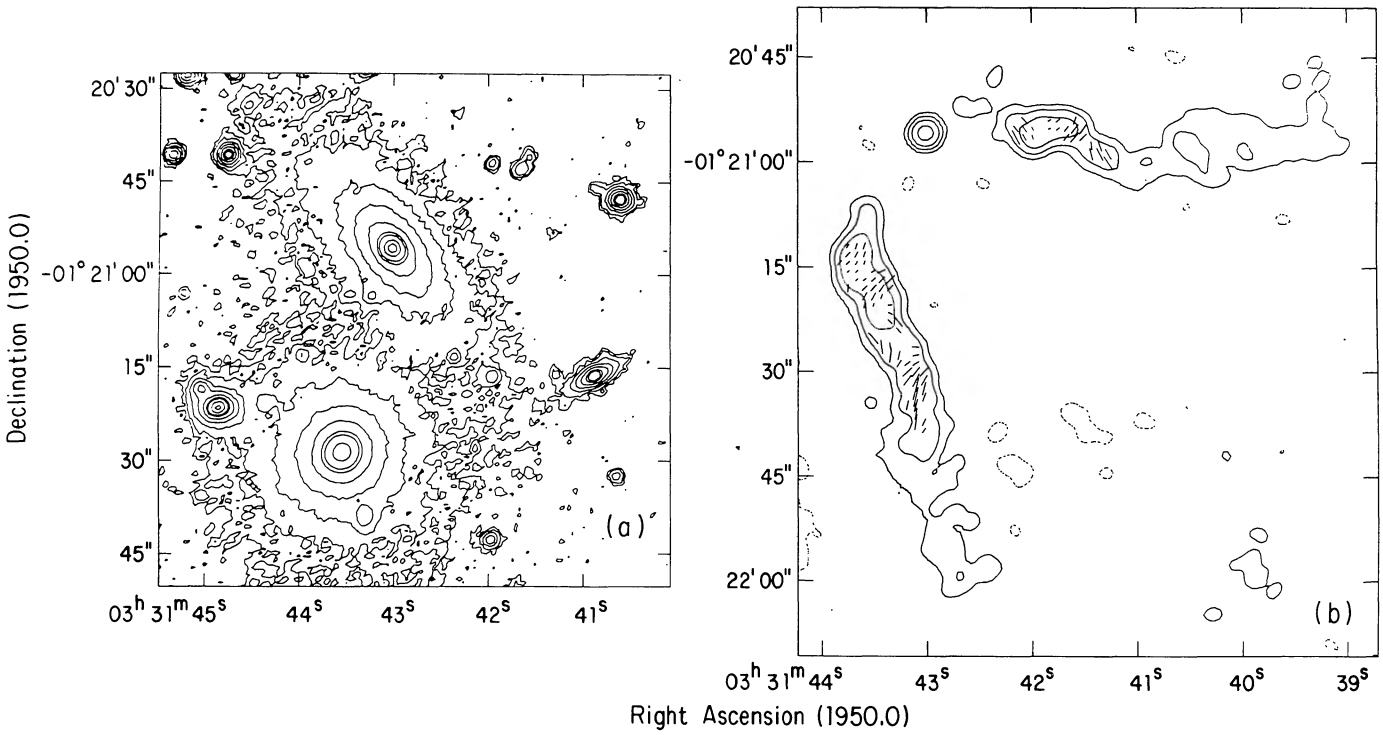


FIG. 10.—3C 89. (*a*) Contours of the *R*-band optical image of the host galaxy of 3C 89. Levels are $1\times10^{-16}\times(-3, 3, 5, 10, 20, 40, 75, 100, 200, 350, 750, 1000)$ ergs $s^{-1}$ $cm^{-2}$ $arcsec^{-2}$. (*b*) Contours of the 6 cm B array VLA image of 3C 98. Levels are $2.3\times10^{-1}\times(-3, 3, 10, 30, 100, 200, 500)$ mJy per restoring beam (3".8 FWHM circular Gaussian). The lengths of the superposed vectors indicate the fractional polarization, and their orientations give the direction of the projected electric field. A vector of length 1" represents a fractional polarization of 16.7%.

© American Astronomical Society • Provided by the NASA Astrophysics Data System

1988ApJS...68..643B

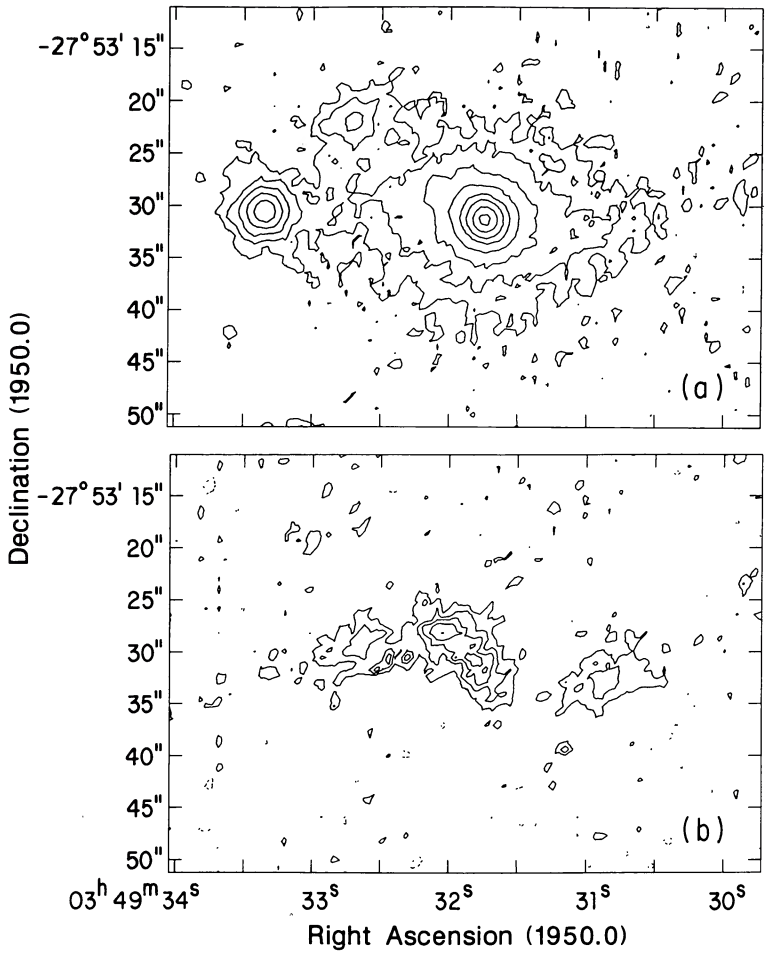


FIG. 11.—PKS 0349−278. (*a*) Contours of the *V*-band optical image of the host galaxy of PKS 0349−278. Levels are (−2, 2, 4, 8, 15, 25, 35, 50, 65) in arbitrary units. (*b*) Contours of the [O III] emission. Levels are $1\times10^{-16}\times(-2, 2, 4, 6, 8, 11)$ ergs $s^{-1}$ $cm^{-2}$ $arcsec^{-2}$. Calibrated using spectrophotometry from Danziger *et al.* (1984).

© American Astronomical Society • Provided by the NASA Astrophysics Data System

1988ApJS...68..643B

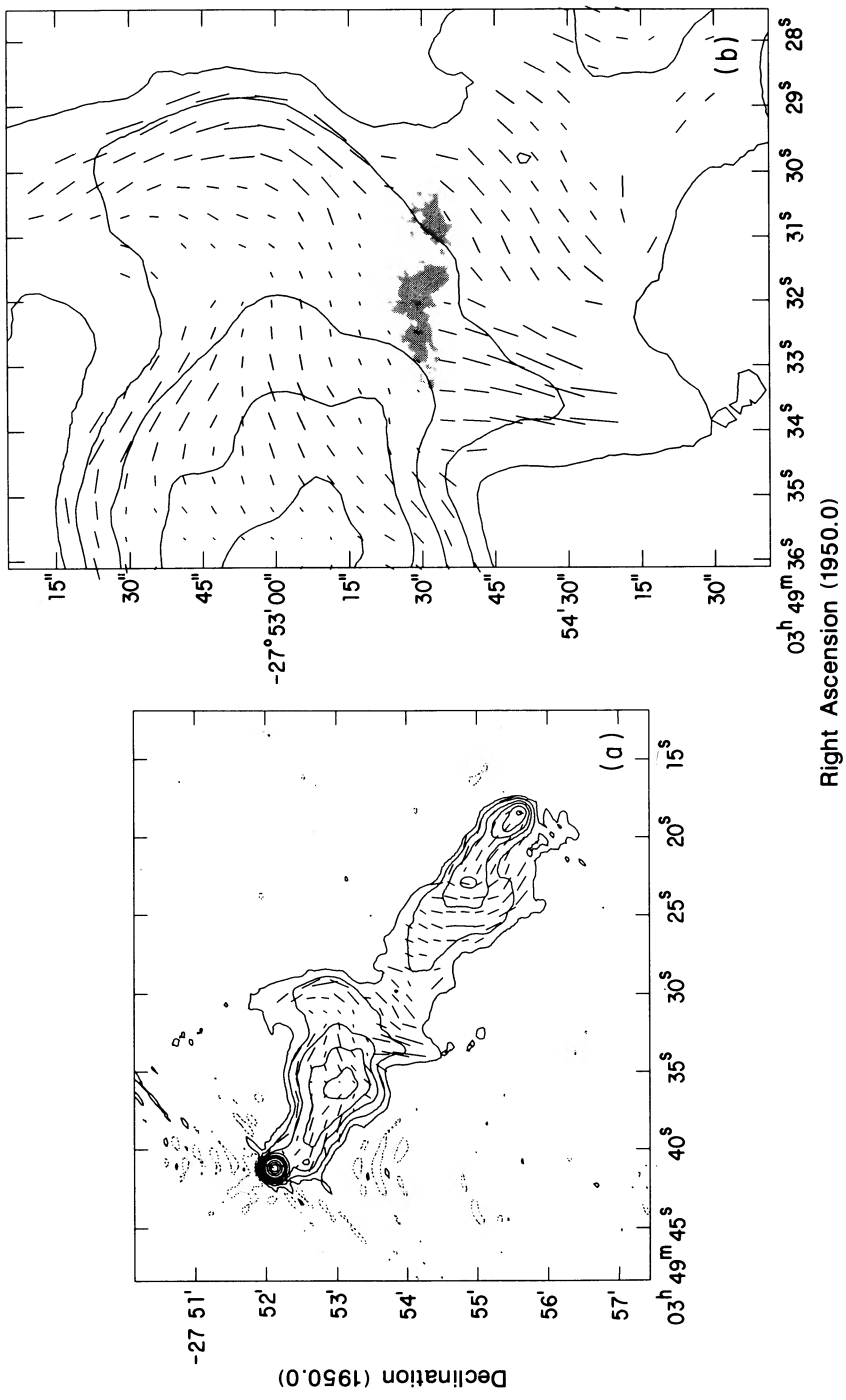


FIG. 12.—PKS 0349 – 278. (*a*) Contours of the 20 cm combined B and C array VLA image. Levels are $3.5\times10^{-1}\times(-3, 3, 15, 50, 100, 200, 350, 500, 1000, 1500, 2000, 2500)$ mJy per restoring beam (10″ FWHM circular Gaussian). The lengths of the superposed vectors indicate the fractional polarization, and their orientations give the direction of the projected electric field. A vector of length 1″ represents a fractional polarization of 2.8%. (*b*) Silhouette of the [O III] emission superposed on the 20 cm combined B and C array VLA image. The radio contours are the same as in (*a*). A vector of length 1″ represents a fractional polarization of 8.3%.



© American Astronomical Society • Provided by the NASA Astrophysics Data System

1988ApJS...68..643B

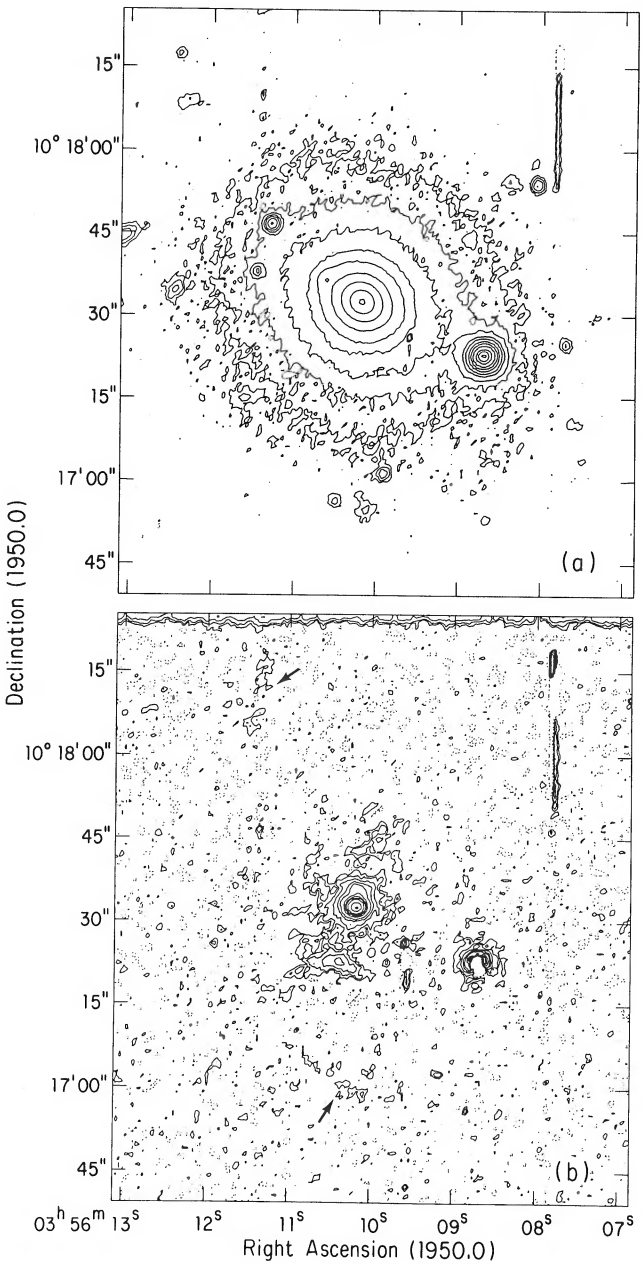


FIG. 13.—3C 98. (*a*) Contours of the *R*-band optical image of the host galaxy of 3C 98. Levels are $1\times10^{-16}\times(-4, 4, 8, 15, 30, 50, 100, 200, 500, 2000, 5000, 10000)$ ergs $s^{-1}$ $cm^{-2}$ $arcsec^{-2}$. (*b*) Contours of the H$\alpha$ + [N II] image. Levels are $1\times10^{-17}\times(-2, 2, 4, 8, 15, 25, 50, 75, 100, 150, 300, 500, 1000)$ ergs $s^{-1}$ $cm^{-2}$ $arcsec^{-2}$. Arrows indicate the location of very faint emission-line gas which we have confirmed spectroscopically.



© American Astronomical Society • Provided by the NASA Astrophysics Data System

1988ApJS...68..643B

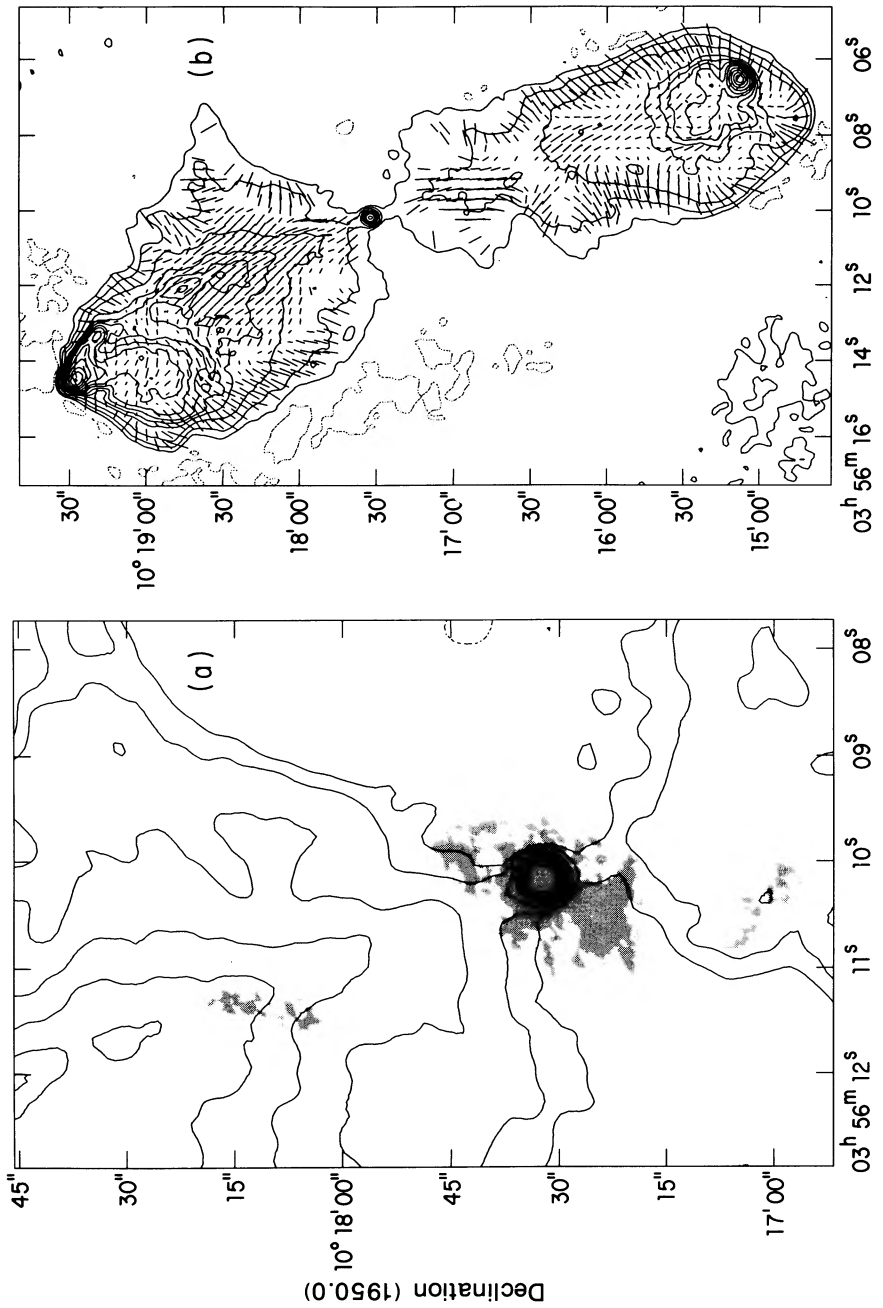


FIG. 14.—3C 98. (*a*) Silhouette of the H$\alpha$+[N II] emission superposed on the contours of the 6 cm VLA C array radio image. The radio contours are at levels of $8.5\times10^{-2}\times(-3, 3, 6, 15, 30, 50, 75, 100)$ mJy per restoring beam (3".8 FWHM circular Gaussian). (*b*) Contours of the 6 cm C VLA image of 3C 98. Levels are $8.5\times10^{-2}\times(-3, 3, 10, 25, 50, 65, 80, 100, 125, 175, 250, 350, 450, 580)$ mJy per restoring beam (3".8 FWHM circular Gaussian). The lengths of the superposed vectors indicate the fractional polarization, and their orientations give the direction of the projected electric field. A vector of length 1" represents a fractional polarization of 6.7%.



© American Astronomical Society • Provided by the NASA Astrophysics Data System

1988ApJS...68..643B

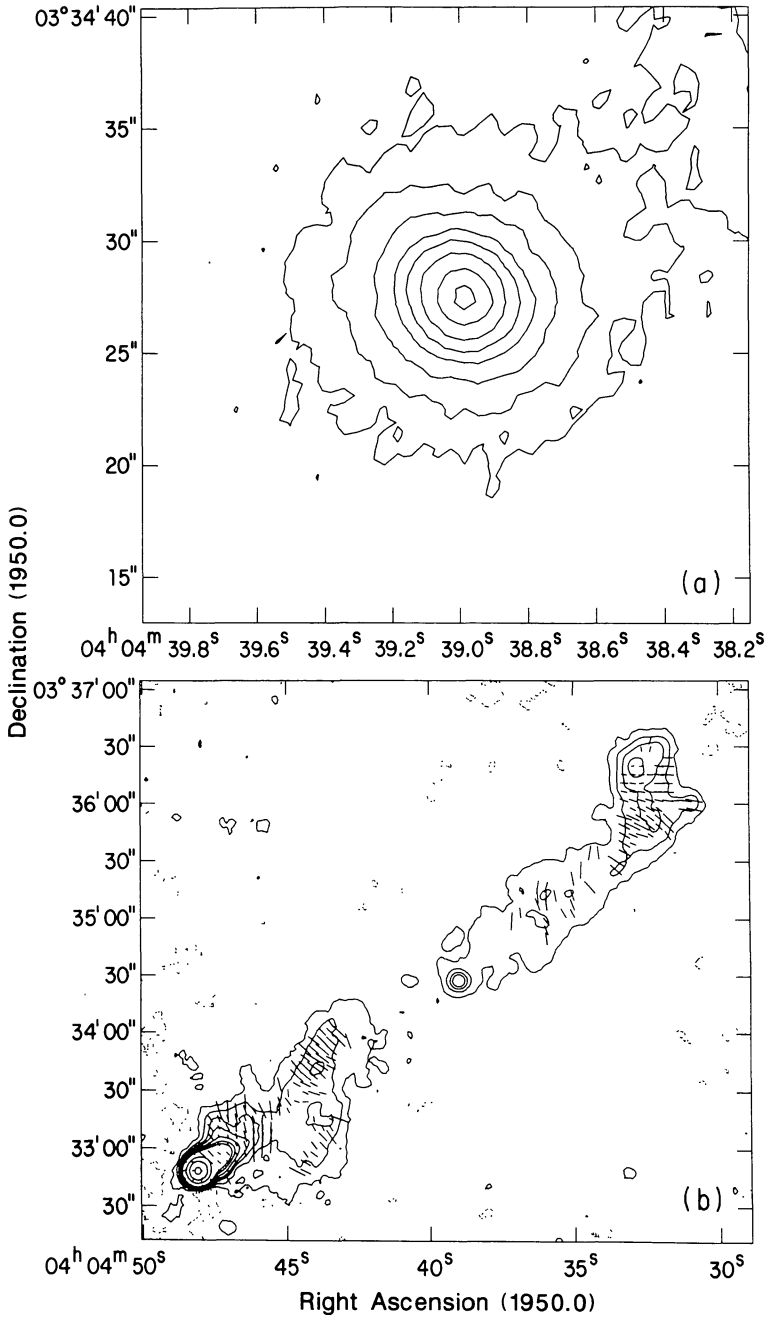


FIG. 15.—3C 105. (*a*) Contours of the *R*-band optical image of the host galaxy of 3C 105. Levels are $1\times10^{-16}\times(-4, 4, 8, 15, 25, 35, 50, 75, 100)$ ergs $s^{-1}$ $cm^{-2}$ $arcsec^{-2}$. (*b*) Contours of the 6 cm combined C and D array VLA image of 3C 105. Levels are $3.6\times10^{-1}\times(-3, 3, 10, 20, 30, 50, 75, 100, 400, 1000, 2500)$ mJy per restoring beam (7″ FWHM circular Gaussian). The lengths of the superposed vectors indicate the fractional polarization, and their orientations give the direction of the projected electric field. A vector of length 1″ represents a fractional polarization of 4.4%.

© American Astronomical Society • Provided by the NASA Astrophysics Data System

1988ApJS...68..643B

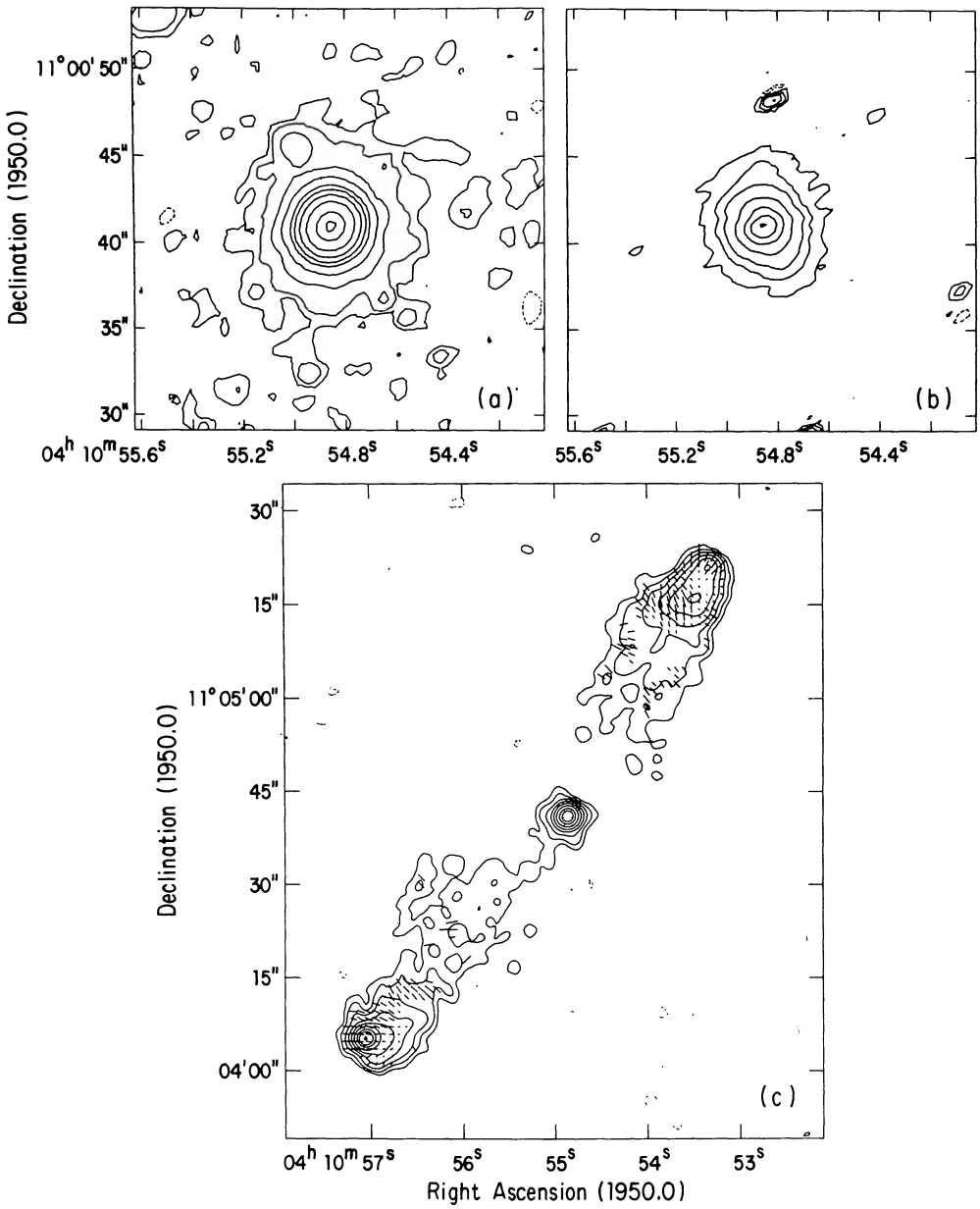


FIG. 16.—3C 109. (*a*) Contours of the *V*-band optical image of the host galaxy of 3C 109. Levels are $1\times10^{-16}\times(-1, 1, 2, 5, 10, 20, 30, 50, 100, 250, 400)$ ergs $s^{-1}$ $cm^{-2}$ $arcsec^{-2}$. (*b*) Contours of the [O III] emission. Levels are $1\times10^{-16}\times(-1, 1, 3, 6, 15, 30, 45, 60)$ ergs $s^{-1}$ $cm^{-2}$ $arcsec^{-2}$. (*c*) Contours of the 6 cm combined B and C array VLA image of 3C 109. Levels are $5.0\times10^{-1}\times(-3, 3, 6, 12, 25, 50, 100, 200, 300, 500)$ mJy per restoring beam (2".25 FWHM circular Gaussian). The lengths of the superposed vectors indicate the fractional polarization, and their orientations give the direction of the projected electric field. A vector of length 1" represents a fractional polarization of 16.7%.

© American Astronomical Society • Provided by the NASA Astrophysics Data System

1988ApJS...68..643B

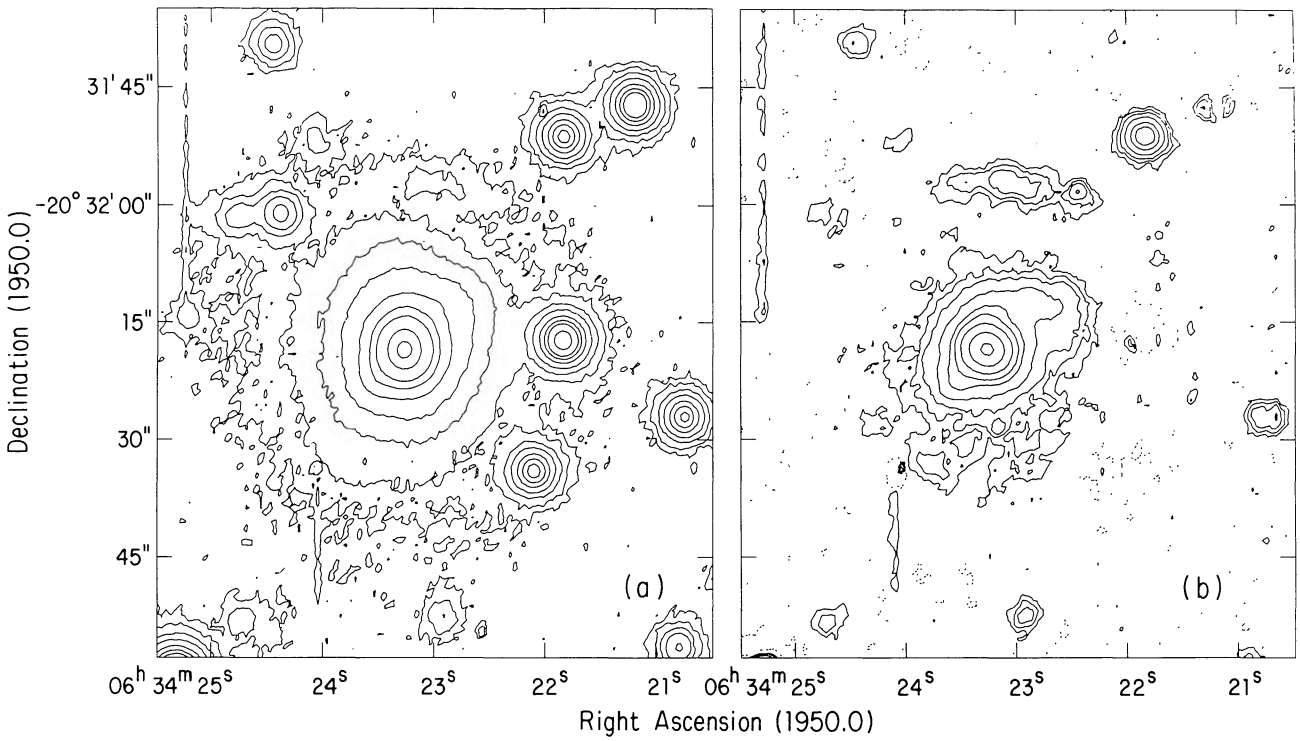


FIG. 17.—PKS 0634−206. (*a*) Contours of the *V*-band optical image of the host galaxy of PKS 0634−206. Levels are $1\times10^{-16}\times(-2, 2, 4, 8, 15, 30, 50, 75, 150, 250, 500, 1000)$ ergs $s^{-1}$ $cm^{-2}$ $arcsec^{-2}$. (*b*) Contours of the H$\alpha$ + [N II] image. Levels are $1\times10^{-17}\times(-1.5, 1.5, 3, 5, 10, 20, 30, 50, 100, 200, 500, 1000, 2000)$ ergs $s^{-1}$ $cm^{-2}$ $arcsec^{-2}$.

© American Astronomical Society • Provided by the NASA Astrophysics Data System

1988ApJS...68..643B

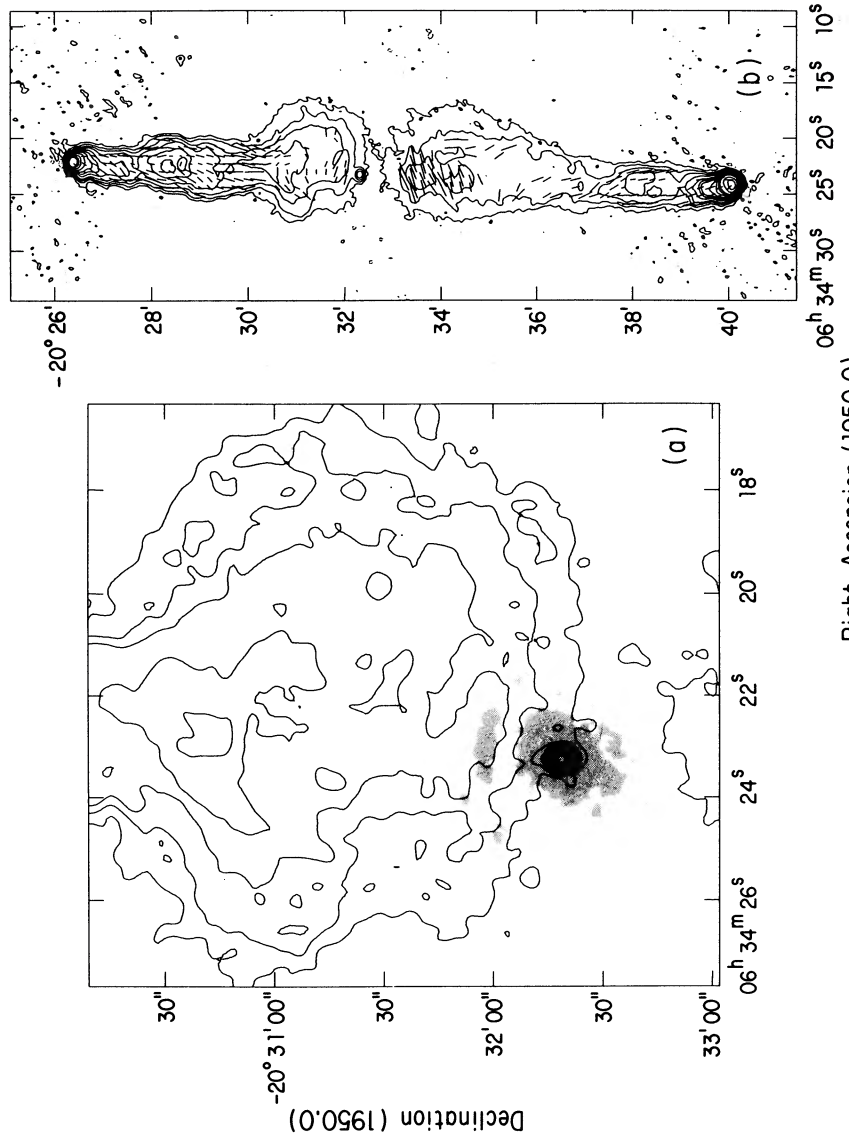


FIG. 18.—PKS 0634 – 206. (*a*) Silhouette of the emission-line image superposed on the contours of the 20 cm combined A/B, B/C, and D array VLA image. Radio levels are $1\times10^{-1}\times(-1, 1, 3, 6, 12, 20, 30, 45, 60, 75, 100)$ mJy per pixel. The pixel size is 1″. The resolution element, or beam, is a 3″.87 × 3″.64 FWHM elliptical Gaussian with its major axis along P.A. 26°.3. (*b*) Contours of the 20 cm B/C array VLA image. Levels are $1.3\times10^{-1}\times(-3, 3, 10, 25, 50, 100, 150, 200, 300, 500, 750, 1000, 2000, 3500, 5500)$ mJy per restoring beam (10″ × 7″ FWHM elliptical Gaussian with major axis along P.A. 80°). The lengths of the superposed vectors indicate the fractional polarization, and their orientations give the direction of the projected electric field. A vector of length 1″ represents a fractional polarization of 2.5%.



© American Astronomical Society • Provided by the NASA Astrophysics Data System

1988ApJS...68..643B

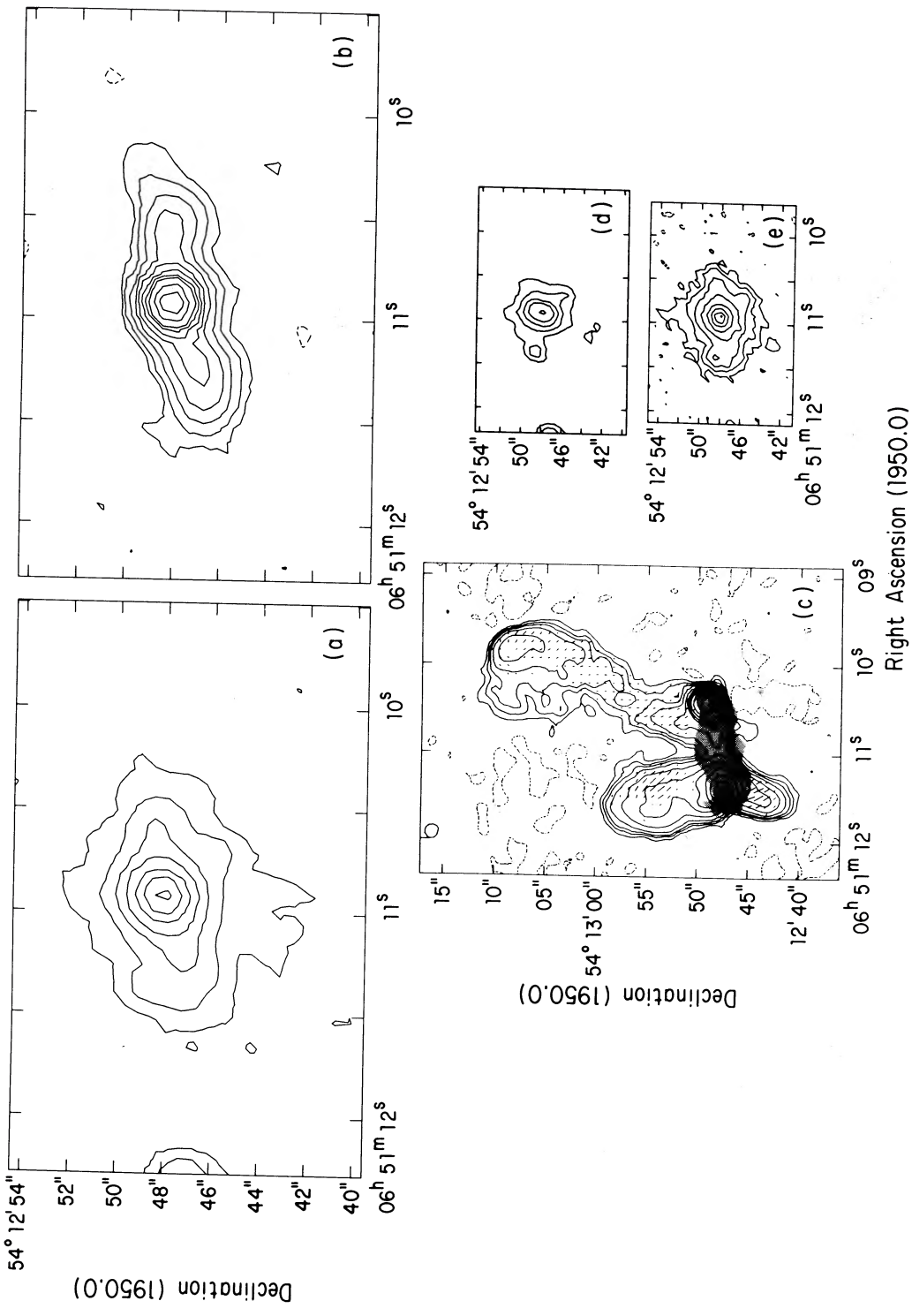


FIG. 19.—3C 171. (*a*) Contours of the *R*-band image of the host galaxy of 3C 171. Levels are $1\times10^{-16}\times(-4, 4, 10, 20, 35, 65, 100, 150)$ ergs $s^{-1}$ $cm^{-2}$ $arcsec^{-2}$. (*b*) Contours of the [O III] emission. Levels are $1\times10^{-17}\times(-12, 12, 24, 45, 75, 120, 180, 240, 300, 450, 600)$ ergs $s^{-1}$ $cm^{-2}$ $arcsec^{-2}$. Calibrated using spectrophotometry of Yee and Oke (1978). (*c*) Silhouette of the [O III] emission superposed on contours of the 20 cm A array VLA image, reproduced from Heckman, van Breugel, and Miley (1984). Radio contours are at $(-1, 1, 2, 3, 5, 10, 20, 30, 50, 100, 250, 500, 1000)$ mJy per restoring beam (1".1 FWHM circular Gaussian). (*c*) Contours of the "line-free" *R*-band optical image (i.e., following subtraction of a flux-scaled version of the [O III] image to remove contaminating emission lines). Levels are $1\times10^{-16}\times(-6, 6, 12, 20, 30, 50)$ ergs $s^{-1}$ $cm^{-2}$ $arcsec^{-2}$. (*e*) Contours of the *V*-band optical image of the host galaxy of 3C 171. Levels are $(-2, 4, 8, 15, 30, 60, 100, 140, 175)$ in arbitrary units.



© American Astronomical Society • Provided by the NASA Astrophysics Data System

1988ApJS...68..643B

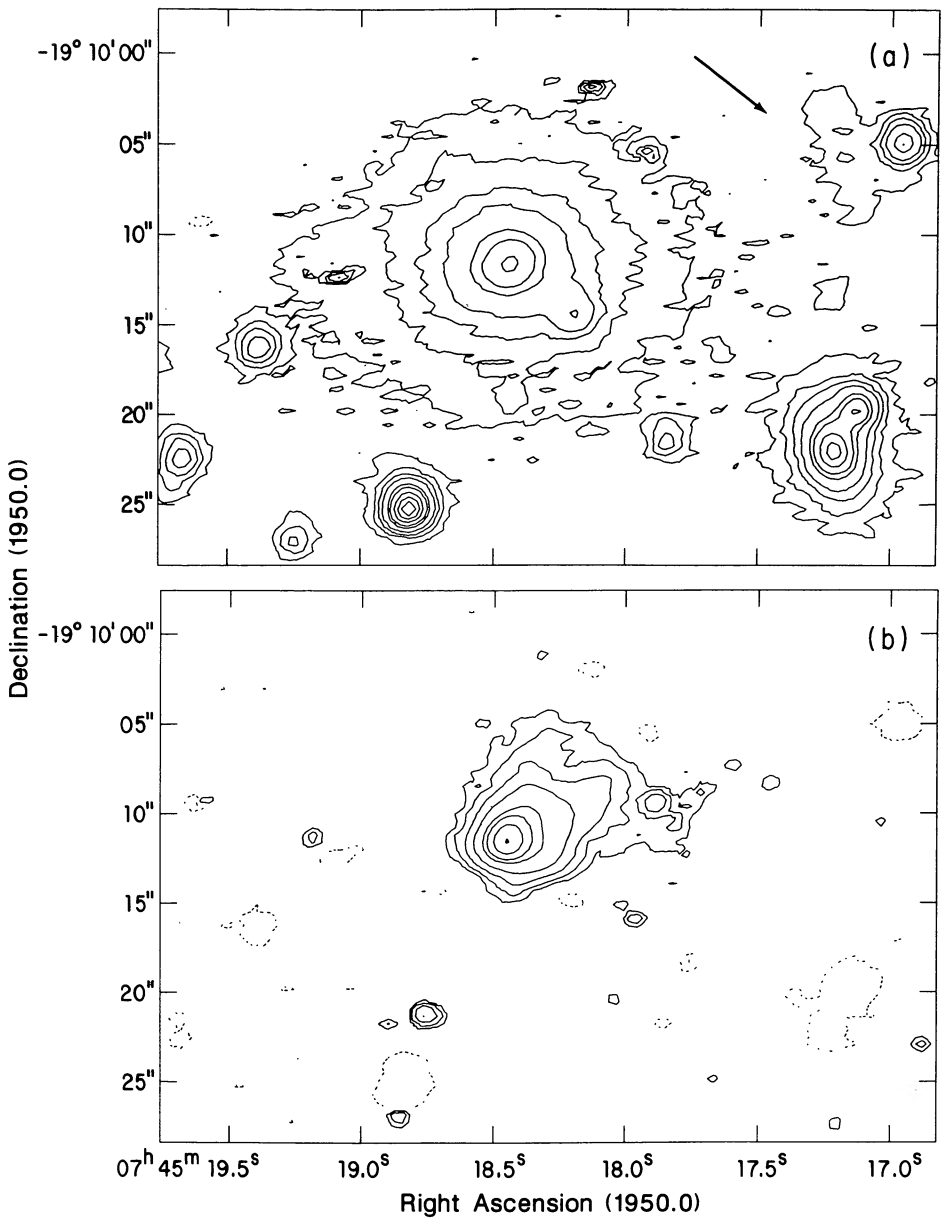


FIG. 20.—PKS 0745−191. (*a*) Contours of the *R*-band optical image of the host galaxy of PKS 0745−191. Levels are $1\times10^{-15}\times(-1.5, 1.5, 3, 5, 8, 15, 20, 30, 40, 50)$ ergs $s^{-1}$ $cm^{-2}$ $arcsec^{-2}$. The arrow points out the unusual arc of emission in the broad-band image. (*b*) Contours of the Hα+[N II] emission at levels of $1\times10^{-16}\times(-1.5, 1.5, 3, 6, 12, 25, 35, 55, 85)$ ergs $s^{-1}$ $cm^{-2}$ $arcsec^{-2}$.

© American Astronomical Society • Provided by the NASA Astrophysics Data System

1988ApJS...68..643B

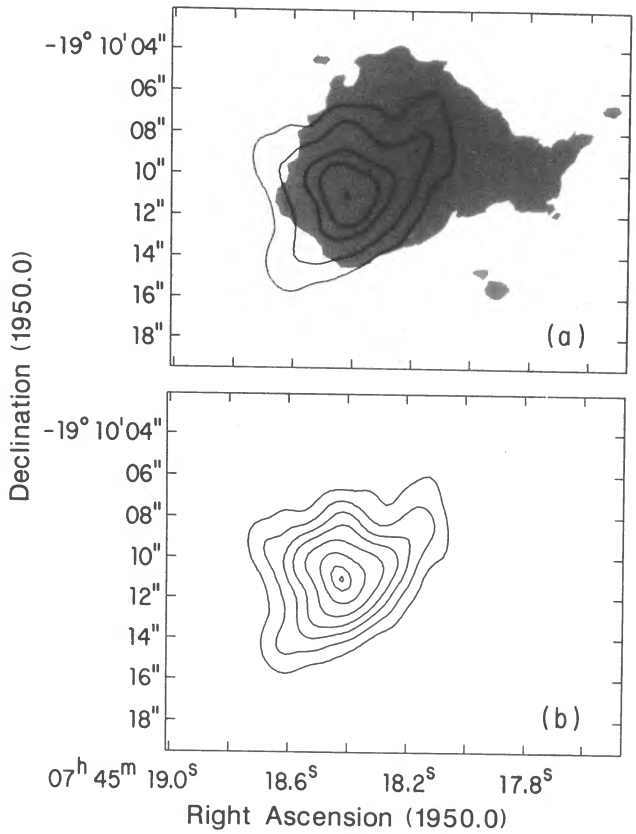


FIG. 21.—PKS 0745−191. (*a*) Silhouette of the Hα + [N II] emission superposed on contours of the 20 cm A array VLA radio image. Radio contours are at levels of 1.4×(−3, 3, 15, 75, 150, 425) mJy per restoring beam (1".76×1".15 FWHM elliptical Gaussian with major axis along P.A. 21°). (*b*) Contours of the 20 cm A array VLA radio image. Radio contours are at levels 1.4×(−3, 3, 10, 25, 50, 100, 200, 350, 425) mJy per restoring beam. The radio image is taken from Baum, O'Dea, and Killeen (1988).



© American Astronomical Society • Provided by the NASA Astrophysics Data System

© American Astronomical Society • Provided by the NASA Astrophysics Data System



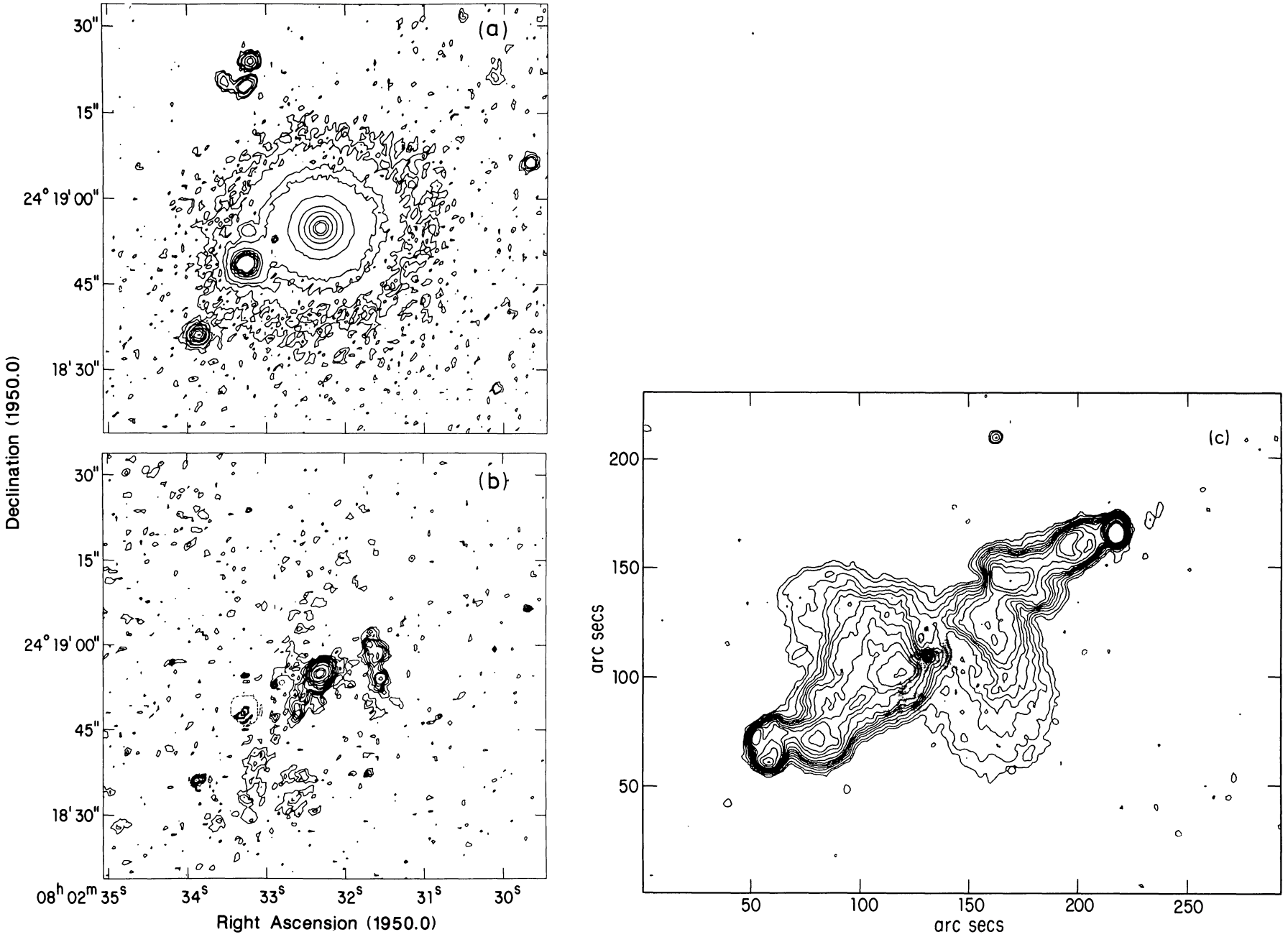


FIG. 22.—3C 192. (*a*) Contours of the *R*-band optical image of the host galaxy of 3C 192. Levels are $1\times10^{-16}\times(-3, 3, 5, 10, 15, 40, 80, 150, 300, 650, 1000)$ ergs $s^{-1}$ $cm^{-2}$ $arcsec^{-2}$. (*b*) Contours of the H$\alpha$ + [N II] emission. Levels are $1\times10^{-17}\times(-10, 2, 4, 6, 8, 10, 15, 20, 30, 50, 100, 300, 500, 1000)$ ergs $s^{-1}$ $cm^{-2}$ $arcsec^{-2}$. (*c*) Silhouette of the H$\alpha$ + [N II] emission superposed on contours of the 18 cm VLA image. Contours are (−0.5, 0.5, 1, 2, 3, 4, 5, 6, 7.5, 10, 12.5, 15, 20, 30, 40, 50) mJy per restoring beam (3″.9 FWHM circular Gaussian). The radio map was kindly provided by S. Spangler.

1988ApJS...68..643B

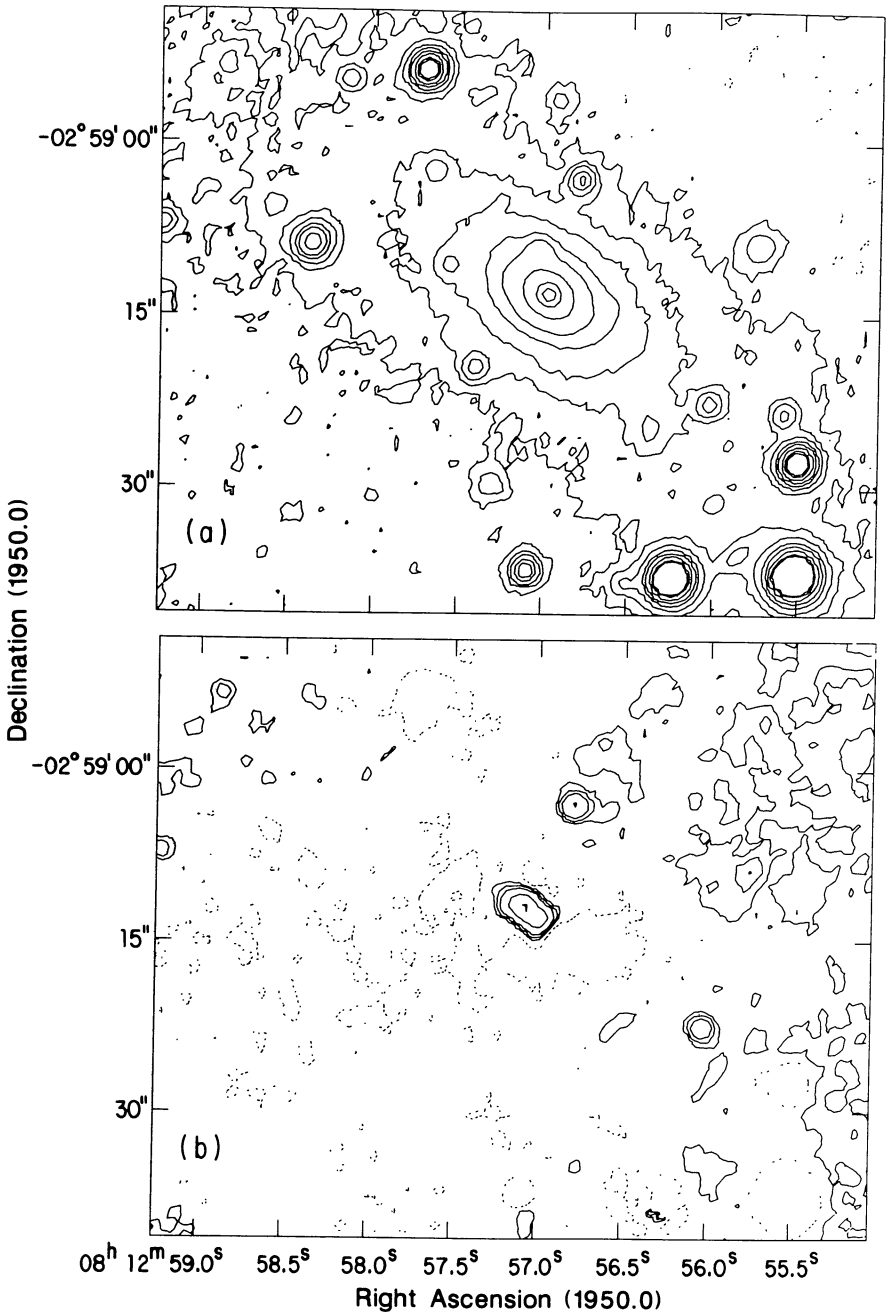


FIG. 23.—3C 196.1 (*a*) Contours of the *V*-band optical image of the host galaxy of 3C 196.1. Levels are $1\times10^{-16}\times(-1, 1, 3, 6, 12, 20, 40, 75, 100)$ ergs $s^{-1}$ $cm^{-2}$ $arcsec^{-2}$. (*b*) Contours of the H$\alpha$ + [N II] emission. Levels are $1\times10^{-17}\times(-5, 2, 6, 12, 35, 75)$ ergs $s^{-1}$ $cm^{-2}$ $arcsec^{-2}$.

© American Astronomical Society • Provided by the NASA Astrophysics Data System

1988ApJS...68..643B

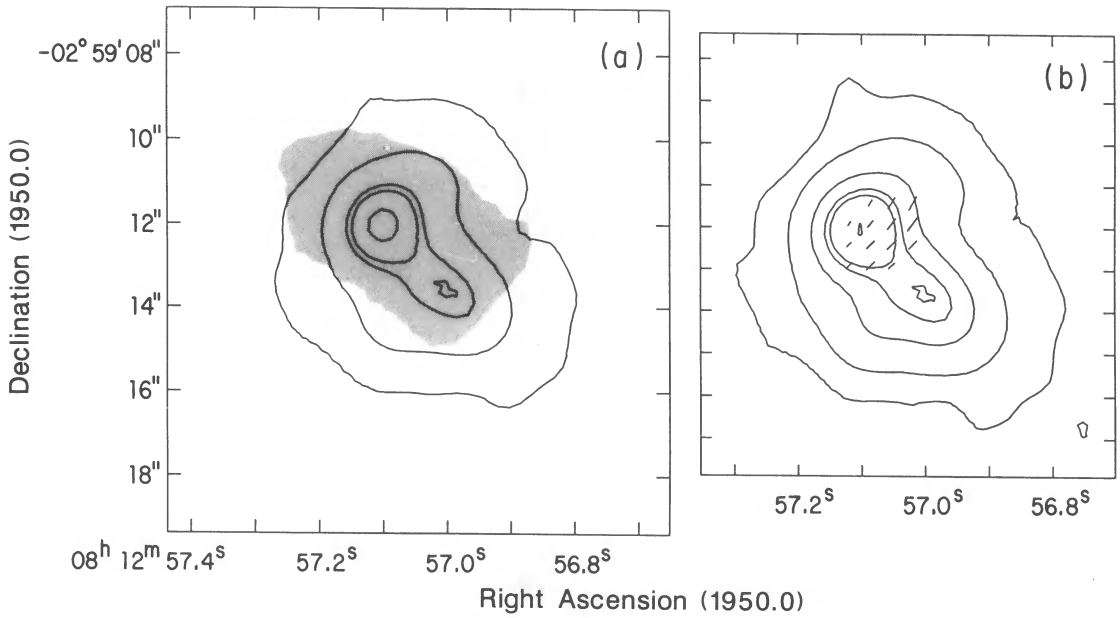


FIG. 24.—3C 196.1 (*a*) Silhouette of the Hα+[N II] emission superposed on contours of the 6 cm B array VLA image. (*b*) Contours of the 6 cm B array VLA image. Levels are $1.4\times10^{-1}\times(-3, 3, 40, 200, 400, 500, 900)$ mJy restoring beam (1″.4×1″.25 FWHM elliptical Gaussian with major axis along P.A. 28°). The lengths of the superposed vectors indicate the fractional polarization, and their orientations give the direction of the projected electric field. A vector of length 1″ represents a fractional polarization of 4.0%.



© American Astronomical Society • Provided by the NASA Astrophysics Data System

1988ApJS...68..643B

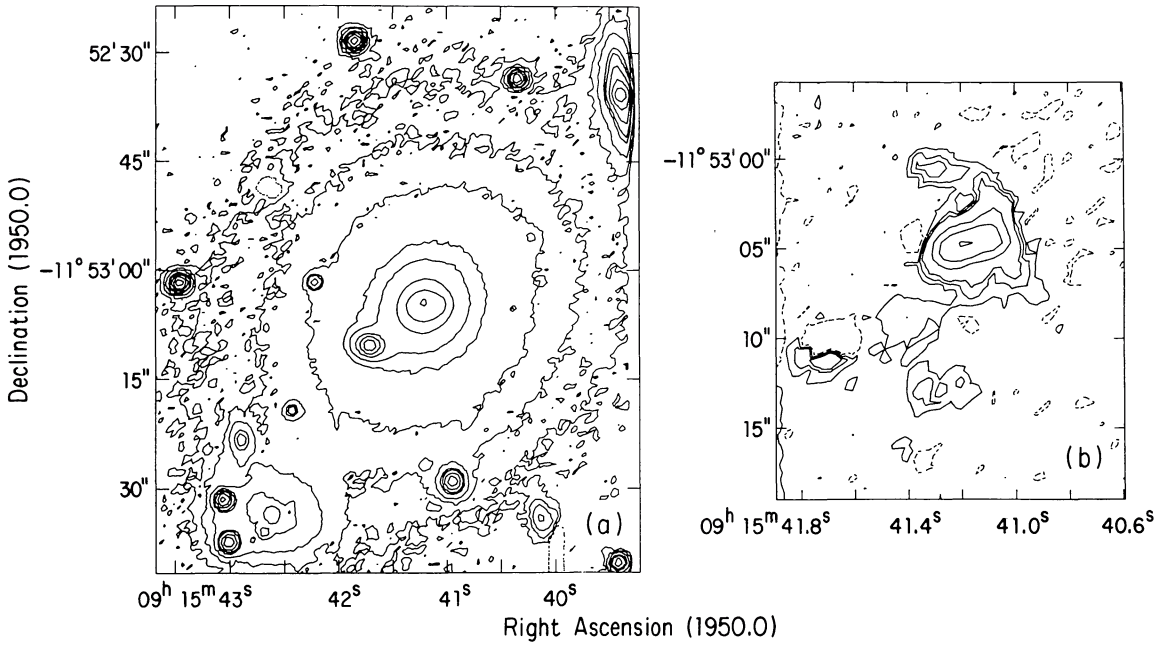


FIG. 25.—3C 218. (*a*) Contours of the *V*-band optical image of the host galaxy of 3C 218. Levels are $1\times10^{-16}\times(-5, 5, 10, 20, 50, 75, 150, 300, 600, 1000)$ ergs $s^{-1}$ $cm^{-2}$ $arcsec^{-2}$. (*b*) Contours of the H$\alpha$ + [N II] image. Levels are $1\times10^{-17}\times(-5, 5, 12, 20, 75, 150, 290)$ ergs $s^{-1}$ $cm^{-2}$ $arcsec^{-2}$.

© American Astronomical Society • Provided by the NASA Astrophysics Data System

1988ApJS...68..643B

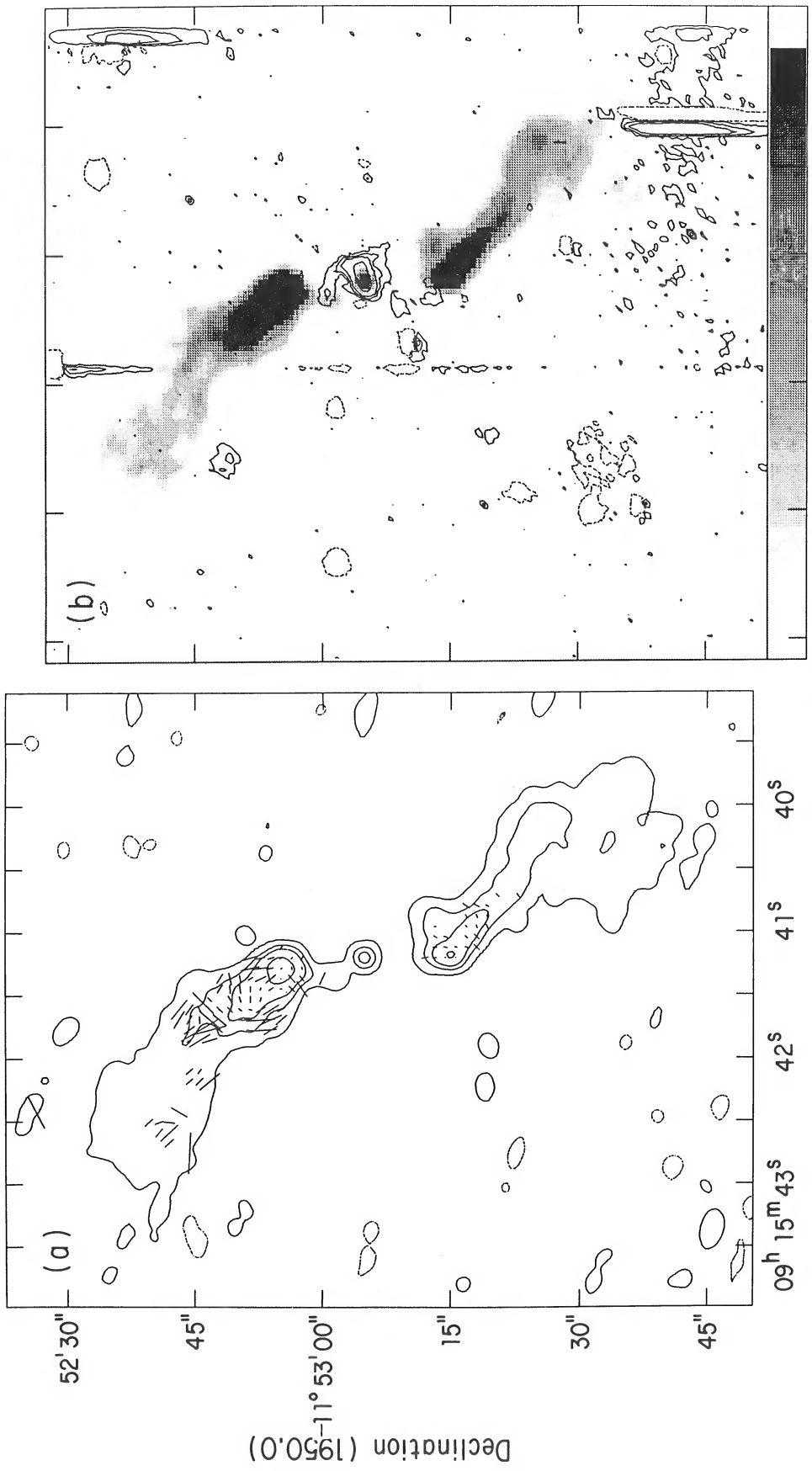


FIG. 26.—3C 218. (*a*) Contours of the 6 cm combined B and C array VLA image of 3C 218. Levels are (−9, 9, 60, 150, 450) mJy per restoring beam (1".85 FWHM circular Gaussian). The lengths of the superposed vectors indicate the fractional polarization and their orientations give the direction of the projected electric field. A vector of length 1" represents a fractional polarization of 3.125%. (*b*) Gray-scale radio superposed on contours of the Hα+[N II] emission.



© American Astronomical Society • Provided by the NASA Astrophysics Data System

1988ApJS...68..643B

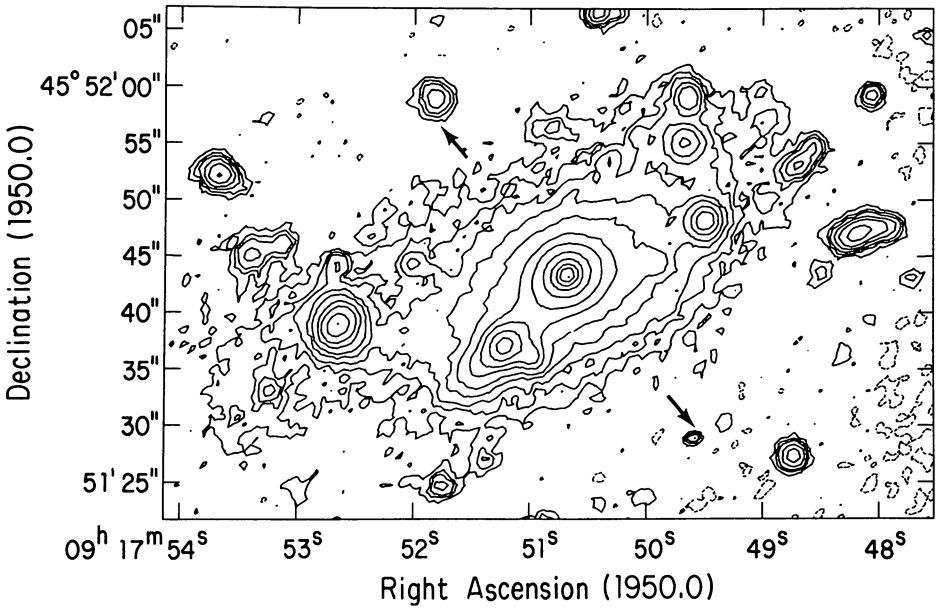


FIG. 27.—3C 219. (*a*) Contours of the *V*-band optical image of the host galaxy of 3C 219, and nearby galaxies. Levels are $1\times10^{-16}\times(-1, 1, 2, 3, 5, 8, 15, 25, 50, 100, 170, 250, 340)$ ergs $s^{-1}$ $cm^{-2}$ $arcsec^{-2}$. Arrows indicate the radio source axis.

© American Astronomical Society • Provided by the NASA Astrophysics Data System

1988ApJS...68..643B

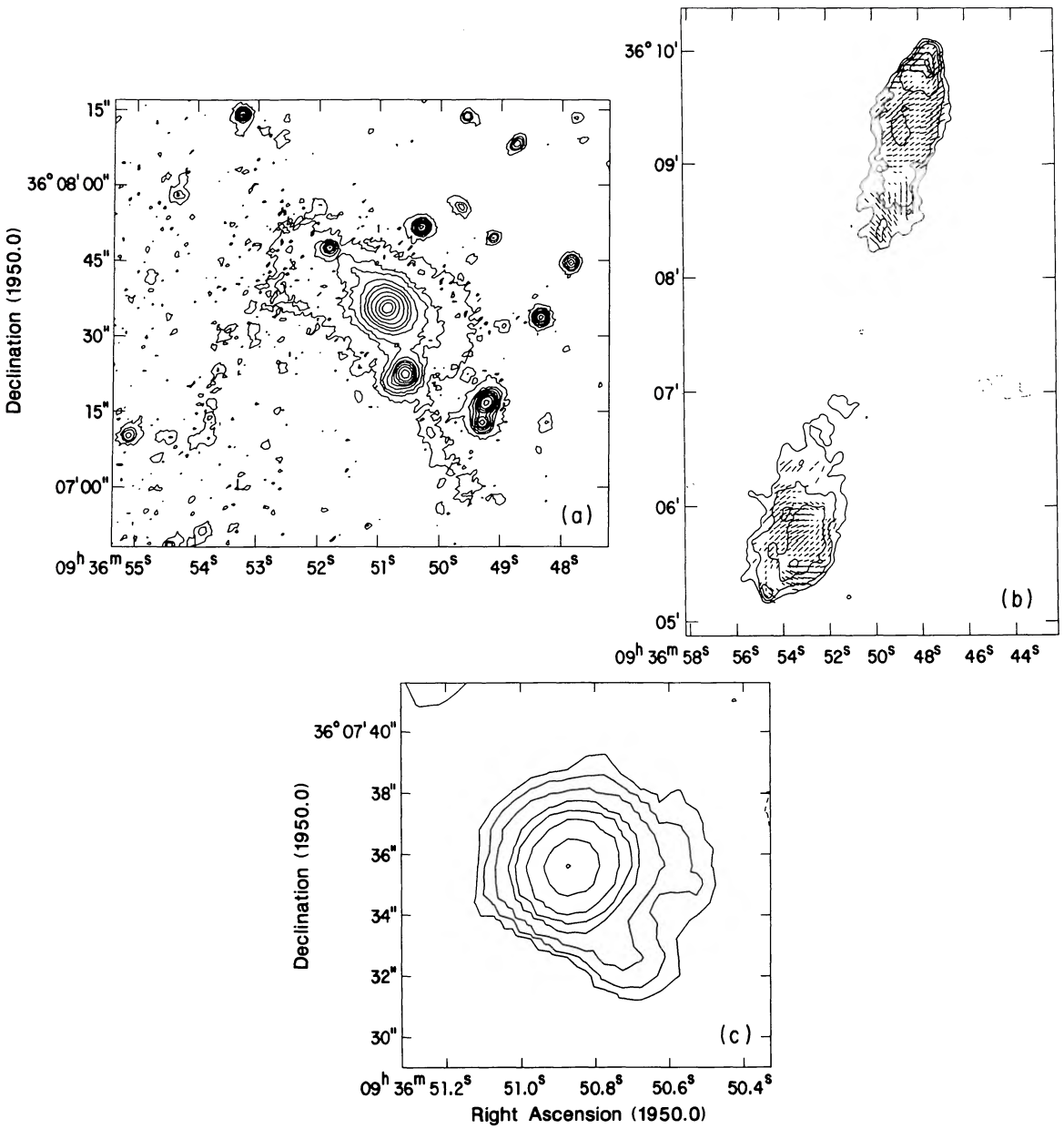


FIG. 28.—3C 223. (*a*) Contours of the *V*-band optical image of the host galaxy of 3C 223. Levels are at $1\times10^{-16}\times(-1.75, 1.75, 4, 6, 10, 15, 20, 30, 50, 100, 195)$ ergs $s^{-1}$ $cm^{-2}$ $arcsec^{-2}$. (*b*) Contours of the 20 cm B array VLA image of 3C 223. Levels are $(-3, 3, 6, 12, 40, 60)$ mJy per restoring beam (3".8 FWHM circular Gaussian). The lengths of the superposed vectors indicate the fractional polarization, and their orientations give the direction of the projected electric field. A vector of length 1" represents a fractional polarization of 6.7%. (*c*) Contours of the H$\alpha$+[N II] emission. Levels are $1\times10^{-17}\times(-3, 3, 6, 12, 30, 50, 100, 280, 550)$ ergs $s^{-1}$ $cm^{-2}$ $arcsec^{-2}$.

© American Astronomical Society • Provided by the NASA Astrophysics Data System

1988ApJS...68..643B

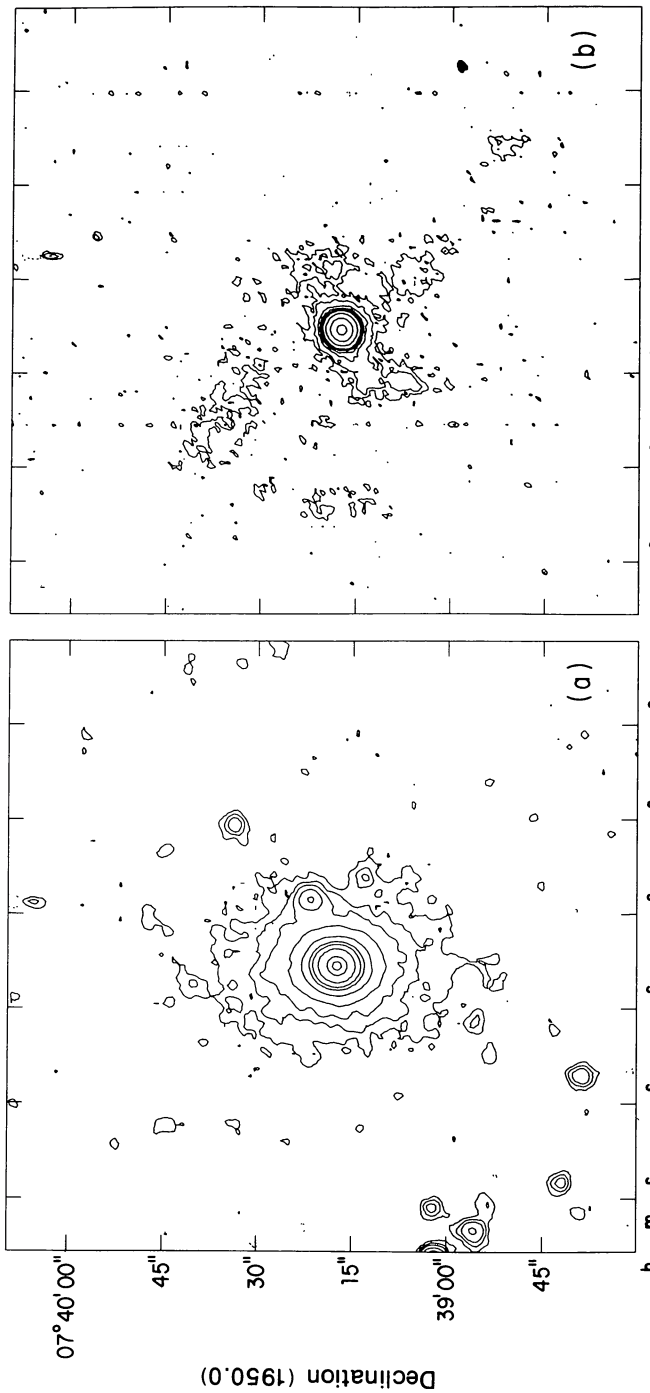


FIG. 29.—3C 227. (*a*) Contours of the *R*-band optical image of the host galaxy of 3C 227. Levels are $1\times10^{-16}\times(-1.5, 1.5, 3, 5, 10, 20, 35, 50, 100, 400, 800, 1250)$ ergs $s^{-1}$ $cm^{-2}$ $arcsec^{-2}$. (*b*) Contours of the H$\alpha$ + [N II] emission. Levels are $1\times10^{-17}\times(-5, 5, 10, 20, 30, 40, 50, 100, 300, 1000)$ ergs $s^{-1}$ $cm^{-2}$ $arcsec^{-2}$.

© American Astronomical Society • Provided by the NASA Astrophysics Data System

1988ApJS...68..643B

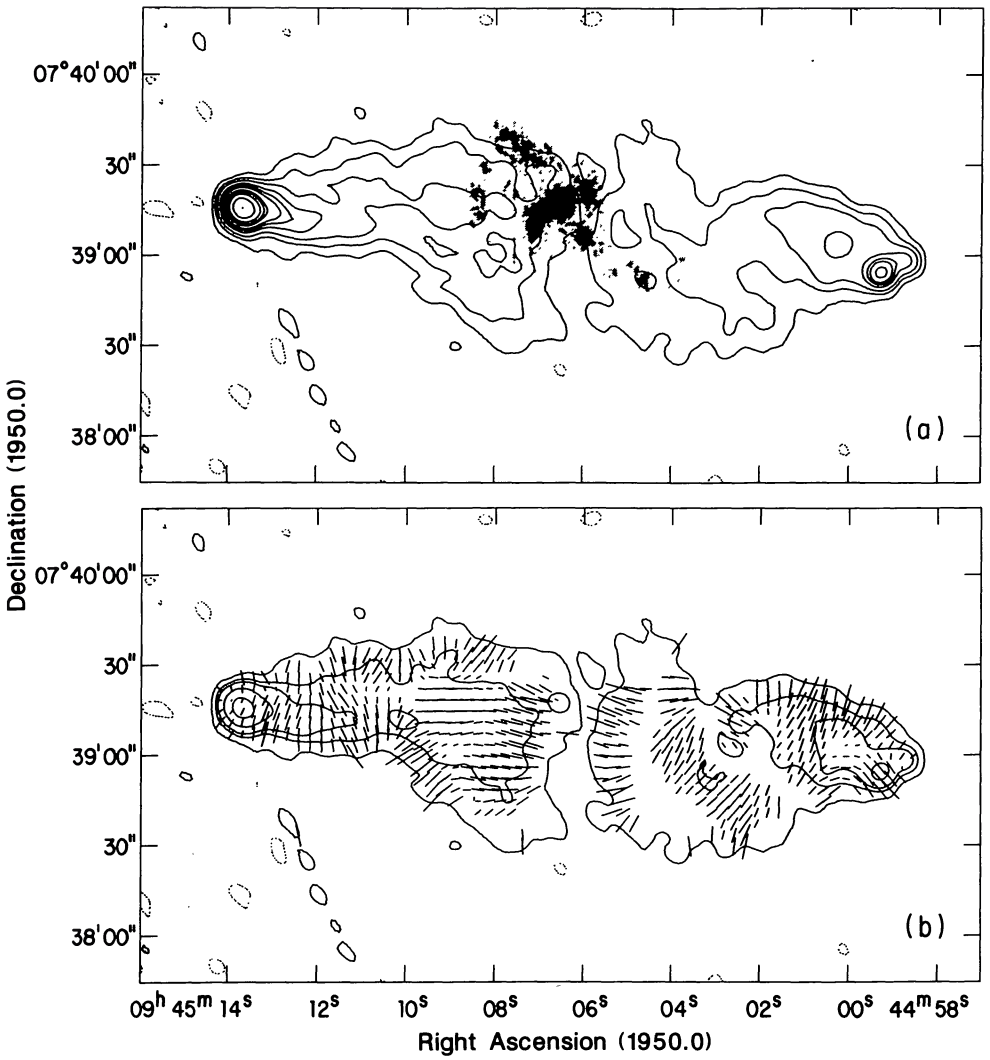


FIG. 30.—3C 227. (*a*) Silhouette of the Hα+[N II] emission superposed on the contours of the 6 cm combined B, C, and D array VLA image. Radio contours are at $7\times10^{-1}$ (−3, 3, 10, 20, 40, 60, 80, 125, 150, 200, 300, 450) mJy per restoring beam (6″.5 FWHM circular Gaussian). (*b*) Contours of the 6 cm combined B, C, and D array VLA image. Levels are $7\times10^{-1}\times$(−3, 3, 15, 30, 100, 300) mJy per restoring beam (6″.5 FWHM circular Gaussian). The lengths of the superposed vectors indicate the fractional polarization and their orientations give the direction of the projected electric field. A vector of length 1″ represents a fractional polarization of 5.3%.

© American Astronomical Society • Provided by the NASA Astrophysics Data System

1988ApJS...68..643B

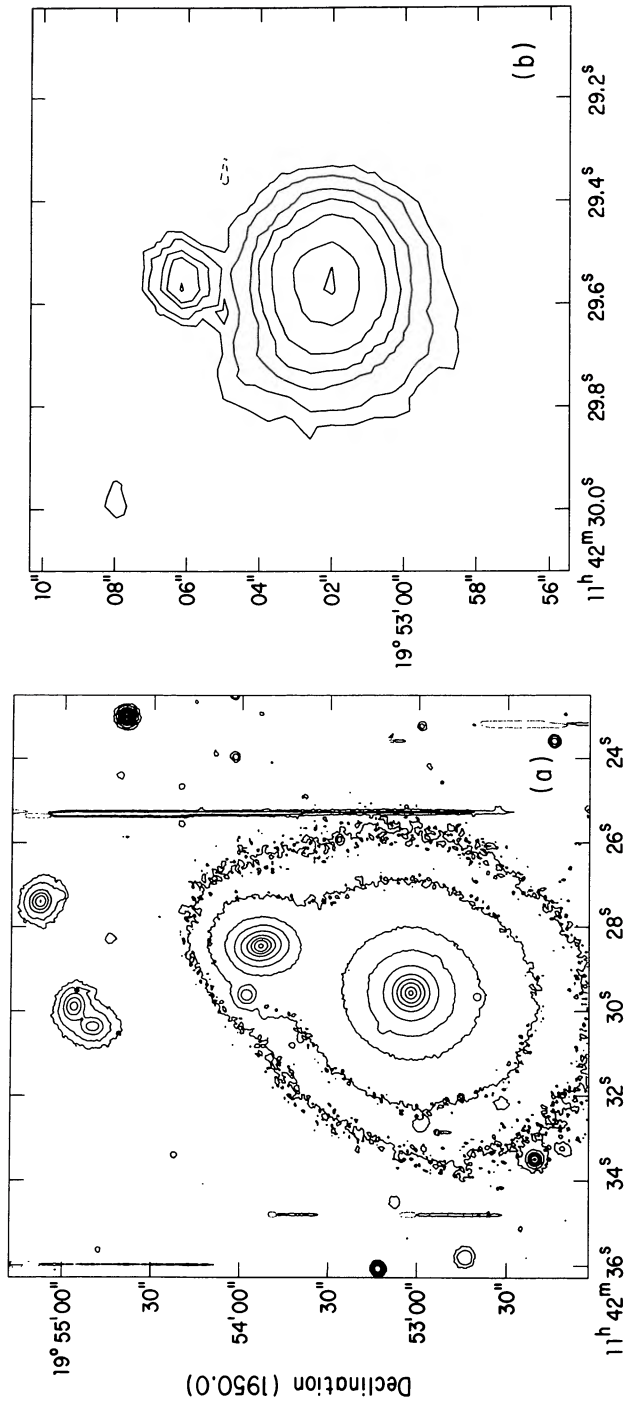


FIG. 31.—3C 264. (*a*) Contours of the *V*-band image of the host galaxy of 3C 442. Levels are $1\times10^{-16}\times(-5, 5, 10, 25, 50, 100, 200, 350, 600, 1200, 2000)$ ergs $s^{-1}$ $cm^{-2}$ $arcsec^{-2}$. (*b*) Contours of the H$\alpha$ + [N II] image. Levels are $1\times10^{-17}\times(-5, 5, 10, 20, 30, 50, 100, 150)$ ergs $s^{-1}$ $cm^{-2}$ $arcsec^{-2}$. The unresolved feature at 19° 53' 06" is a cosmic-ray hit.

© American Astronomical Society • Provided by the NASA Astrophysics Data System

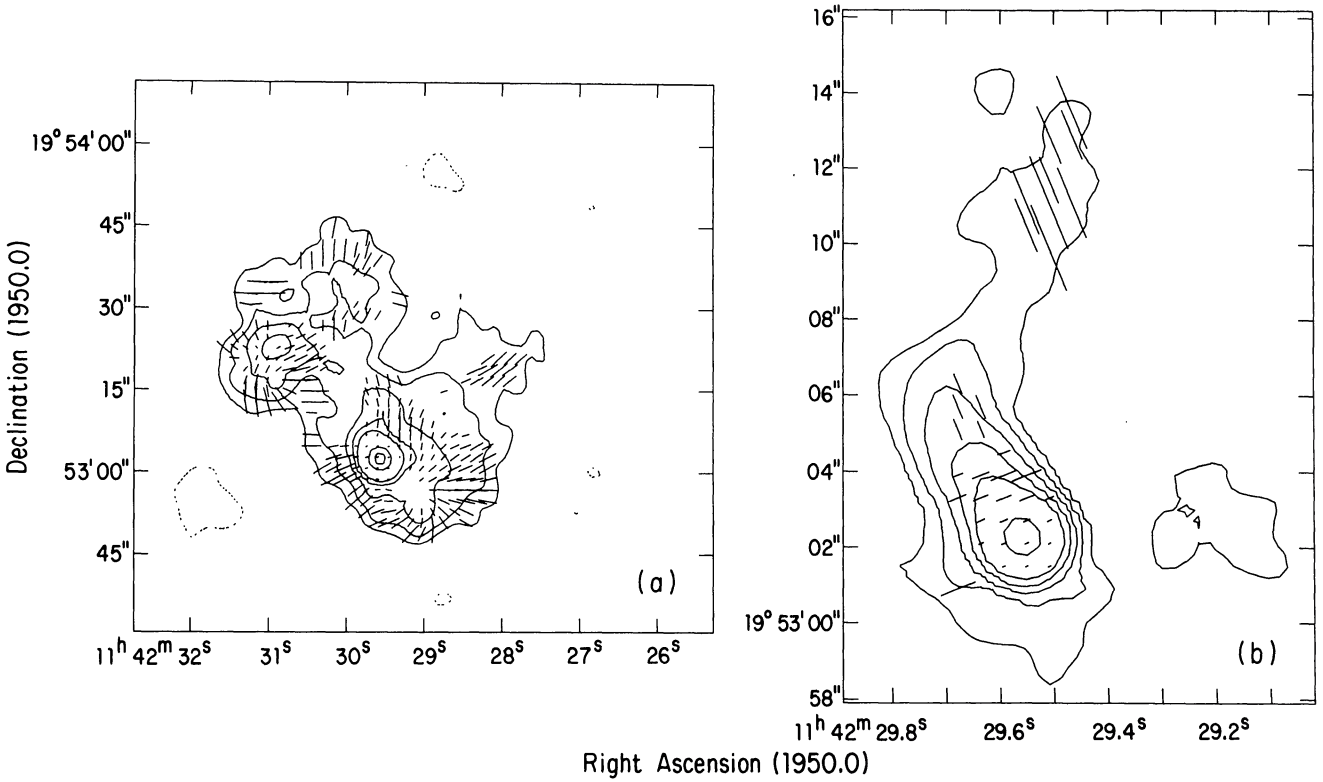


FIG. 32.—3C 264. (*a*) Contours of the 6 cm radio VLA C array map. Levels are $5.8\times10^{-1}\times(-3, 3, 6, 12, 25, 50, 300, 500)$ mJy per restoring beam (3".8 FWHM circular Gaussian). The lengths of the superposed vectors indicate the fractional polarization, and their orientations give the direction of the projected electric field. A vector of length 1" represents a fractional polarization of 10%. (*b*) Contours of the 6 cm radio VLA B array map. Levels are $5.8\times10^{-1}$ $(-3, 3, 6, 12, 25, 50, 300, 500)$ mJy per restoring beam (1".15 FWHM circular Gaussian).

© American Astronomical Society • Provided by the NASA Astrophysics Data System

1988ApJS...68..643B

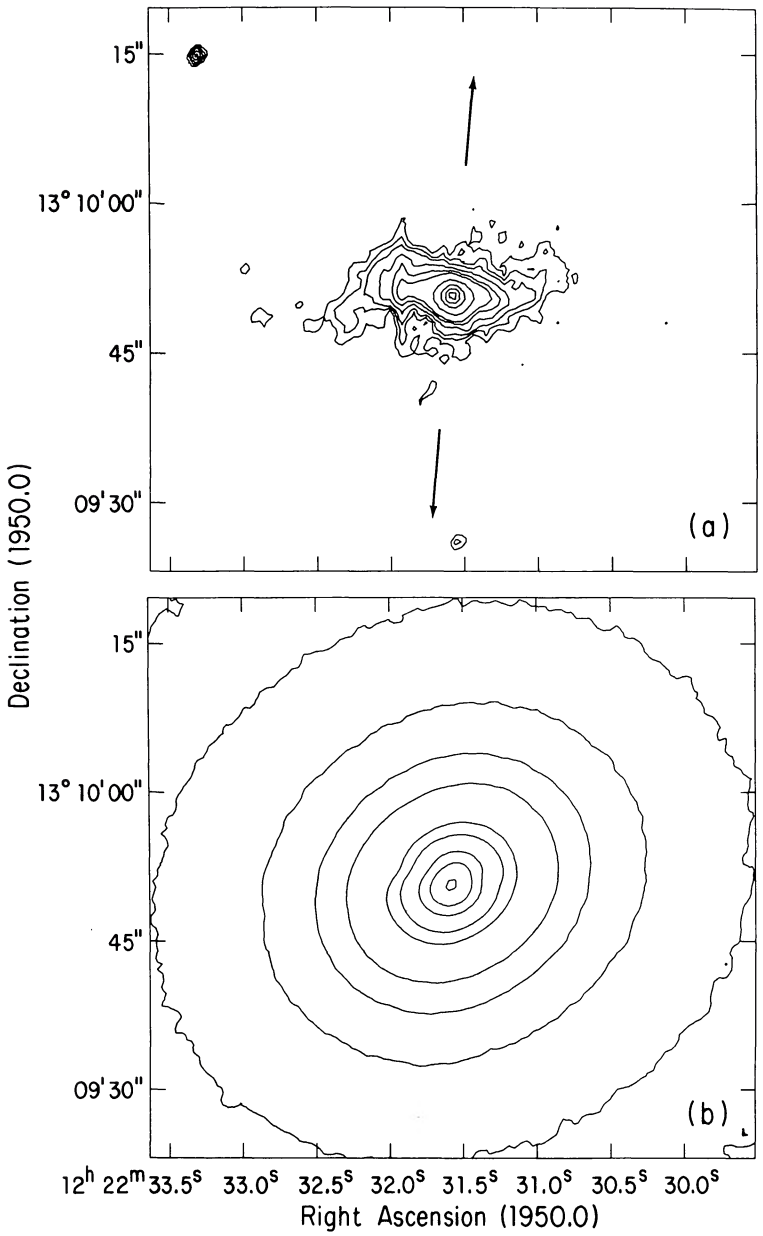


FIG. 33.—3C 272.1. (*a*) Contours of the Hα+[N II] image. Levels are $1\times10^{-17}\times(-10, 10, 20, 30, 50, 75, 100, 200, 375, 550, 725)$ ergs $s^{-1}$ $cm^{-2}$ $arcsec^{-2}$. Calibrated using spectrophotometry from Hansen, Noorgard-Nielsen, and Jorgensen (1985). (*b*) Contours of the *R*-band optical image of the host galaxy of 3C 272.1 (M 84). Levels are (8, 15, 30, 50, 75, 150, 200, 325, 450, 650) in arbitrary units.

© American Astronomical Society • Provided by the NASA Astrophysics Data System

1988ApJS...68..643B

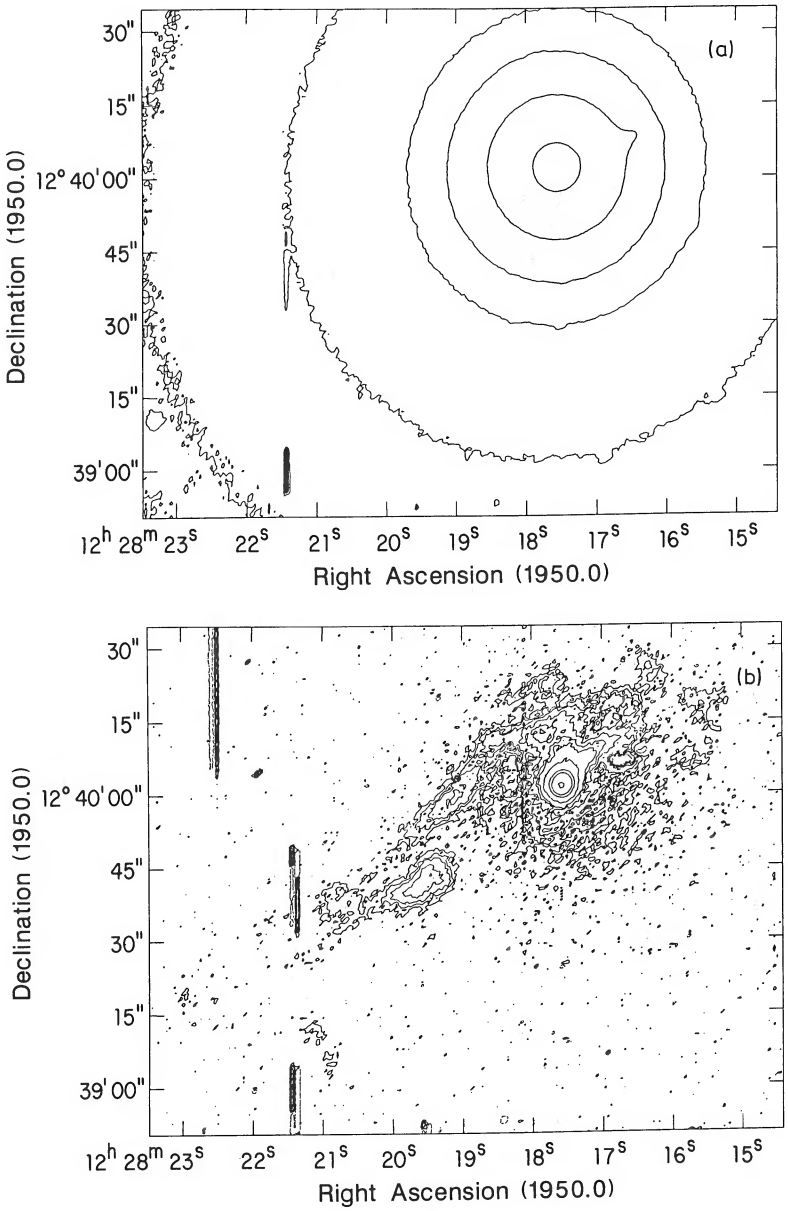


FIG. 34.—3C 274. (*a*) Contours of the *R*-band optical image of the inner part of M 87, the host galaxy of 3C 274. Levels are $1\times10^{-16}\times(-10, 10, 20, 30, 50, 75, 100, 200, 500, 800, 1500, 4000)$ ergs $s^{-1}$ $cm^{-2}$ $arcsec^{-2}$. (*b*) Contours of the H$\alpha$+[N II] emission. Levels are $1\times10^{-17}\times(-10, 10, 20, 30, 50, 75, 100, 200, 500, 800, 1800)$ ergs $s^{-1}$ $cm^{-2}$ $arcsec^{-2}$.



© American Astronomical Society • Provided by the NASA Astrophysics Data System

1988ApJS...68..643B

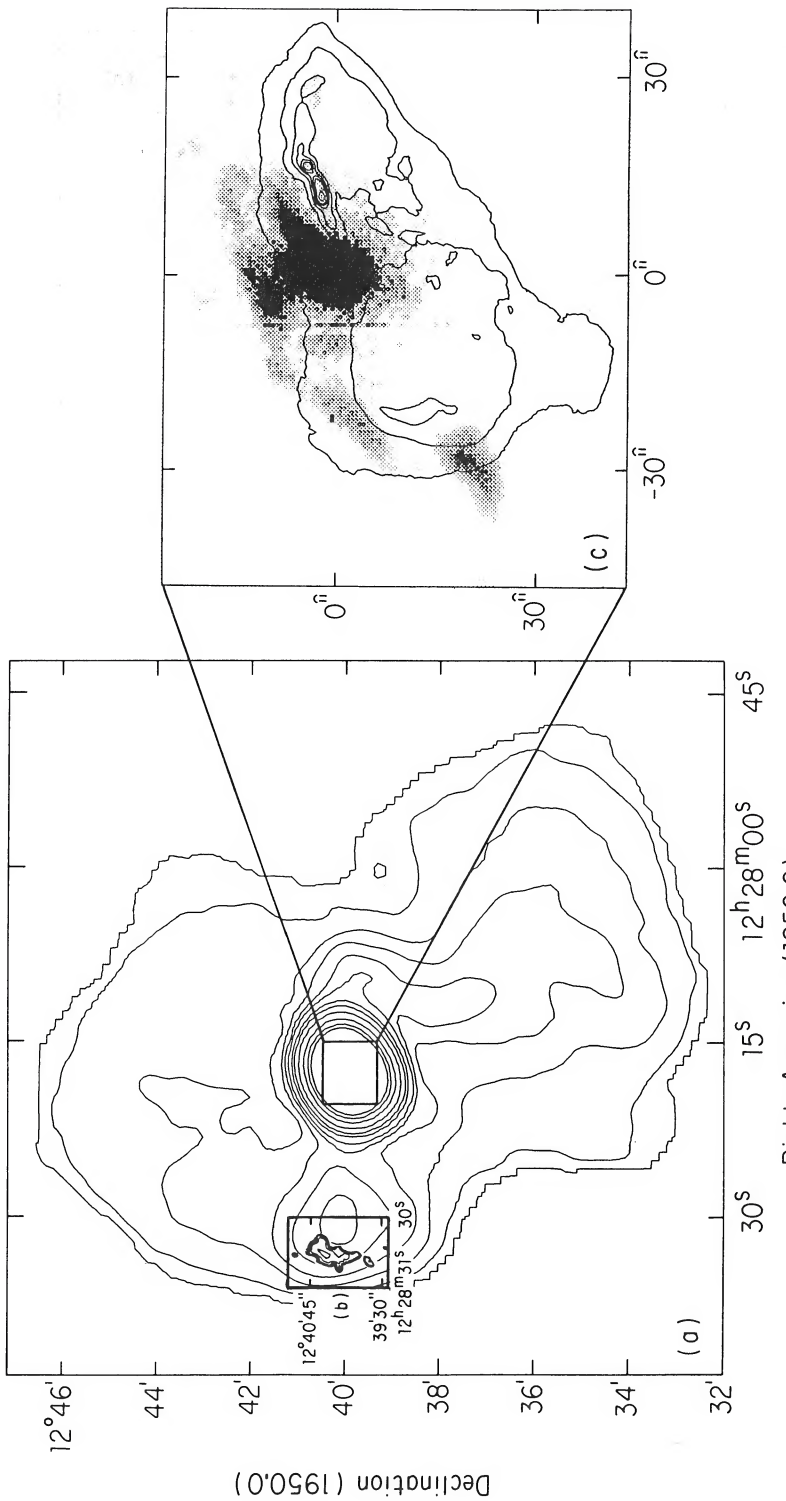


FIG. 35.—3C 274. Reproduced from Baum and Heckman (1987) (*a*) Contours of the 20 cm total emission of 40″ resolution, courtesy of Frazer Owen. Contour levels are at $5\times10^{-5}\times(-5, 5, 100, 300, 500, 750, 1000, 1500, 2000, 3000, 5000, 7500, 10000)$ Jy per pixel, where each pixel is 10″ on a side. (*b*) Contours of the H$\alpha$ + [N II] emission, in arbitary units. (*c*) Gray-scale representation of the H$\alpha$ + [N II] emission superposed on contours of the 20 cm total intensity emission at 1″.1 resolution (radio map courtesy of Frazer Owen, Tim Cornwell, and Phil Hardee). Contour levels are $2\times10^{-4}\times(3, 10, 25, 50, 75, 100, 150, 200, 300, 400, 500, 750, 1000)$ Jy per pixel, where each pixel is 0″.19 on a side.



© American Astronomical Society • Provided by the NASA Astrophysics Data System

1988ApJS...68..643B

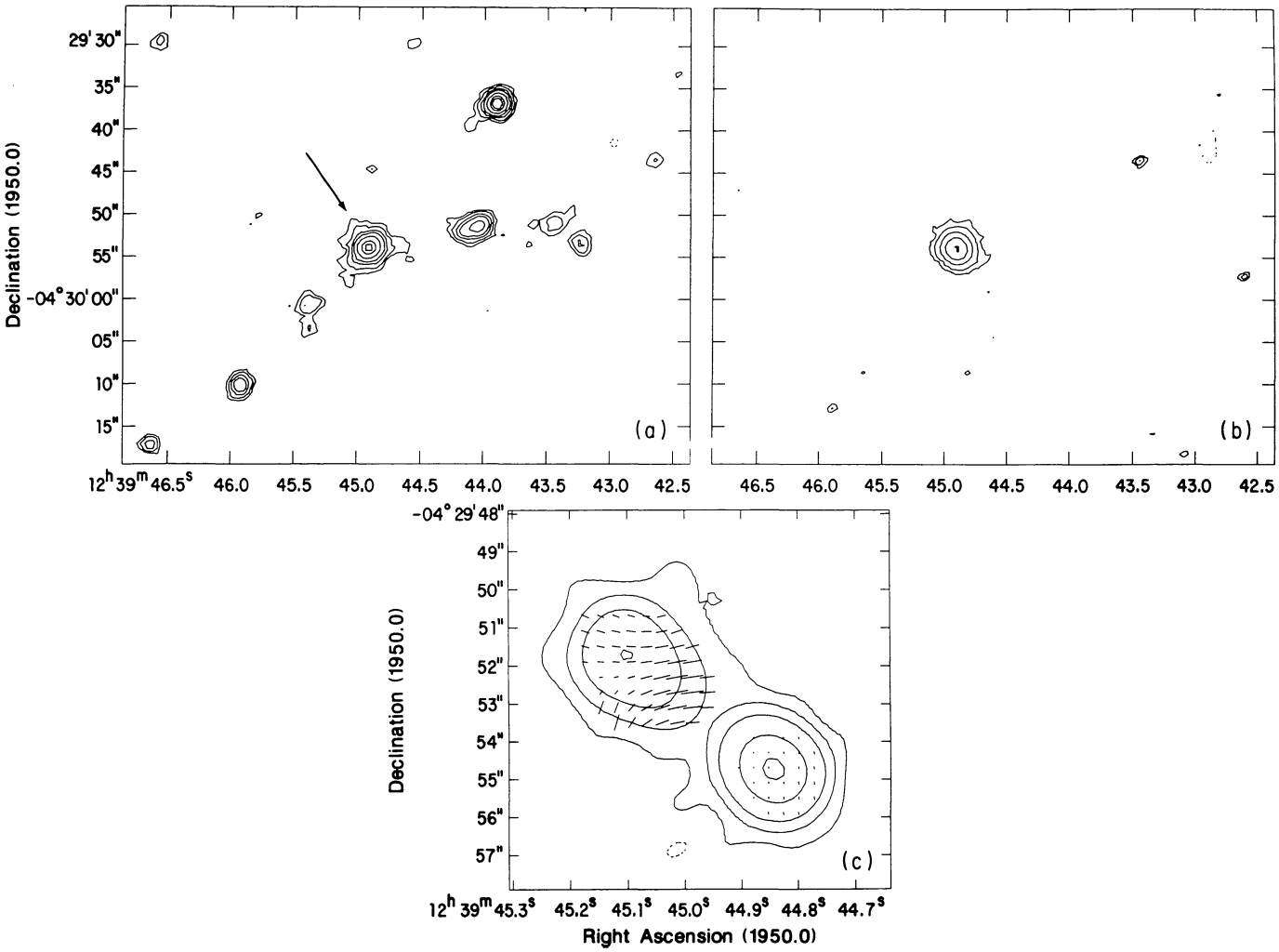


FIG. 36.—3C 275. (*a*) Contours of the *R*-band optical image of the environs of the host galaxy of 3C 275. The arrow points to the radio galaxy. Levels are (−7, 7, 10, 15, 20, 30, 45, 55) in arbitrary units. (*b*) Contours of the [O III] emission. Levels are (−2.5, 2.5, 6, 15, 35, 80) in arbitrary units. (*c*) Contours of the 6 cm B array VLA image. Levels are $7\times10^{-1}\times(-4, 4, 25, 75, 300, 700)$ mJy per restoring beam (1″.4 FWHM circular Gaussian). The lengths of the superposed vectors indicate the fractional polarization and their orientations give the direction of the projected electric field. A vector of length 1″ represents a fractional polarization of 33.3%.

© American Astronomical Society • Provided by the NASA Astrophysics Data System

1988ApJS...68..643B

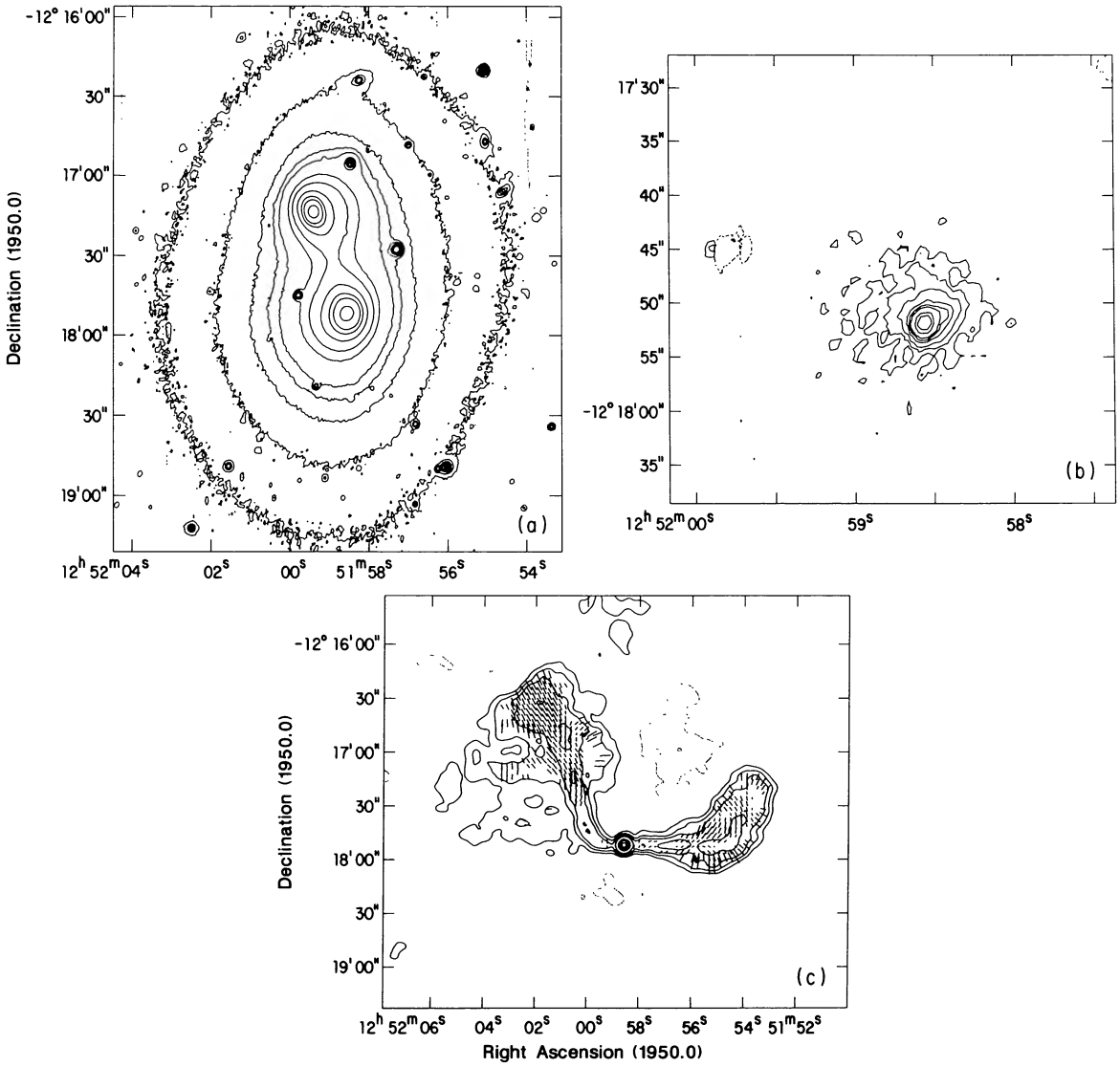


FIG. 37.—3C 278. (*a*) Contours of the *R*-band optical image of the host galaxy of 3C 278. Levels are $1\times10^{-16}\times(-10, 10, 25, 50, 75, 100, 200, 300, 500, 750, 1000, 2000)$ ergs $s^{-1}$ $cm^{-2}$ $arcsec^{-2}$. (*b*) Contours of the H$\alpha$+[N II] emission. Levels are $1\times10^{-17}\times(-6, 6, 12, 25, 50, 75, 100, 200, 300, 500)$ ergs $s^{-1}$ $cm^{-2}$ $arcsec^{-2}$. (*c*) Contours of the 6 cm C array VLA image of 3C 278. Levels are $6.5\times10^{-1}\times(-3, 3, 6, 10, 20, 50, 75, 100)$ mJy per restoring beam (5″.8 FWHM circular Gaussian). The lengths of the superposed vectors indicate the fractional polarization and their orientations give the direction of the projected electric field. A vector of length 1″ represents a fractional polarization of 8.3%.

© American Astronomical Society • Provided by the NASA Astrophysics Data System

1988ApJS...68..643B

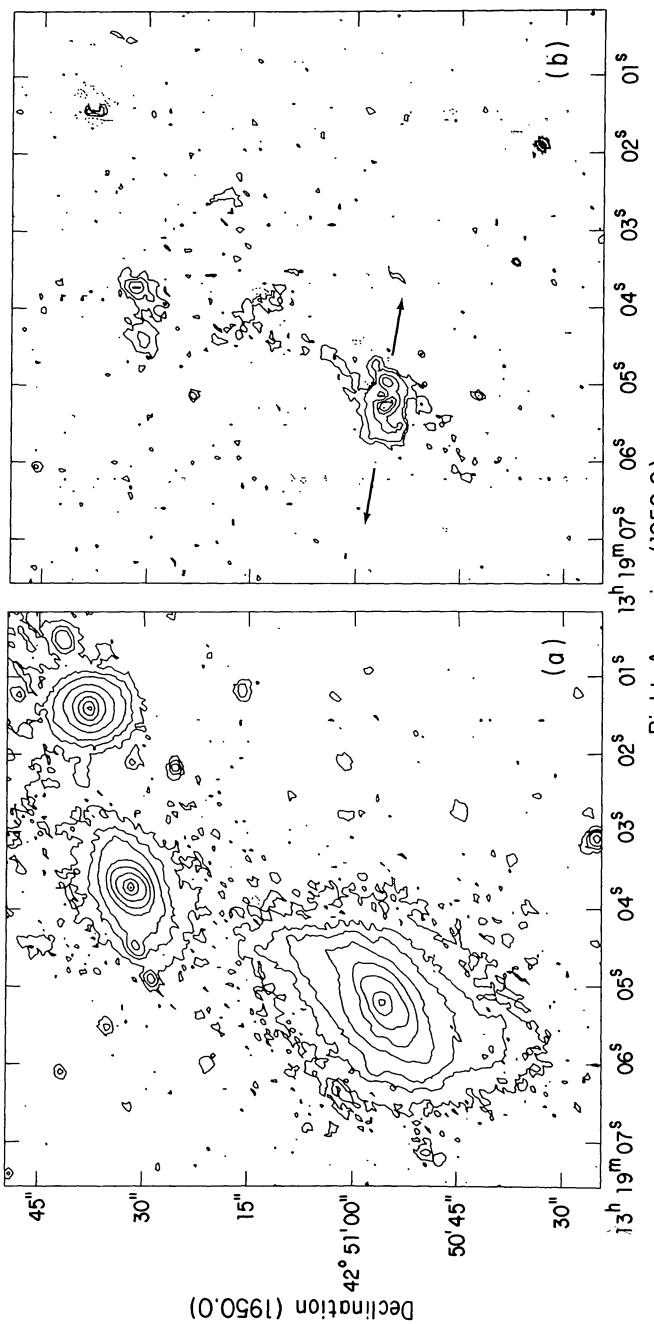


FIG. 38.—3C 285. (*a*) Contours of the *R*-band optical image of the host galaxy of 3C 285 and two smaller galaxies. Levels are $1\times10^{-16}\times(-2, 2, 5, 10, 25, 50, 100, 250, 500, 700)$ ergs $s^{-1}$ $cm^{-2}$ $arcsec^{-2}$. (*b*) Contours of the H$\alpha$+[N II] image. Levels are $1\times10^{-17}\times(-3.5, 3.5, 10, 35, 70, 100, 140)$ ergs $s^{-1}$ $cm^{-2}$ $arcsec^{-2}$. Arrows indicate the radio source axis.

© American Astronomical Society • Provided by the NASA Astrophysics Data System

1988ApJS...68..643B

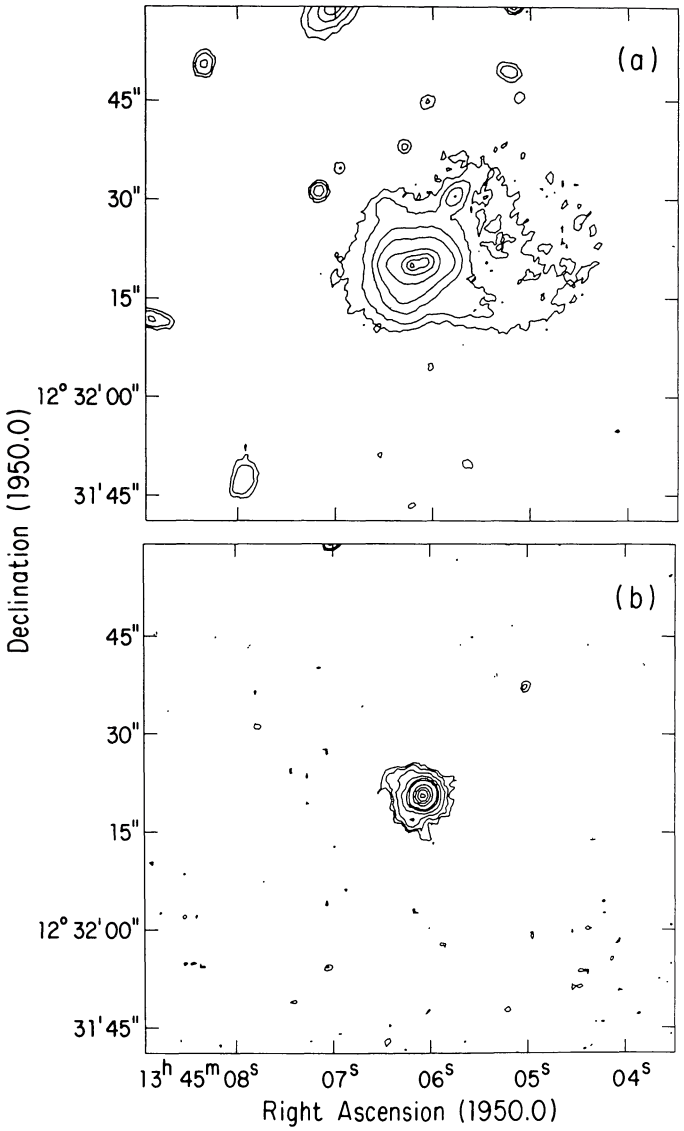


FIG. 39.—PKS 1345+125. (*a*) Contours of the *R*-band optical image of the host galaxy of PKS 1345+125. Levels are (−5, 5, 10, 25, 50, 100, 175, 300, 400, 1000) in arbitrary units. (*b*) Contours of the Hα+[N II] image. Levels are $1\times10^{-17}\times(-3, 3, 5, 10, 20, 35, 50, 150, 300, 500, 800)$ ergs $s^{-1}$ $cm^{-2}$ $arcsec^{-2}$. Calibrated using spectrohotometry from Grandi (1977) and Gilmore and Shaw (1986).

© American Astronomical Society • Provided by the NASA Astrophysics Data System

1988ApJS...68..643B

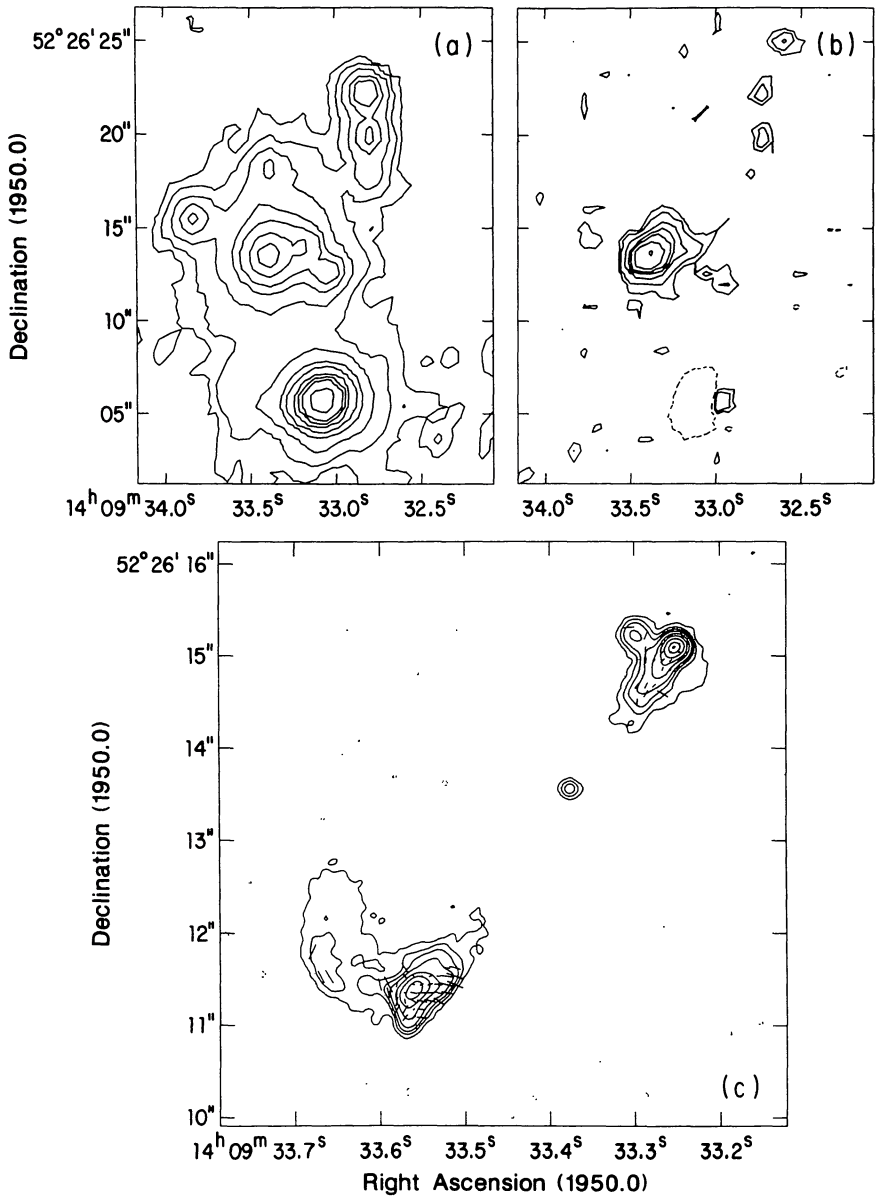


FIG. 40.—3C 295. (*a*) Contours of the *R*-band optical image of the host galaxy of 3C 295. Levels are $1\times10^{-16}\times(-3, 3, 5, 10, 20, 30, 50, 75, 100, 200)$ ergs $s^{-1}$ $cm^{-2}$ $arcsec^{-2}$. (*b*) Contours of the [O III] emission. Levels are $1\times10^{-17}\times(-3, 3, 5, 10, 15, 20, 30, 55, 100)$ ergs $s^{-1}$ $cm^{-2}$ $arcsec^{-2}$. (*c*) Contours of the 2 cm A array VLA image. Levels are $3\times10^{-1}\times(-3, 3, 10, 20, 40, 100, 200, 400, 750, 1000)$ mJy per restoring beam (0″.1 FWHM circular Gaussian). The lengths of the superposed vectors indicate the fractional polarization, and their orientation given the direction of the projected electric field. A vector of length 1″ reepresents a fractional polarization of 222%.

© American Astronomical Society • Provided by the NASA Astrophysics Data System

1988ApJS...68..643B

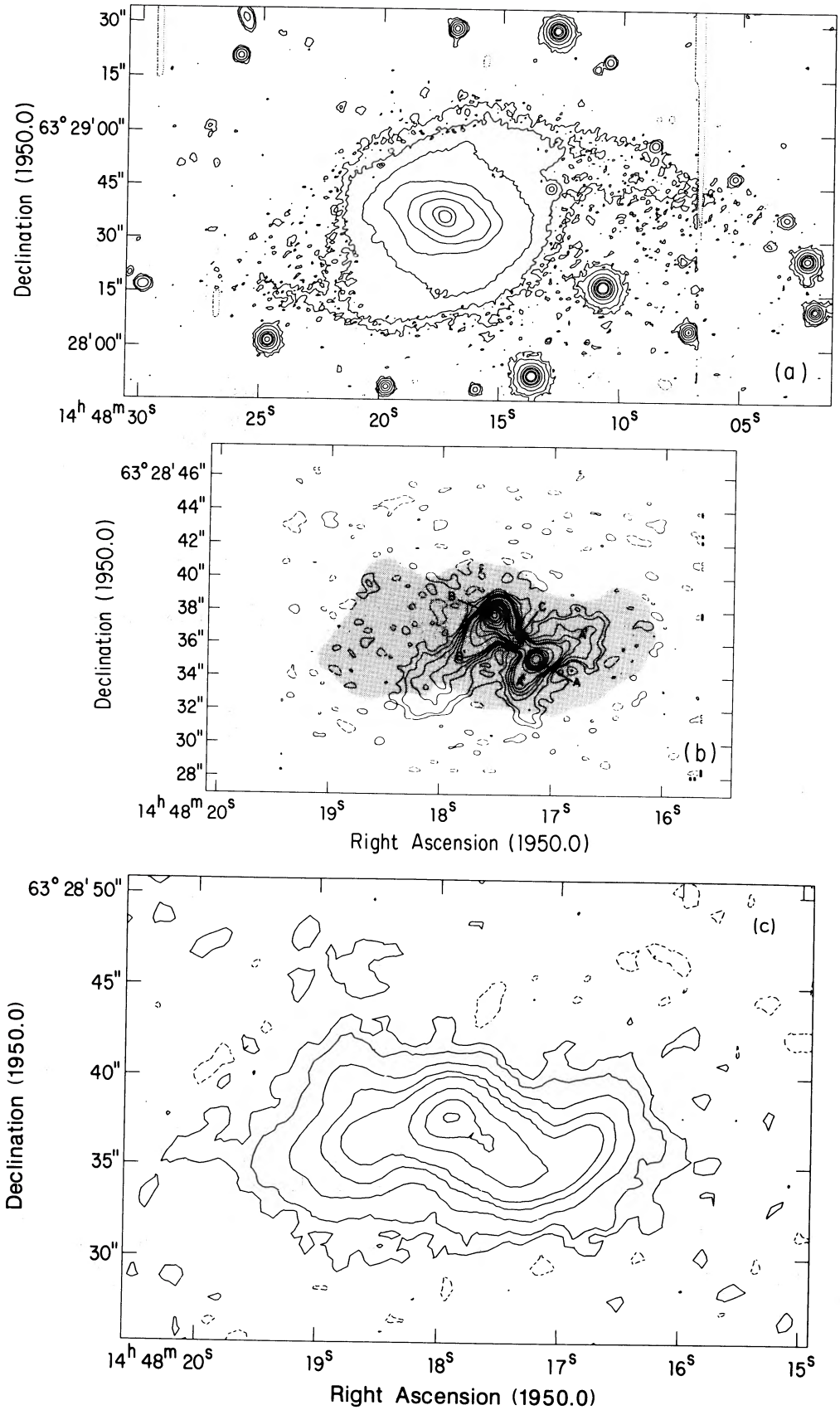


FIG. 41.—3C 305. (*a*) Contours of *R*-band optical image of the host galaxy of 3C 305. Levels are (−5, 5, 10, 30, 100, 250, 500, 1500, 3000), in arbitrary units. (*b*) Silhouette of the Hα + [N II] emission superposed on the contours of the radio emission. The contours of the line emission are at $1\times10^{-16}\times$ (1, 7.5, 30, 75, 140) ergs $s^{-1}$ $cm^{-2}$ $arcsec^{-2}$. The contours of the 6 cm radio emission are reproduced from Heckman *et al.* 1982. Levels are (−1.0, −0.5, 0.5, 1, 2, 3, 4, 5, 10, 15, 20, 29, 38, 60, 90, 120, 160, 200) mJy per restoring beam (0.″5 FWHM circular Gaussian). (*c*) Contours of the Hα + [N II] emission. Levels are $1\times10^{-17}\times(-2, 2, 5, 15, 40, 80, 300, 750, 1300)$ ergs $s^{-1}$ $cm^{-2}$ $arcsec^{-2}$. Calibrated using spectrophotometry from Heckman *et al.* (1982).



© American Astronomical Society • Provided by the NASA Astrophysics Data System

1988ApJS...68..643B

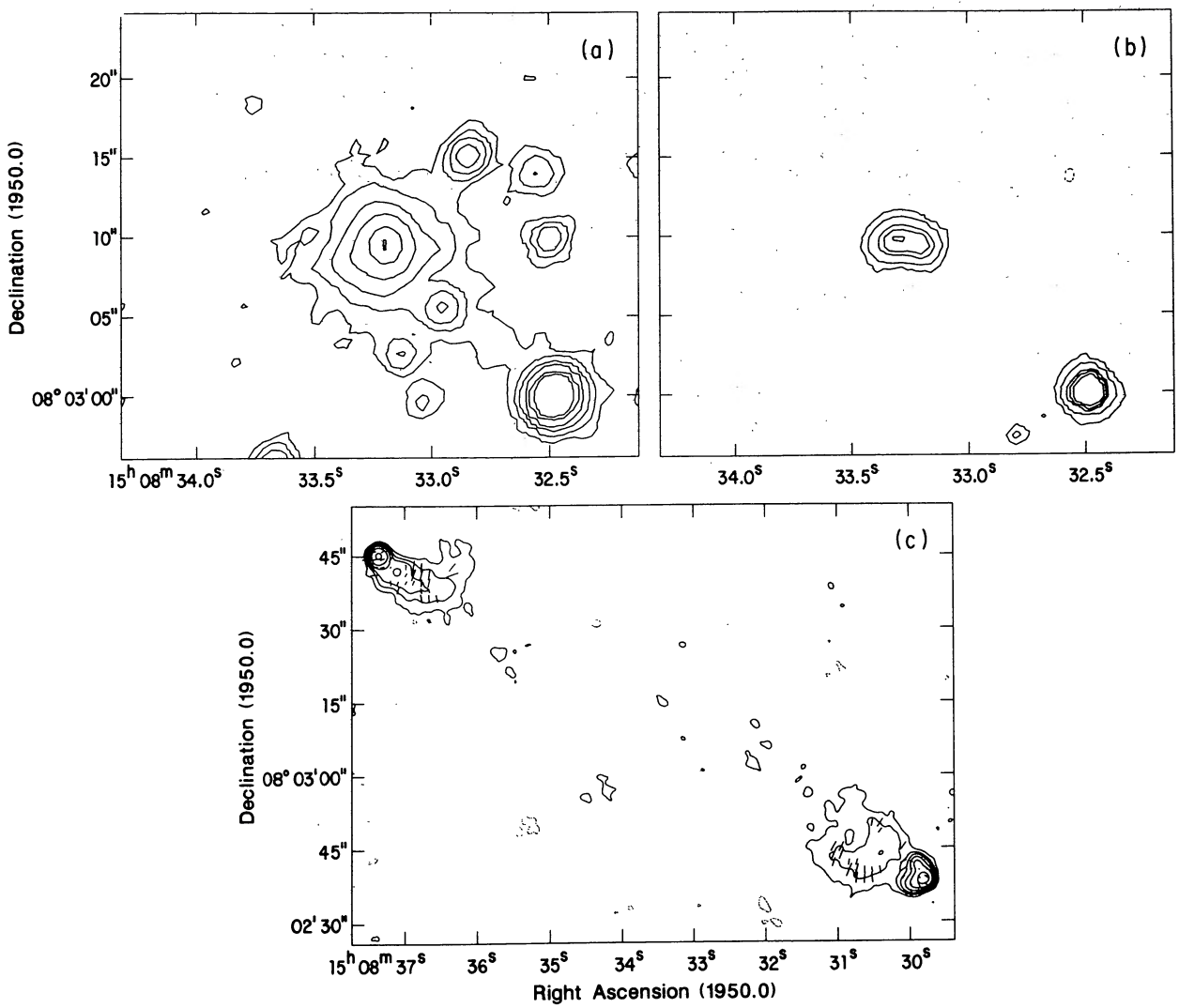


FIG. 42.—3C 313. (*a*) Contours of the *R*-band optical image of the host galaxy of 3C 313. Levels are $1\times10^{-16}\times(-4, 4, 8, 15, 30, 75, 150)$ ergs $s^{-1}$ $cm^{-2}$ $arcsec^{-2}$. (*b*) Contours of the [O III] emission. Levels are $1\times10^{-17}\times(-4, 4, 10, 25, 35, 50)$ ergs $s^{-1}$ $cm^{-2}$ $arcsec^{-2}$. (*c*) Contours of the 6 cm B array VLA image. Levels are $3.6\times10^{-1}\times(-3, 3, 10, 20, 45, 100, 300)$ mJy per restoring beam (2″ FWHM circular Gaussian). The length of the superposed vectors indicate the fractional polarization, and their orientations give the direction of the projected electric field. A vector of length 1″ represents a fractional polarization of 16.7%.

© American Astronomical Society • Provided by the NASA Astrophysics Data System

1988ApJS...68..643B

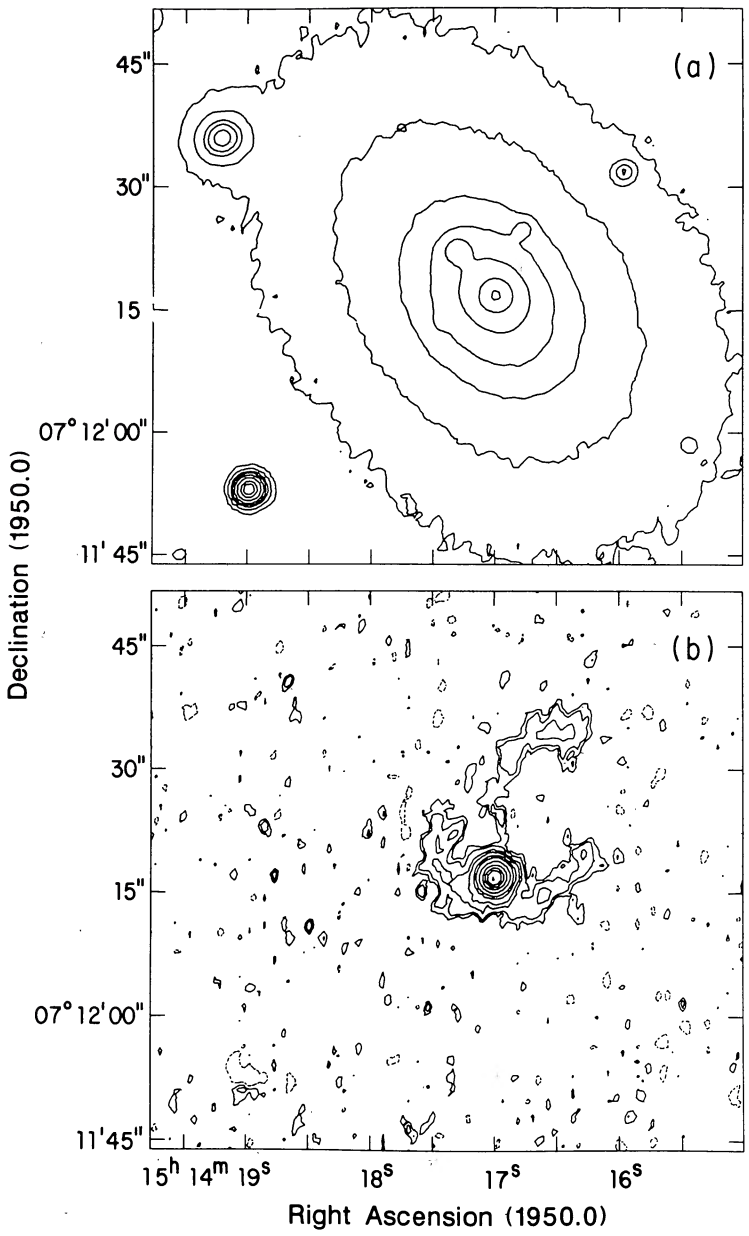


FIG. 43.—3C 317. (*a*) Contours of the *R*-band optical image of the host galaxy of 3C 317. Levels are (−5, 5, 10, 20, 30, 50, 100, 200, 300, 500, 750, 1000) in arbitrary units. (*b*) Contours of the Hα + [N II] emission. Levels are $1\times10^{-17}\times(-3, 3, 5, 10, 15, 25, 35, 60, 100, 150, 200, 300)$ ergs $s^{-1}$ $cm^{-2}$ $arcsec^{-2}$. Calibrated using spectrophotometry from Cohen and Osterbrock (1981).

© American Astronomical Society • Provided by the NASA Astrophysics Data System

1988ApJS...68..643B

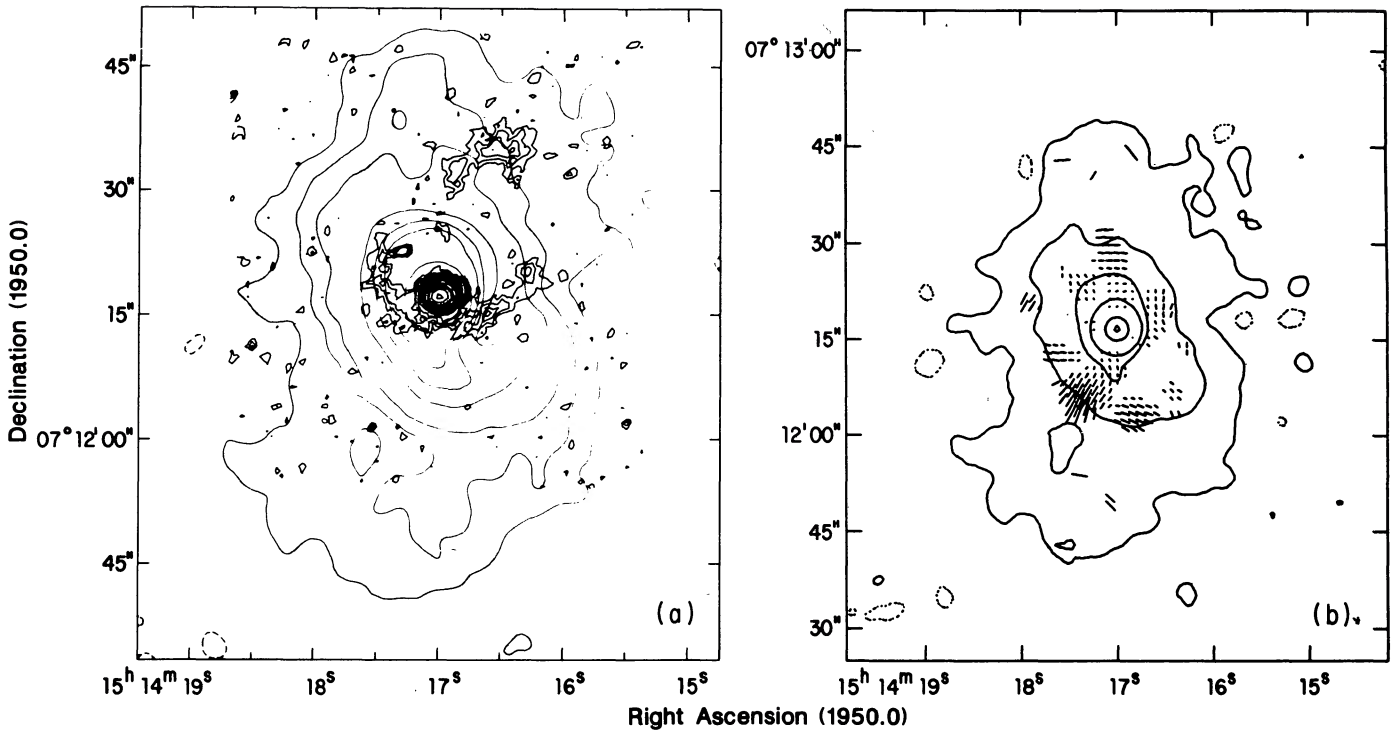


FIG. 44.—3C 317. (*a*) Contours of the Hα+[N II] emission superposed on the contours of the 6 cm combined B, C, and D array VLA image, reproduced from Baum and Heckman (1987). (*b*) Contours of the 6 cm combined B, C, and D array VLA image. Levels are $2.0\times10^{-1}\times(-3, 3, 25, 75, 100, 200, 1000, 1600)$ mJy per restoring beam (4″ FWHM circular Gaussian). The lengths of the superposed vectors indicate the fractional polarization, and their orientations give the direction of the projected electric field. A vector of length 1″ represents a fractional polarization of 11.1%.

© American Astronomical Society • Provided by the NASA Astrophysics Data System

1988ApJS...68..643B

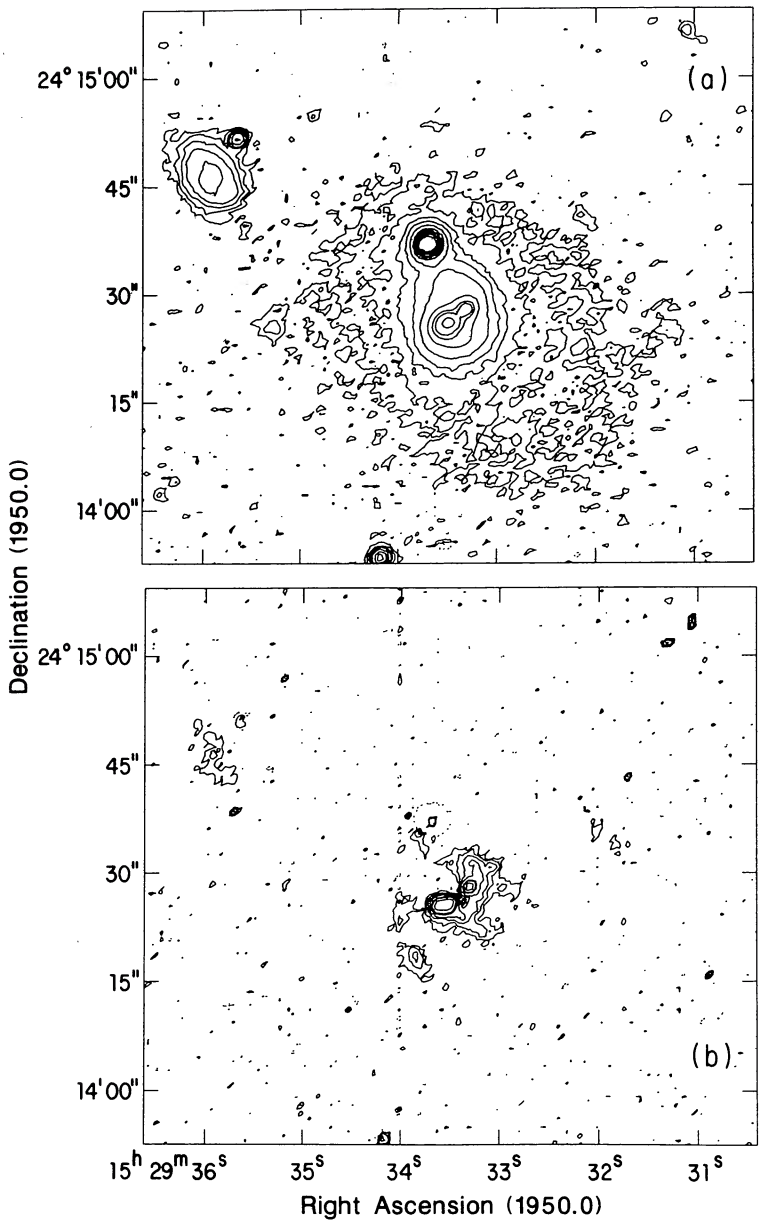


FIG. 45.—3C 321. (*a*) Contours of the *R*-band optical image of the host galaxy of 3C 321. Levels are (−8, 8, 16, 30, 50, 100, 250, 500, 750, 1500, 2500, 5000) in arbitrary units. (*b*) Contours of the Hα + [N II] emission. Levels are $1\times10^{-16}\times(-1.8, 1.8, 4, 8, 15, 30, 45, 90, 200, 300, 500, 1000)$ ergs $s^{-1}$ $cm^{-2}$ $arcsec^{-2}$. Calibrated using spectrophotometry from van Breugel (1987, private communication).

© American Astronomical Society • Provided by the NASA Astrophysics Data System

1988ApJS...68..643B

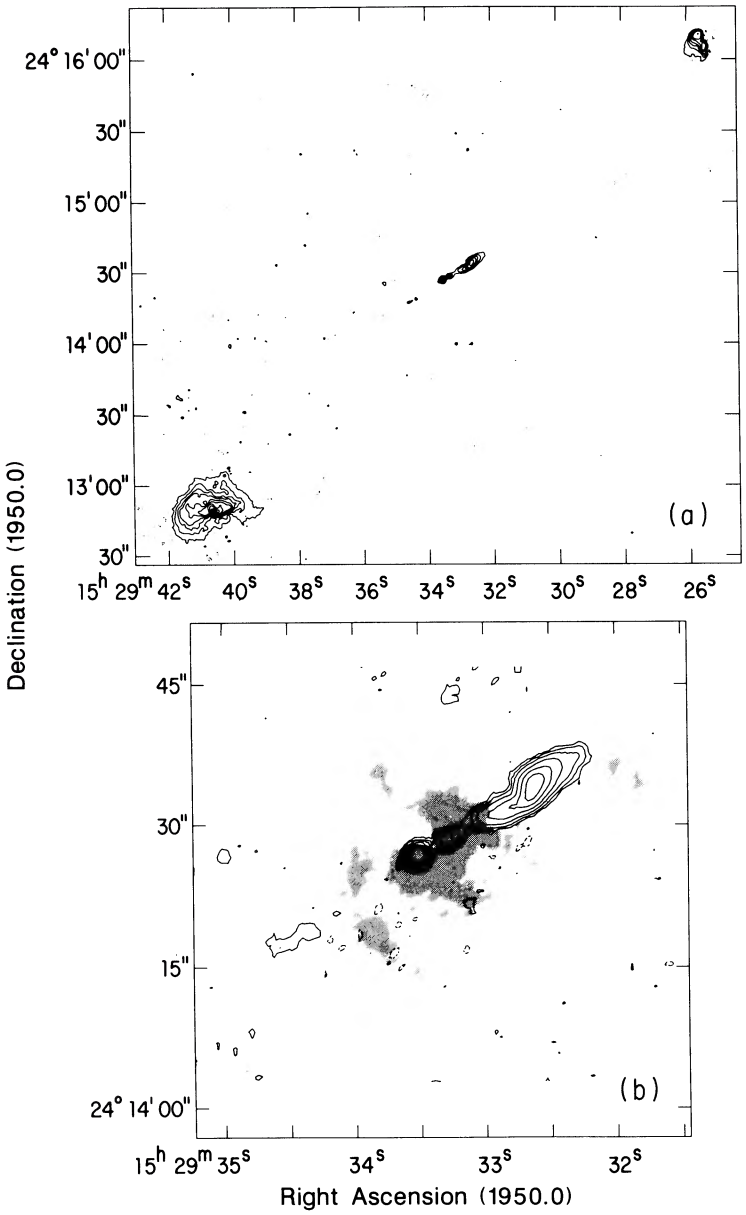


FIG. 46.—3C 321. (*a*) Contours of the 20 cm combined A and B array VLA image of 3C 321. Levels are $2.0\times10^{-1}\times(-3, 3, 10, 20, 30, 50, 75, 150, 300, 600, 1000, 1500, 2000)$ mJy per restoring beam (1".37 FWHM circular Gaussian). (*b*) Silhouete of the H$\alpha$ + [N II] emission superposed on the contours of the 20 cm combined A and B array VLA image. The radio contours are at levels of $1.3\times10^{-1}\times(-3, 3, 6, 12, 25, 45, 70, 100)$ mJy per restoring beam (1".37 FWHM circular Gaussian).



© American Astronomical Society • Provided by the NASA Astrophysics Data System

1988ApJS...68..643B

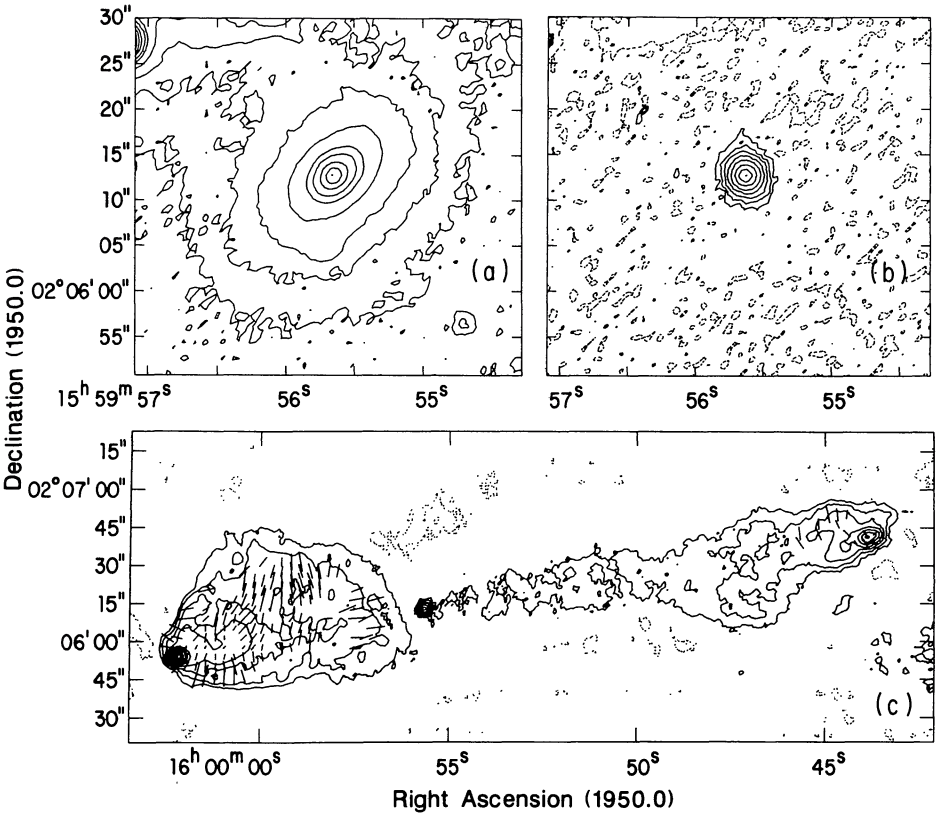


FIG. 47.—3C 327. (*a*) Contours of the *R*-band optimal image of the host galaxy of 3C 327. Levels are (−5, 5, 10, 20, 30, 50, 100, 200, 300, 500, 750, 1000) in arbitrary units. (*b*) Contours of the Hα+[N II] emission. Levels are $1\times10^{-17}\times(-10, 10, 25, 50, 100, 200, 400, 700, 1000)$ ergs $s^{-1}$ $cm^{-2}$ $arcsec^{-2}$. Calibrated using spectrophotometry from Costero and Osterbrock (1977). (*c*) Contours of the 6 cm combined B, C, and D array VLA image. Levels are $3.8\times10^{-1}\times(-3, 3, 6, 12, 25, 50, 75, 100, 150, 200, 235, 285)$ mJy per restoring beam (2″.94 circular Gaussian FWHM). The length of the superposed vectors indicate the fractional polarization, and their orientations give the direction of the projected electric field. A vector of length 1″ represents a fractional polarization of 5.7%.

© American Astronomical Society • Provided by the NASA Astrophysics Data System

1988ApJS...68..643B

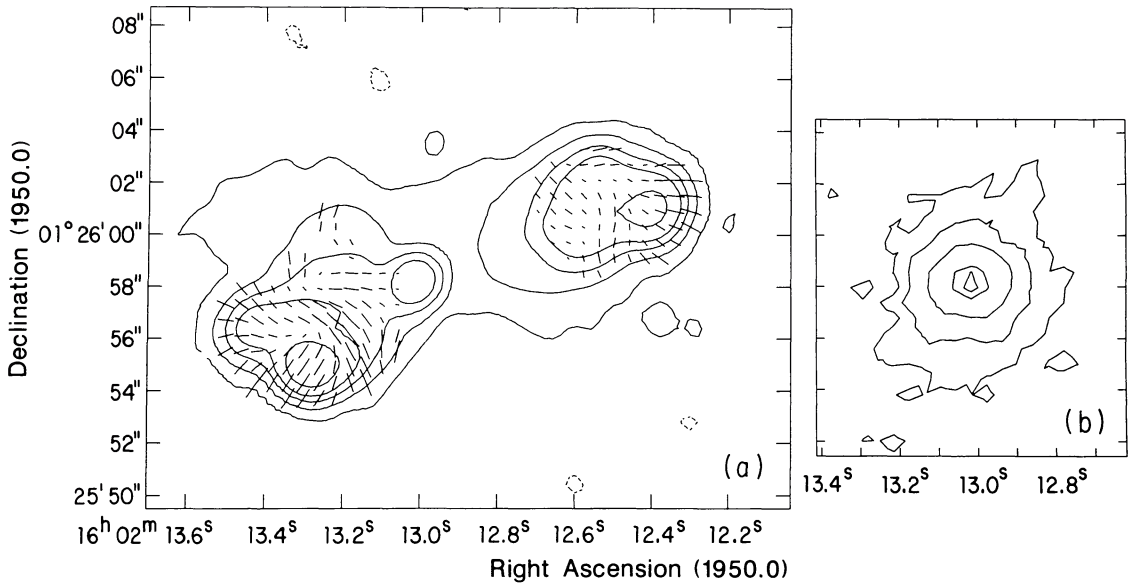


FIG. 48.—3C 327.1. (*a*) Contours of the 6 cm B array VLA image of 3C 327.1. Levels are $2.0\times10^{-1}\times(-3, 3, 25, 75, 150, 350)$ mJy per restoring beam (1".4 FWHM circular Gaussian). The lengths of the superposed vectors indicate the fractional polarization, and their orientations give the direction of the projected electric field. A vector of length 1" represents a fractional polarization of 22.2%. (*b*) Contours of the *R*-band optical image of the host galaxy of 3C 327.1. Levels are $1\times10^{-16}\times(-2, 2, 4, 10, 25, 30)$ ergs $s^{-1}$ $cm^{-2}$ $arcsec^{-2}$.

© American Astronomical Society • Provided by the NASA Astrophysics Data System

1988ApJS...68..643B

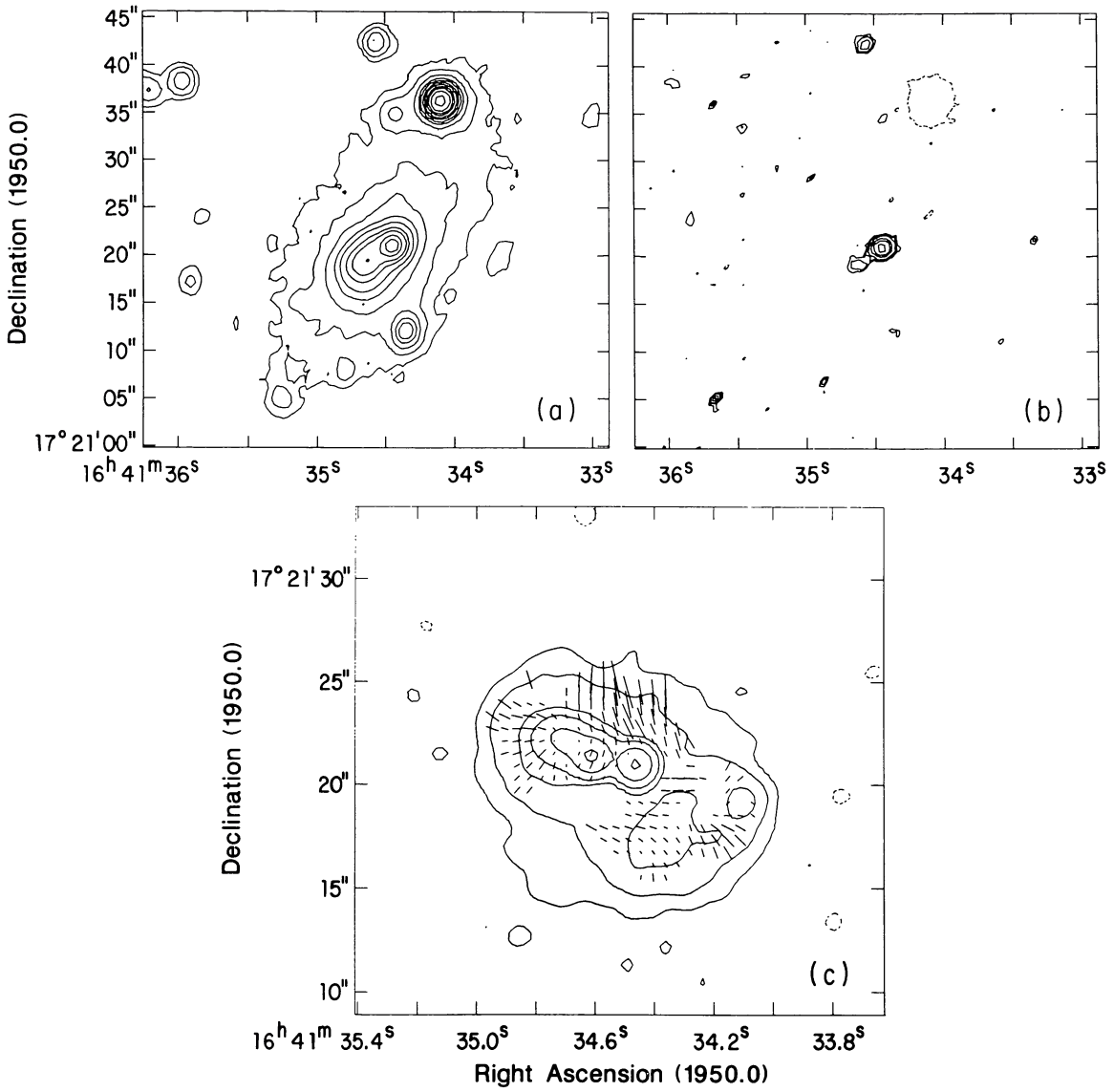


FIG. 49.—3C 346. (*a*) Contours of the *R*-band optical image of the host galaxy of 3C 346. Levels are (−5, 5, 10, 20, 35, 50, 75, 100, 150, 200, 300, 500, 750, 1000) in arbitrary units. (*b*) Contours of the H$\alpha$+[N II] emission. Levels are (−2, 2, 3, 5, 10, 15, 25, 50, 100, 250, 500) in arbitrary units. (*c*) Contours of the 6 cm B array VLA image of 3C 346. Levels are $2.25\times10^{-1}\times(-3, 3, 20, 80, 150, 400, 1000)$ mJy per restoring beam (1″.2 FWHM circular Gaussian). The lengths of the superposed vectors indicate the fractional polarization, and their orientations give the direction of the projected electric field. A vector of length 1″ represents a fractional polarization of 27.8%.

© American Astronomical Society • Provided by the NASA Astrophysics Data System

1988ApJS...68..643B

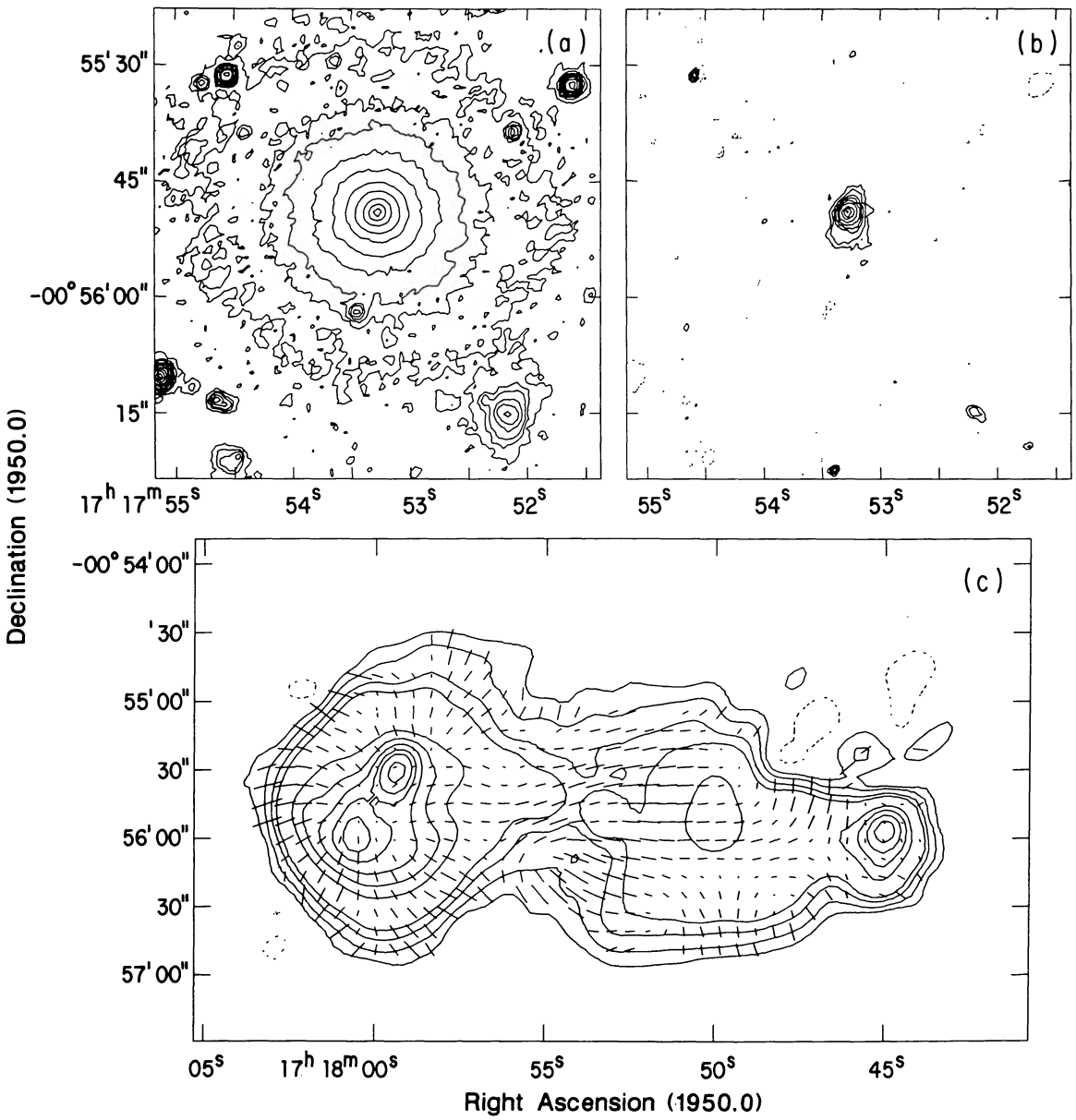


FIG. 50.—3C 353. (*a*) Contours of the *V*-band optical image of the host galaxy of 3C 353. Levels are $1\times10^{-16}\times(-4, 4, 8, 12, 20, 30, 50, 80, 150, 300, 750, 1000)$ ergs $s^{-1}$ $cm^{-2}$ $arcsec^{-2}$. (*b*) Contours of the H$\alpha$+[N II] emission. Levels are $1\times10^{-17}\times(-5, 5, 10, 20, 30, 50, 100, 250, 400, 600)$ ergs $s^{-1}$ $cm^{-2}$ $arcsec^{-2}$. (*c*) Contours of the 6 cm D array VLA image. Levels are $(-12, 12, 30, 60, 90, 225, 300, 375, 450, 510, 600)$ mJy per restoring beam (13″ circular Gaussian FWHM). The lengths of the superposed vectors indicate the fractional polarization, and their orientations give the direction of the projected electric field. A vector of length 1″ represents a fractional polarization of 5.0%.

© American Astronomical Society • Provided by the NASA Astrophysics Data System

1988ApJS...68..643B

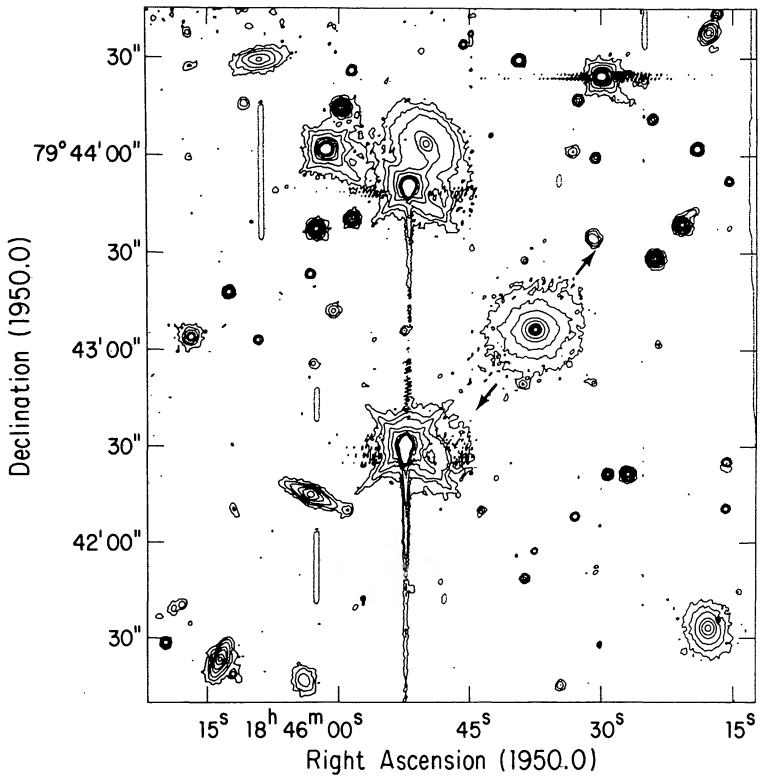


FIG. 51.—3C 390.3. Contours of the *V*-band optical image of the host galaxy of 3C 390.3 and nearby galaxies. Levels are $1\times10^{-16}\times(-5, 5, 10, 20, 50, 100, 300, 700, 1500, 3000)$ ergs $s^{-1}$ $cm^{-2}$ $arcsec^{-2}$. Arrows indicate the radio source axis.

© American Astronomical Society • Provided by the NASA Astrophysics Data System

1988ApJS...68..643B

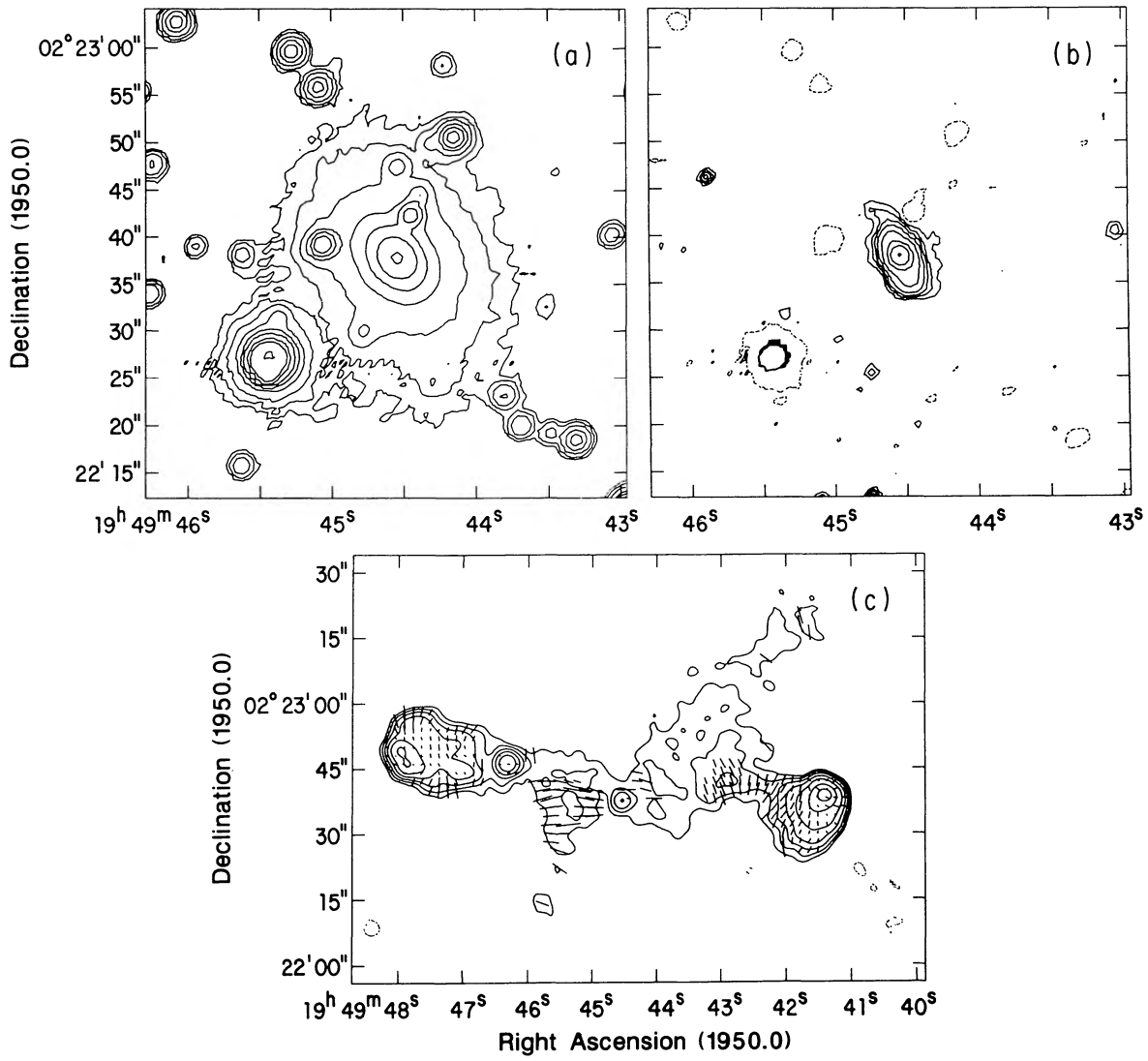


FIG. 52.—3C 403. (*a*). Contours of the *R*-band image of the host galaxy of 3C 403. Levels are (−3, 3, 5, 10, 25, 50, 100, 300, 750, 3000) in arbitrary units. (*b*) Contours of the Hα+[N II] emission. Levels are (−1, 1, 2, 3, 5, 10, 25, 45, 90) in arbitrary units. (*c*) Contours of the 6 cm combined B and C array image of 3C 403. Levels are $5.5\times10^{-1}\times(-3, 3, 6, 12, 25, 55, 125, 200)$ mJy per restoring beam (3.″2 FWHM circular Gaussian). The lengths of the superposed vectors indicate the fractional polarization, and their orientations give the direction of the projected electric field. A vector of length 1″ represents a fractional polarization of 13.3%.

© American Astronomical Society • Provided by the NASA Astrophysics Data System

1988ApJS...68..643B

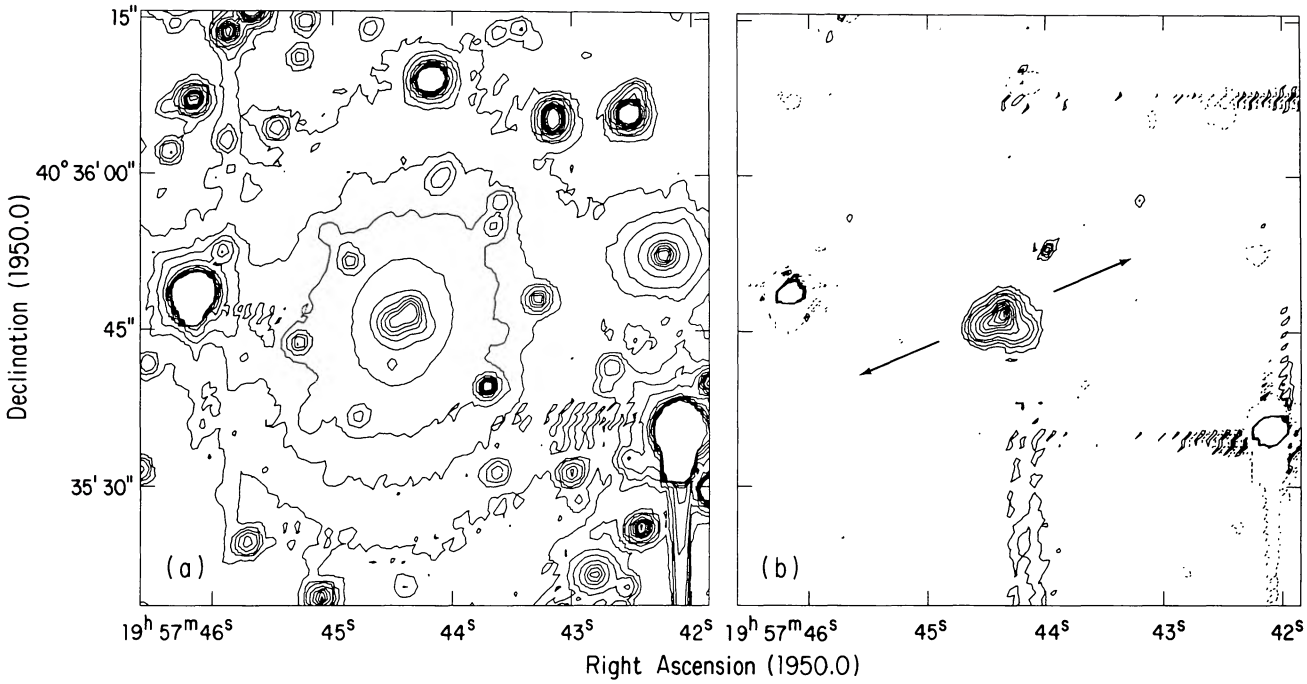


FIG. 53.—3C 405. (*a*) Contours of the *V*-band optical image of the host galaxy of 3C 405. Levels are $1\times10^{-16}\times(-8, 8, 15, 25, 50, 100, 150, 200, 250, 300, 399)$ ergs $s^{-1}$ $cm^{-2}$ $arcsec^{-2}$. (*b*) Contours of the [O III] emission. Levels are $1\times10^{-16}\times(-4, 4, 8, 15, 25, 50, 75, 100, 125, 150, 175, 200)$ ergs $s^{-1}$ $cm^{-2}$ $arcsec^{-2}$. Calibrated using spectrophotometry from Osterbrock and Miller (1975).

© American Astronomical Society • Provided by the NASA Astrophysics Data System

1988ApJS...68..643B

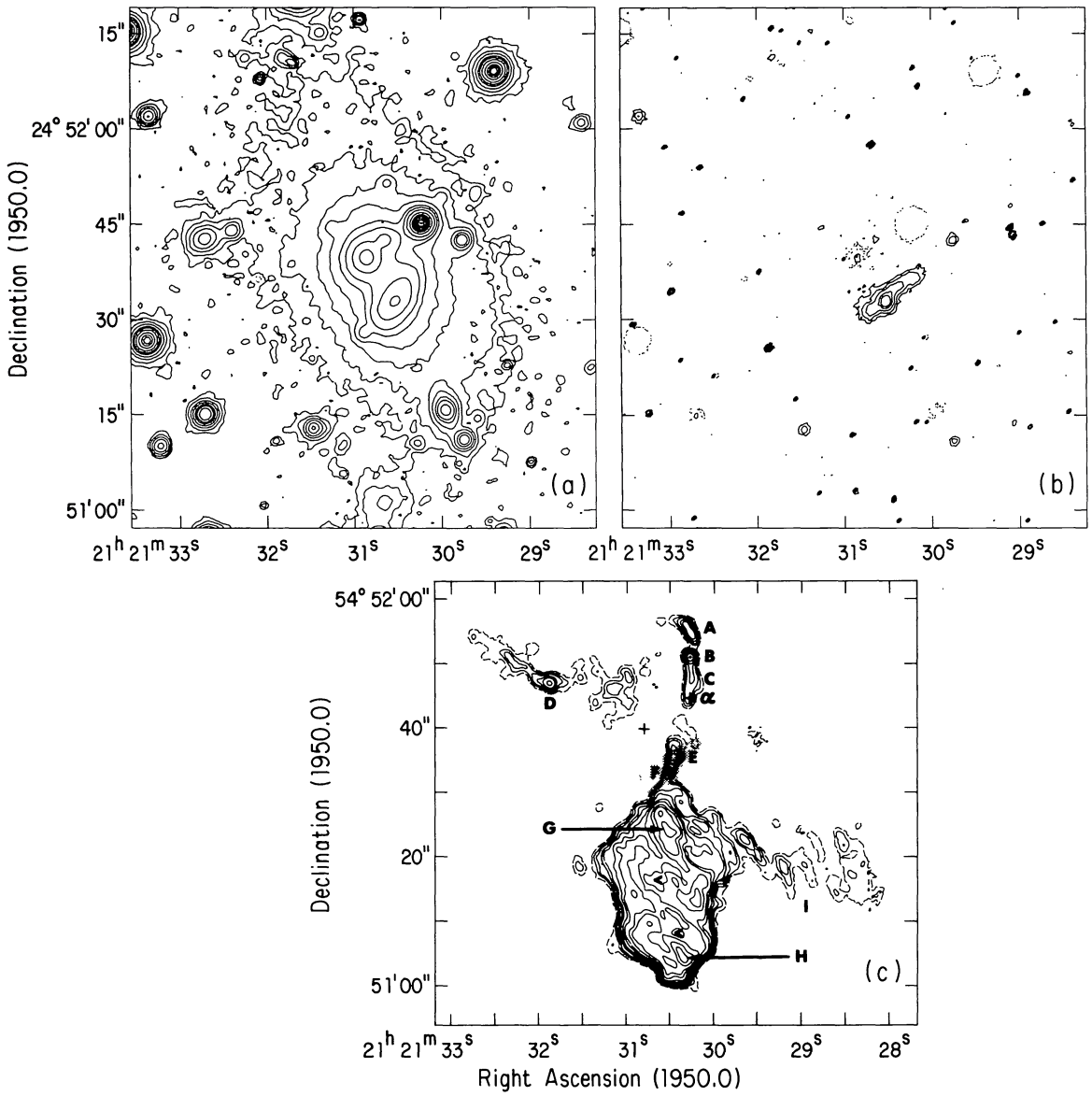


FIG. 54.—3C 433. (*a*) Contours of the *V*-band optical image of the host galaxy of 3C 433. Levels are $1\times10^{-16}\times(-2, 2, 4, 8, 15, 30, 50, 100, 250, 500, 750, 1000, 1500, 2000, 2500)$ ergs $s^{-1}$ $cm^{-2}$ $arcsec^{-2}$. (*b*) Contours of the H$\alpha$+[N II] image. Levels are $1\times10^{-16}\times(-2, 2, 5, 10, 20, 30, 50, 100, 150)$ ergs $s^{-1}$ $cm^{-2}$ $arcsec^{-2}$. (*c*) Silhouette of the H$\alpha$+[N II] image superposed on contours of the 6 cm radio emission. The radio contours are reproduced from van Breugel *et al.* (1983). Levels are (1 [*dashed line*], 1.5, 2, 3, 4, 6, 9, 16, 24, 32, 64) mJy per restoring beam (1".2 FWHM circular Gaussian).

© American Astronomical Society • Provided by the NASA Astrophysics Data System

1988ApJS...68..643B

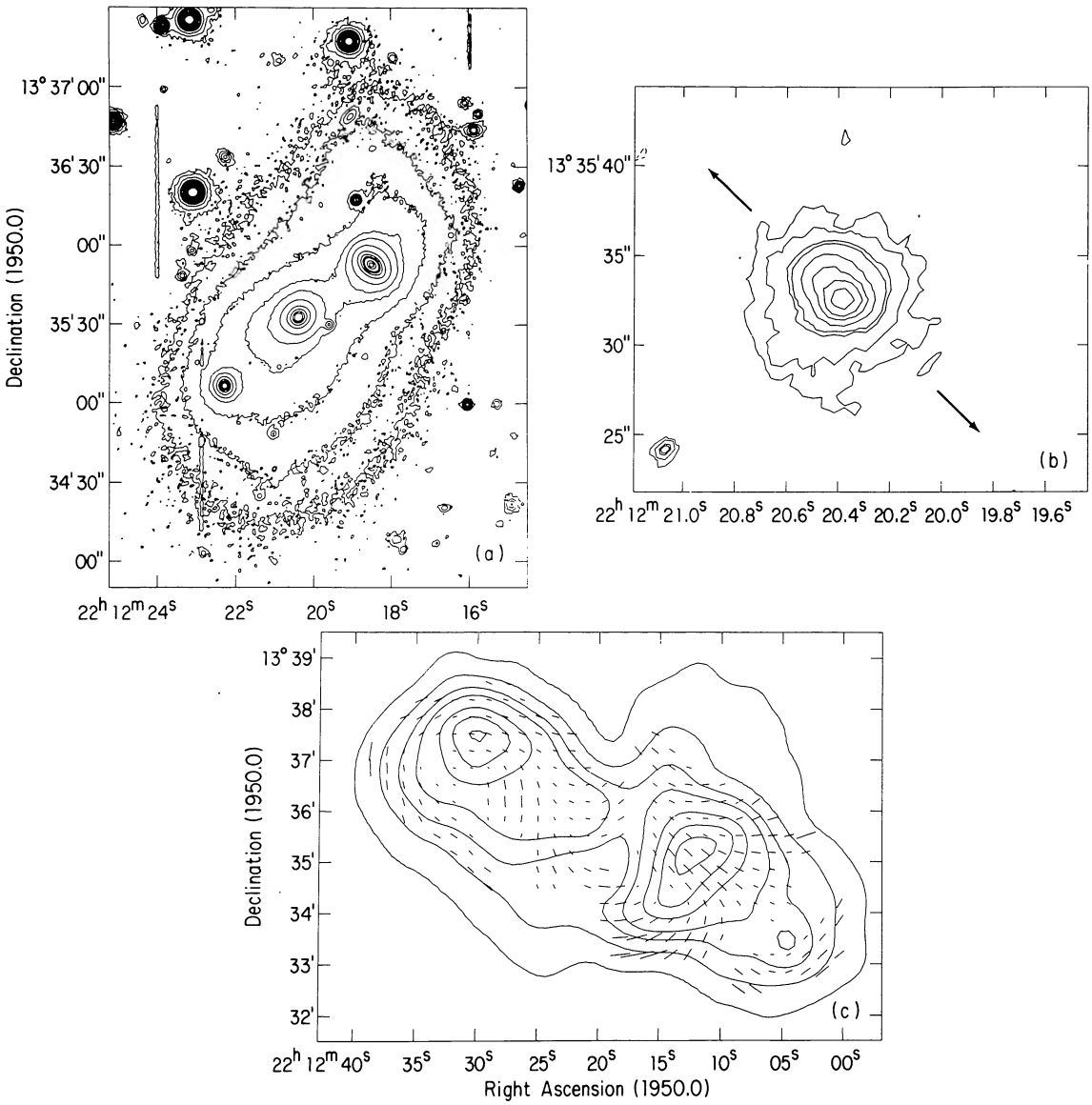


FIG. 55.—3C 422. (*a*) Contours of the *R*-band optical image of the host galaxy of 3C 442. The radio source is identified with the central of the three galaxies. Levels are $1\times10^{-16}\times(-6, 6, 12, 25, 50, 80, 150, 300, 500, 750, 1000, 2000, 3000)$ ergs $s^{-1}$ $cm^{-2}$ $arcsec^{-2}$. (*b*) Contours of the H$\alpha$ + [N II] image. Levels are $1\times10^{-17}\times(-6, 6, 12, 25, 30, 50, 75, 100, 140, 180)$ ergs $s^{-1}$ $cm^{-2}$ $arcsec^{-2}$. Arrows indicate the radio source axis. (*c*) Contours of the 21 cm radio VLA D array image. Levels are $(-6, 6, 30, 60, 86, 130, 160, 180)$ mJy per restoring beam (50″ FWHM circular Gaussian). The lengths of the superposed vectors indicate the fractional polarization, and their orientations give the direction of the projected electric field. A vector of length 10″ represents a fractional polarization of 1%.

© American Astronomical Society • Provided by the NASA Astrophysics Data System

1988ApJS...68..643B



interstellar medium associated with the host galaxy of 3C 405, or (3) the intracluster medium.

Optical broad-band imaging of the host galaxy of 3C 405 has been reported by Thompson (1984). Pierce and Stockton (1986) have studied, spectroscopically and with narrow-band imagining, the extended emission-line region in the center of the galaxy. Our [O III] image of 3C 405 shows the unusual emission-line morphology associated with the inner parts of this galaxy. We confirm that the central northern peak seen in the broad-band galaxy image is dominated by line emission, while the line emission associated with the southeastern peak has a smaller equivalent width. The position of the radio source core appears to be intermediate between these two peaks and may be coincident with a peak in the very high angular resolution broad-band image obtained by Thompson (1984).

*3C 433 (2121 + 54).*—Van Breugel *et al.* (1983) report optical, radio, and X-ray observations of 3C 433. This radio source is associated with the southern of a pair of galaxies in a common elliptical envelope at $z = 0.1016$ on the edge of a cluster of galaxies (MMS). The two nuclei are separated by $\sim 8''.3$ (14 kpc). The radio source has a very peculiar morphology for its high radio luminosity. The source has a jet to the north which bends slightly to the west before vanishing. To the south, an edge-brightened lobe (containing the majority of the radio flux in the interferometric maps) is detected. Finally, radio emission is detected to the west-northwest and east-southeast, giving the source an X-shaped morphology. Our H$\alpha$ + [N II] image shows nuclear emission plus a slightly curving filament which extends 8″ (14 kpc) to the northwest and 5″ (8.5 kpc) to the southeast, along an axis which is askew to the radio jet by $\sim 36°$.

*3C 442 (2212 + 13).*—The radio source 3C 442 is associated with the central galaxy of three galaxies in a line, each of which is separated in projection by $\sim 35''$ (17 kpc) from the adjacent galaxy. The galaxy is the brightest member of an extended cluster of richness class 0 (MMS). Our H$\alpha$ + [N II] image shows nuclear line emission, surrounded by a roughly circular region of extended emission with a diameter of $\sim 8''$ (4 kpc) and a curving tail of line emission extending to the southeast. The radio source 3C 442 is roughly 8′.7 (260 kpc) in extent and is the lowest radio luminosity source in our sample that has hotspots which are clearly visible at the ends of the extended radio emission. Our 6 cm C array VLA snapshot image shows unresolved hotspots of roughly equal flux density at opposite ends of the source and the radio core. The two hotspots are not collinear with the nucleus, the line connecting the two hotspots being displaced northwest of the core. At 20 cm in the D array at 50″ resolution, 3C 442 shows a northeastern hotspot and a somewhat dimmer hotspot at the southwestern end of the source. Interior to the dim southwestern hotspot, roughly halfway to the core, but displaced slightly northward of the line joining the hotspot and the core, is a most unusual, bright, resolved region of radio emission which is elongated transverse to the radio axis. Lower resolution radio maps of 3C 442 at 408 and 1407 MHz have been presented by Mackay (1969).

## VII. CONCLUDING REMARKS

In this paper, we present radio, optical broad-band, and optical emission-line images of a total of 42 radio sources. In future papers, we will present the numerical and statistical results of these observations and discuss their implications. However, a few qualitative remarks are in order here. We note that extended optical-line–emitting gas is extremely common in powerful radio galaxies and that individual emission-line nebulae can be quite striking. In 3C 227 a single filament appears to reach for $\sim 100$ kpc. In PKS 0349 − 278, 3C 63, 3C 218, 3C 272.1, and 3C 285 the brightest line emission comes from a region which has an S shape, and in 3C 63, PKS 0349 − 278, and 3C 285 long filaments appear to form bridges between the host galaxy and a nearby companion. Many of the galaxies also exhibit peculiarites in the distribution of their optical continuum light. We note the 70 kpc continuum-emitting tails in 3C 223 and the possible 13 kpc arc of continuum light found 35 kpc from the nucleus of PKS 0745 − 191 at the center of a rich "cooling flow" cluster of galaxies. Subsequent papers will present parameters derived from these data and discuss the statistical results of this work and their implications, including a detailed examination of the relationship between the extended radio structure and the line-emitting gas.

We thank the staff at NRAO and at KPNO for their help, Kerry Hilldrup for supporting AIPS on the Convex C-1 at NRAO in Charlottesville where much of the data reduction was done, Thad Polk and Don Wells for developing the geometrical software that was used to superpose the radio and optical images, and George Kessler for his work on the figures. S. A. B. and T. M. H. acknowledge support from NSF grant AST85-15896. S. A. B. thanks NRAO for the award of a predoctoral research associateship, Chris O'Dea for comments on the paper, and D. Mint for moral support.

## REFERENCES

Abramopoulus, F., and Ku, W. H.-M. 1983, *Ap. J.*, **271**, 446.
Arnaud, K. A., Fabian, A. C., Eales, S. A., Jones, C., and Forman, W. 1984, *M.N.R.A.S.*, **211**, 981.
Arnaud, K. A., Johnstone, R. M., Fabian, A. C., Crawford, C. S., Nulsen, P. E. J., Shafer, R. A., and Mushotzky, R. F. 1987, *M.N.R.A.S.*, **227**, 241.
Baars, J. W. M., Genzel, R., Pauliny-Toth, I. I. K., and Witzel, A. 1977, *Astr. Ap.*, **61**, 99.
Baum, S. A., and Heckman, T. M. 1987. In *Radio Continuum Processes in Clusters of Galaxies*, ed. C. P. O'Dea and J. M. Uson (Greenbank: NRAO), p. 119.
Baum, S. A., O'Dea, C. P., and Killeen, N. E. B. 1988, in preparation.
Begelman, M. C., Blandford, R. D., and Rees, M. J. 1984, *Rev. Mod. Phys.*, **56**, 255.
Begelman, M. C., and Blandford, R. D. 1987, *Nature*, **330**, 46.
Bignell, R. C., and Perley, R. A. 1985. In *Synthesis Imaging*, ed. R. A. Perley, F. R. Schwab, and A. H. Bridle (Green Bank: NRAO), p. 49.
Bolton, J. G., and Ekers, J. 1966, *Australian J. Phys.*, **19**, 559.
Bridle, A. H., Perley, R. A., and Henriksen, R. N. 1986, *A.J.*, **92**, 534.
Bridle, A. H., and Vallee, J. P. 1981, *A.J.*, **86**, 1165.
Burbidge, E. M., and Burbidge, G. R. 1971, *Ap. J.* (*Letters*), **163**, L21.
Burbidge, G. R., and Crowne, A. H. 1979, *Ap. J. Suppl.*, **40**, 583.
Burstein, D., and Heiles, C. 1982, *A.J.*, **87**, 1165.
Canizares, C. R., Stewart, G. C., and Fabian, A. C. 1983, *Ap. J.*, **272**, 449.
Chincarini, G., and Rood, H. J. 1977, *Ap. J.*, **214**, 351.
Clavel, J., and Wamsteker, W. 1987, *Ap. J.* (*Letters*), **320**, L9.
Cohen, R. D., and Osterbrock, E. 1981, *Ap. J.*, **243**, 81.

© American Astronomical Society • Provided by the NASA Astrophysics Data System

1988ApJS...68..643B



Costero, R., and Osterbrock, D. E. 1977, *Ap. J.*, **211**, 675.
Danziger, I. J., Fosbury, R. A. E., Goss, W. M., Bland, J., and Boksenberg, A. 1984, *M.N.R.A.S.*, **208**, 589.
Dickens, R. F., and Moss, C., 1976, *M.N.R.A.S.*, **174**, 47.
Dieckvoss, W. 1975, **AGK3 Star Catalogue** (Hamburg: Hamburger Sternwarte).
Dreher, J. W., Carilli, C. L., and Perley, R. A. 1987, *Ap. J.*, **316**, 611.
Eather, R. H., and Reasoner, D. L. 1969, *Applied Optics*, **8**, 227.
Ekers, R., and Simkin, S. 1983, *Ap. J.*, **265**, 85.
Elvis, M., Schreier, E. J., Tonry, J., Davis, M., and Huchra, J. P. 1981, *Ap. J.*, **246**, 20.
Fabbiano, G., Doxsey, R. E., Johnston, M., Schwartz, D. A., and Schwartz, J. 1979, *Ap. J.* (*Letters*), **230**, L67.
Fabian, A. C., Arnaud, K. A., Nulsen, P. E., Watson, M. G., Stewart, G. C., McHardy I., Smith, A., Cooke, B., Elvis, M., and Mushotsky, R. F. 1985, *M.N.R.A.S.*, **216**, 923.
Fanaroff, B. L., and Riley, F. M. 1974, *M.N.R.A.S.*, **167**, 31p.
Feigelson, E. D., Wood, P. A. D., Schreier, E. J., Harris, D. W., and Reid, M. J. 1986, *Ap. J.*, **312**, 101.
Ford, H. C., and Butcher, H. 1979, *Ap. J. Suppl.*, **41**, 147.
Forman, W., Jones, C. 1982, *Ann. Rev. Astr. Ap.*, **20**, 547.
Fosbury, R. A. E. 1986. In *Structure and Evolution of Active Galactic Nuclei*, ed. G. Givricin, F. Mardirossian, M. Mezzetti, and M. Ramonella (Dordrecht: Reidel), p. 297.
Fosbury, R. A. E. Tadhunter, C. N., Bland, J., and Danziger, I. J. 1984, *M.N.R.A.S.*, **208**, 955.
Gavazzi, G., Perola, G. C., and Jaffe, W. 1981, *Astr. Ap.*, **103**, 35.
Gilmore, G., and Shaw, M. A. 1986, *Nature*, **321**, 750.
Grandi, S. A. 1977, *Ap. J.*, **215**, 446.
Grandi, S. A., and Osterbrock, D. E. 1978, *Ap. J.*, **220**, 783.
Hansen, L., Norgaard-Nielsen, H. U., and Jorgensen, H. E. 1985, *Astr. Ap.*, **149**, 442.
_____. 1987, *Astr. Ap., Suppl.* **71**, 465.
Hargrave, P. J., and Ryle, M. 1974, *M.N.R.A.S.* **166**, 305.
Harris, A. 1972, *M.N.R.A.S.*, **158**, 1.
Heckman, T. M., Carty, T. J., and Bothun, G. D. 1985, *Ap. J.*, **288**, 122.
Heckman, T. M., Miley, G. H., Balick, B., van Breugel, W. J. M., and Bothun, H. R. 1982, *Ap. J.*, **262**, 529.
Heckman, T. M., Smith, E. P., Baum, S. A., van Breugel, W. J. M., Miley, G. K., Illingworth, G. D., Bothun, G. D., and Balick, B. 1986, *Ap. J.*, **311**, 526 (H86).
Heckman, T. M., van Breugel, W. J. M., Miley, G. H. 1984, *Ap. J.*, **286**, 509.
Henry, J. P., and Henriksen, M. J. 1986, *Ap. J.*, **301**, 689.
Hoessel, J. G., Borne, K. D., and Schneider, D. P. 1985, *Ap. J.*, **293**, 94.
Hogbom, J. 1974, *Astr. Ap. Suppl.*, **15**, 417.
Hogbom, J. A. 1979, *Astr. Ap. Suppl.*, **36**, 173.
Hogg, D. E., MacDonald, G. H., Conway, R. G., and Wade, C. M. 1969, *A.J.*, **74**, 1206.
Hu, E. M., Cowie, L. L., and Wang, Z. 1985, *Ap. J. Suppl.*, **59**, 447.
Kato, T., Tebara, H., Inoue, M., and Aizu, K. 1987, *Nature*, **329**, 223.
Killeen, N. E. B., Bicknell, G. V., and Ekers, R. D. 1986, *Ap. J.*, **302**, 306.
Koski, A. T. 1978, *Ap. J.*, **223**, 56.
Katanyi C. 1980, Astr. Ap. **83**, 245.
Laing, R. A., and Bridle, A. H. 1987, *M.N.R.A.S.*, **228**, 557.
Lauer, T. 1987, preprint
Leahy, J. P., and Williams, A. G. 1984, *M.N.R.A.S.*, **210**, 929.
Lynds, R., and Petrosian, V. 1986, *Bull. A.A.S.*, **18**, 1014.
Mackay, C. D. 1969, *M.N.R.A.S.*, **145**, 31.
Maltby, P., Mathews, T. A., and Moffet, A. T. 1963, *Ap. J.*, **137**, 153.
Mathews, T. A., Morgan, W. W., and Schmidt, M. 1964, *Ap. J.*, **140**, 35 (MMS).
McCarthy, P. J., van Breugel, W., Heckman, T., Miley, G., Filippenko, A. V., and Baum, S. A. 1988, in preparation.
O'Dea, C. P., and Owen, F. N. 1985, *A.J.*, **90**, 927.
O'Dea, C. P., Owen, F. N., and Keel, W. 1986, *Canadian J. Phys.*, **64**, 313.
O'Donoghue, A. 1987, in *Radio Continuum Processes in Clusters of Galaxies*, ed. C. P. O'Dea and J. M. Uson (Greenbank: NRAO), p. 142.
O'Donoghue, A., and Owen, F. N. 1987, in *Radio Continuum Processes in Clusters of Galaxies*, ed. C. P. O'Dea and J. M. Uson (Greenbank: NRAO), p. 155.
Osterbrock, D. E., Koski, A. T., and Phillips, M. M. 1975, *Ap. J.* (*Letters*), **197**, L41.
_____. 1976, *Ap. J.*, **206**, 898.
Osterbrock, D. E., and Miller, J. S. 1975, *Ap. J.*, **197**, 535.
Owen, F., and Rudnick, L. 1976, *Ap. J.* (*Letters*), **205**, L1.
Owen, F. N., O'Dea, C. P., Inoue, M., and Eilek, J. A. 1985, *Ap. J.* (*Letters*), **294**, L85.
Owen, F., O'Dea, C. P., and Keel, W. 1987, preprint.
Parma, P., de Ruiter, H. R., Fanti, C., and Fanti, R. 1986, *Astr. Ap. Suppl.*, **64**, 135.
Perley, R. A., Dreher, J. D., and Cowan, J. J. 1984, *Ap. J.* (*Letters*), **285**, L35.
Pierce, M. J., and Stockton, A. 1986, *Ap. J.*, **305**, 204.
Rao, A. P. 1987, in *Radio Continuum Processes in Clusters of Galaxies*, ed. C. P. O'Dea and J. M. Uson (Greenbank: NRAO), p. 79.
Saikia, D. J., Subrahmanya, C. R., Patnaik, A. R., Unger, S. W., Cornwell, T. J., Graham, D. A., and Prabhu, T. P. 1986, *M.N.R.A.S.*, **219**, 545.
Sandage, A. 1966, *Ap. J.*, **145**, 1.
_____. 1972, *Ap. J.*, **178**, 25 (S72).
Sandage, A., and Hardy, E. 1973, *Ap. J.*, **183**, 743.
Schilizzi, R. T., Lockhart, I. A., and Wall, J. V. 1972, *Australian J. Phys.*, **25**, 545.
Schmidt, M. 1965, *Ap. J.*, **141**, 1.
_____. 1966, *Ap. J.*, **146**, 7.
Schwab, F. 1980, *Proc. SPIE*, **231**, 18.
_____. 1984, *A.J.*, **89**, 1076.
Simkin, S. M. 1979, *Ap. J.*, **234**, 56.
_____. 1986, *Ap. J.* (*Letters*), **222**, L55.
Simkin, S. M., and Michel, A. 1986, *Ap. J.* (*Letters*), **300**, L5.
Simmons, J. F. L., and Stewart B. G. 1985, *Astr. Ap.*, **142**, 100.
Soucail, G., Fort, B., Meiller, Y., and Picat, J. P. 1987, *Astr. Ap.*, **172**, L14.
Smithsonian Astrophysical Observatory. 1966, *Smithsonian Astrophysical Observatory Star Catalog* (Washington, DC: Smithsonian Institution).
Spinrad, H., Djorgovski, S., Marr, J., and Aguilar, L. 1985, *Pub. A.S.P.*, **93**, 932.
Spinrad, H., and Stauffer, J. R. 1982, *M.N.R.A.S.*, **200**, 153.
Thompson, A. R., Clark, B. G., Wade, C. M., and Napier, P. J. 1980, *Ap. J. Suppl.*, **44**, 151.
Thompson, L. A. 1984, *Ap. J.* (*Letters*), **279**, L47.
Unger, S. W., Booler, R. V., and Pedlar, A. 1984, *M.N.R.A.S.*, **207**, 679.
van Breugel, W. 1986, *Canadian J. Phys.*, **64**, 392.
van Breugel, W., Balick, B., Heckman, T., Miley, G., and Helfand, D. 1983, *A.J.*, **88**, 42.
van Breugel, W., Heckman, T., and Miley, G. 1984, *Ap. J.*, **276**, 79.
van Breugel, W. J. M., Heckman, T. M., Miley, G. K., and Filippenko, A. V. 1986, *Ap. J.*, **311**, 58.
Vinokur, M. 1965, *Ann. d'Ap.*, **28**, 412.
Wade, C. M. 1960, *Observatory*, **80**, 235.
Wardle, J. F. C., and Kronberg, P. P. 1974, *Ap. J.*, **194**, 249.
Wirth, A., Smarr, L., and Gallagher, J. S. 1982, *A.J.*, **87**, 602.
Wyndham, J. D. 1966, *Ap. J.*, **144**, 459.
Yee, H. K. C., and Oke, J. B. 1978, *Ap. J.*, **226**, 753.

STEFI ALISON BAUM: Radiosterrenwacht, Postbus 2, 7990 AA, Dwingeloo, The Netherlands

ALAN H. BRIDLE: National Radio Astronomy Observatory, Edgemont Road, Charlottesville, VA 22901

TIMOTHY M. HECKMAN: Astronomy Program, University of Maryland, College Park, MD 20742

GEORGE K. MILEY: Homewood Campus, Space Telescope Science Institute, Baltimore, MD 21218

WIL J. M. VAN BREUGEL: Radio Astronomy Laboratory, University of California, 601 Campbell Hall, Berkeley, CA 94720

© American Astronomical Society • Provided by the NASA Astrophysics Data System